VOL. 14 NO. 4 AUGUST 1967
PUBLISHED MONTHLY
completing volume 14

JOURNAL OF

ELECTROANALYTICAL CHEMISTRY

AND INTERFACIAL ELECTROCHEMISTRY

International Journal devoted to all Aspects of Electroanalytical Chemistry, Double Layer Studies, Electrokinetics, Colloid Stability, and Electrode Kinetics.

ELSEVIER

GENERAL INFORMATION

See also Suggestions and Instructions to Authors which will be sent free, on request to the Publishers.

Types of contributions

(a) Original research work not previously published in other periodicals.
(b) Reviews on recent developments in various fields.
(c) Short communications.
(d) Bibliographical notes and book reviews.

Languages

Papers will be published in English, French or German.

Submission of papers

Papers should be sent to one of the following Editors:

Professor J. O'M. Bockris, John Harrison Laboratory of Chemistry, University of Pennsylvania, Philadelphia 4, Pa. 19104, U.S.A.
Dr. R. H. Ottewill, Department of Chemistry, The University, Bristol 8, England.
Dr. R. Parsons, Department of Chemistry, The University, Bristol 8, England. Until June 1967: Gates and Crellin Laboratories of Chemistry, California Institute of Technology, Pasadena, Calif. 91109, U.S.A.
Professor C. N. Reilley, Department of Chemistry, University of North Carolina, Chapel Hill, N.C. 27515, U.S.A.

Authors should preferably submit two copies in double-spaced typing on pages of uniform size. Legends for figures should be typed on a separate page. The figures should be in a form suitable for reproduction, drawn in Indian ink on drawing paper or tracing paper, with lettering etc. in thin pencil. The sheets of drawing or tracing paper should preferably be of the same dimensions as those on which the article is typed. Photographs should be submitted as clear black and white prints on glossy paper. Standard symbols should be used in line drawings, the following are available to the printers:

All references should be given at the end of the paper. They should be numbered and the numbers should appear in the text at the appropriate places.
A summary of 50 to 200 words should be included.

Reprints

Fifty reprints will be supplied free of charge. Additional reprints can be ordered at quoted prices. They must be ordered on order forms which are sent together with the proofs.

Publication

The *Journal of Electroanalytical Chemistry and Interfacial Electrochemistry* appears monthly and has four issues per volume and three volumes per year.

Subscription price: £ 18.18.0 or $ 52.50 or Dfl. 189.00 per year; £ 6.6.0 or $ 17.50 or Dfl. 63.00 per volume; plus postage. Additional cost for copies by air mail available on request. For advertising rates apply to the publishers.

Subscriptions

Subscriptions should be sent to:

ELSEVIER PUBLISHING COMPANY, P.O. Box 211, Amsterdam, The Netherlands.

ELECTROANALYTICAL CHEMISTRY AND INTERFACIAL ELECTROCHEMISTRY
Elsevier Publishing Company, Amsterdam – Printed in The Netherlands

THE LOCATIONS OF INFLECTION POINTS ON TITRATION CURVES FOR SYMMETRICAL REDOX REACTIONS

JAMES A. GOLDMAN
Department of Chemistry, Polytechnic Institute of Brooklyn, Brooklyn, New York (U.S.A.)
(Received October 31st, 1966)

INTRODUCTION

The question of whether or not the location of the equivalence point coincides with the point of maximum slope on redox titration curves had been previously investigated by KOLTHOFF AND FURMAN[1]. A numerical evaluation was made of the variation of potential in the titration of a solution of ferric ion with a solution of cuprous ion. The slope of the titration curve was evaluated at 0.1% prior, and 0.1% subsequent, to the equivalence point. From this, it was concluded that the location of the maximum slope "occurs just at the equivalence point" and that the "curve is symmetrical on both sides of this point". However, in retrospection, it should be recognized that this numerical example could hardly be expected to provide evidence of any small deviations from symmetry because the difference between the values of the two formal potentials is fairly large, *viz.*, 0.44 V = $\Delta E^{\circ\prime}$.

Indeed, these authors later present a mathematical formulation of the variation in the value of the slope of the titration curve applicable to this same example, *i.e.*, $Fe^{3+} + Cu^{+} = Fe^{2+} + Cu^{2+}$. The conclusion was, that for any symmetrical ($n_1 = n_2$, *i.e.*, both reversible electron transfer couples involve the *same* number of electrons so that the general representation of the titration reaction is: $Ox_1 + Red_2 = Red_1 + Ox_2$) redox reaction, the "theoretical maximum [of the slope of the titration curve] occurs *before* the equivalence point". No approximations were required in the mathematical derivation used to arrive at this conclusion. It is further stated that "in cases where the titration is practical, ... the difference is so small that it can hardly be estimated". By use of an approximation, it was, however, possible to demonstrate that the magnitude of the slope just prior to the equivalence point is *always greater* than at the equivalence point, but that the "difference is actually so small that it will not be observed". It was emphasized that the approximations used are "only of the same order" as the difference between the value at the point of maximum slope and that at the equivalence point. *Only* for titrations where $\Delta E^{\circ\prime} \geqslant$ 591 mV, was it possible, by use of further approximations, to numerically evaluate the fraction titrated at which the point of maximum slope occurs. The general conclusion was that "even in the simple case ... we get equations which are impracticable and difficult to solve".

The next major theoretical investigation of the properties of redox titration curves was made by MURGULESCU AND DRAGULESCU[2] who demonstrated that, rigorously, the inflection point (corresponding to the point of maximum slope) can

never coincide with the equivalence point even when the redox titration reaction is symmetrical. This was evident, before any approximations were made, from the equation presented for d^2E/df^2 (f represents the fraction titrated). However, after the introduction of approximations, the general equation presented for the evaluation of the location of the inflection point predicts that the inflection point *does* coincide with the equivalence point in a symmetrical redox reaction. Nevertheless, it was proposed that the value of this equation was its utility for characterization of asymmetrical redox reactions. However, it should be noted that it was indeed a more general equation than any presented by KOLTHOFF AND FURMAN[1].

Because a general equation[3,4] has recently been presented for the description of titration curves for homogeneous and symmetrical redox reactions, it is now appropriate to re-investigate the location of inflection points on these curves. It will be demonstrated that *no* approximations are required in the following theoretical treatment of curves for *symmetrical* reactions and that the location of the point of *minimum* slope, as well as that of the maximum slope, may be readily determined. It is confirmed that the point of *maximum* slope always *precedes* the equivalence point, whereas it is newly shown that the point of *minimum* slope *always occurs subsequent* to the point at which $f = \frac{1}{2}$. However, there are values of $\Delta E^{\circ\prime}$ for which the titration curve possesses neither a point of maximum nor minimum slope. In addition, the equations presented are rigorously valid for the evaluation of the locations of the inflection points on curves for *any* value of $\Delta E^{\circ\prime}$ *where* these points exist.

THE EXISTENCE AND LOCATIONS OF THE INFLECTION POINTS

For homogeneous and symmetrical redox reactions of the type

$$n_2 \mathrm{Ox}_1 + n_1 \mathrm{Red}_2 = n_2 \mathrm{Red}_1 + n_1 \mathrm{Ox}_2 \tag{1}$$

where a solution containing Red_2 is being titrated *with* a solution containing Ox_1, the fraction titrated at any potential, E, may be calculated from

$$f = \{1 + k \exp(n_1 \psi)\}/\{1 + k \exp(-n_2 \psi)\} \tag{2}$$

where $\psi = (F/RT)(E - E^*)$, $k = \exp(-n\delta)$, $\delta = (F/RT)\Delta E^{\circ\prime}$, $n = n_1 n_2/(n_1 + n_2)$, and $\Delta E^{\circ\prime} = (RT/n_1 n_2 F) \ln K$. The equivalence-point potential is designated by E^*, K represents the equilibrium constant for the reaction defined by eqn. (1), and R, T and F have their customary significance.

Because only symmetrical (where $n_1 = n_2 = p$) reactions are to be considered, eqn.(2) may be rewritten as

$$f = \{1 + k \exp(p\psi)\}/\{1 + k \exp(-p\psi)\} \tag{3}$$

from which one obtains

$$\frac{dE}{df} = \frac{RT}{F} \frac{[1 + k \exp(-p\psi)]^2}{pk[2k + \exp(p\psi) + \exp(-p\psi)]} \tag{4}$$

With the restriction that $n_1 = n_2 = p$, eqn.(4) may also be readily obtained from the more general equation previously presented[5]. Equation(4), which permits the evaluation, at any point, of the slope of the titration curve, may conveniently be rewritten as

$$\frac{dE}{df} = \frac{RT}{F} \frac{[1+k\exp(-p\psi)]^2}{2pk[k+\cosh(p\psi)]} \tag{5}$$

which form is somewhat more convenient for the numerical evaluation of dE/df. It should be noted that the slope is *always positive* and never equal to zero.

At the equivalence point, $\psi = 0$, so that[5]

$$\left(\frac{dE}{df}\right)_{f=1} = \frac{RT}{F} \frac{1+k}{2pk} \tag{6}$$

Differentiation of eqn. (4) yields

$$\frac{d^2E}{df^2} = -\frac{[1+k\exp(-p\psi)]}{k} Q \frac{dE}{df} \tag{7}$$

where

$$Q = \frac{2k[\exp(-p\psi)][2k+\exp(p\psi)+\exp(-p\psi)]}{[2k+\exp(p\psi)+\exp(-p\psi)]^2} + \frac{[1+k\exp(-p\psi)][\exp(p\psi)-\exp(-p\psi)]}{[2k+\exp(p\psi)+\exp(-p\psi)]^2} \tag{8}$$

and Q may be conveniently rewritten as

$$Q = \frac{2k[\exp(-p\psi)][k+\cosh(p\psi)]+[1+k\exp(-p\psi)]\sinh(p\psi)}{2[k+\cosh(p\psi)]^2} \tag{9}$$

At the equivalence point

$$\left(\frac{d^2E}{df^2}\right)_{f=1} = -\frac{(1+k)}{k} Q^* \left(\frac{dE}{df}\right)_{f=1} \tag{10}$$

and from eqn. (9)

$$Q^* = k/(1+k) \tag{11}$$

so that

$$\left(\frac{d^2E}{df^2}\right)_{f=1} = -\left(\frac{dE}{df}\right)_{f=1} = -\frac{RT}{F} \cdot \frac{1+k}{2pk} \tag{12}$$

It is thus apparent that the second derivative is always negative at the equivalence point, and therefore that the equivalence point must always be located *subsequent* to the inflection point corresponding to the location of the point of maximum slope. This is in agreement with the earlier conclusions in the literature[1,2].

At the inflection points it is necessary that $d^2E/df^2 = 0$. Then, because $1+k\exp(-p\psi)$ and dE/df are always finite, positive, and never equal to zero, it is merely required that $Q = 0$. Equating the numerator of Q to zero, yields after some rearrangement

$$k = \frac{-[\tanh(p\psi_i)][\exp(p\psi_i)]}{2+\tanh(p\psi_i)} - \frac{2k^2/\cosh(p\psi_i)}{2+\tanh(p\psi_i)} \tag{13}$$

for the relationship existing between ψ_i—the value of ψ at the inflection point—and the corresponding value of k.

It is evident that for k to have physical significance ($k \geqslant 0$), the values of ψ_i that satisfy eqn.(13) must be negative. Thus, again it is verified that the inflection

point *precedes* the equivalence point. As $p\psi_i \to 0$, it is seen that eqn.(13) becomes: $k = -k^2$. The values of k that satisfy this equality are 0 and -1. The latter possesses no physical significance but the former corresponds to an infinitely large difference between the two formal potentials ($k = \exp(-0.5p)(F/RT)\Delta E^{\circ\prime}$). Therefore, it is to be expected that as the potential difference ($\Delta E^{\circ\prime}$) increases, the difference between the location of the equivalence point and that of the inflection point will decrease.

Equation(13) has been solved, using the method of successive approximations, to obtain values of $p\psi_i$ for various values of k, and the results are presented in Table 1. For each value of $p\psi_i$, the corresponding value of f_i was calculated from eqn. (3), and the slope, pS_i, was calculated from eqn.(5). For purposes of comparison, the value of the slope, pS^* at $f = 1$ is also given.

TABLE 1

THE LOCATIONS OF THE POINTS OF MAXIMUM SLOPE

$n_1 = n_2 = p$, 25°

$p\Delta E^{\circ\prime}$ (mV)	k	$-p(E_i - E^*)$ (mV)	f_i	pS_i	pS^*
50	0.378	—	no inflection	—	46.9
100	0.143	11.04	0.897	108.1	102.7
150	0.0539	3.08	0.9878	252.5	252.1
200	0.0204	1.10	0.9983	642.7	642.2
250	0.00775	0.403	0.9998	1670	1669.7
300	0.00291	0.150	0.99998	4425.2	4424.7

The first column lists values of $p\Delta E^{\circ\prime}$. The values in all succeeding columns have been calculated for 25°. The second column lists the values of k calculated from $k = \exp(-p\Delta E^{\circ\prime}F/2RT)$. In the third column are listed the values of $p(E_i - E^*)$, *viz.*, $(RT/F)p\psi_i$ obtained from the corresponding values of k by use of eqn.(13). E_i represents the potential at the point of maximum slope and E^*, the equivalence-point potential. The fourth column lists the values of f at this inflection point, calculated by use of eqn.(3), and the figures in the fifth and sixth columns were calculated by the use of eqns.(5) and (6), respectively. Some of the values in the sixth column differ from those previously presented[5] which were not directly calculated from the present eqn.(6) but rather evaluated (with no special caution exercised with respect to significant figures) from $(dE/df)_{f=1}$ expressed as a function of the equilibrium constant for eqn.(1). If $p = 2$, then for $\Delta E^{\circ\prime} = 50$ mV, the *second* entry in the first column must be used, and $E_i - E^*$ will be only -5.52 mV; f_i will occur at 0.897, but S_i will now be 54 as compared to $51.4 = S_i^*$.

It is evident from Table 1 that as the difference between the two formal potentials increases, the value of f_i approaches unity, so that with $p\Delta E^{\circ\prime} \geqslant 300$ mV, the point of maximum slope is indeed hardly distinguishable from the equivalence point, as has always been presumed. For any particular value of $p\Delta E^{\circ\prime}$, the magnitude of the slope at the inflection point, pS_i, is always greater than that at the equivalence point where the slope is pS^*, but as the value of $p\Delta E^{\circ\prime}$ increases, the difference between the values of the two slopes becomes increasingly negligible. For any particular value of $\Delta E^{\circ\prime}$, the differences between E_i and E^*, and between S_i and S^*,

decrease as the value of p increases. When $p\Delta E^{\circ\prime} = 50$ mV, no point of maximum slope exists.

Therefore, it is concluded that in titration curves for symmetrical redox reactions, the point of maximum slope can never coincide with the equivalence point but must always precede it. As the difference between the two formal potentials becomes increasingly positive, the difference between the locations of the two points becomes less, so that for any practical titration (where the formal potential difference is sufficiently positive) the difference between the locations of the equivalence point and the point of maximum slope will be too small to be experimentally observed.

Investigation of the properties of eqn.(13) shows that for a particular value of k there are actually two values of $p\psi_i$ which are physically meaningful mathematical solutions. The values of $p(E_i - E^*)$ in Table 1 correspond to values of $p\psi_i$ such that $|p\psi_i| < 1$ so that $p\psi_i \to 0$ as $k \to 0$. However, as $p\psi_i \to -\infty$, it is found that $\exp(p\psi_i) \to k$ so that in eqn.(13): $k \to -(-1)k/(2-1) - 2k^2/(\infty)(2-1) = k$. In other words, values of $p\psi_i < -1$ are also physically meaningful mathematical solutions of eqn.(13). Whenever $|p\psi_i| > 1$, the inflection point corresponds to the point of *minimum* slope, whereas whenever $|p\psi_i| < 1$, the inflection point corresponds to the point of *maximum* slope.

TABLE 2

THE LOCATIONS OF THE POINTS OF MINIMUM SLOPE

$n_1 = n_2 = p$, 25°

$p\Delta E^{\circ\prime}$ (mV)	k	$-p(E_i - E^*)$ (mV)	f_i	pS_i	pS at $f = \frac{1}{2}$	$-p(E - E^*)$ at $f = \frac{1}{2}$
50	0.378	—	no inflection	—	78.4	30.4
100	0.143	44.68	0.593	96.1	97.1	50.97
150	0.0539	74.47	0.507	101.4	101.8	75.14
200	0.0204	99.90	0.5008	102.57	102.59	100.02
250	0.00775	124.8	0.50008	102.678	102.70	125.01
300	0.00291	149.95	0.50003	102.680	102.706	150.005

At the point of minimum slope, values of f_i, and S_i may be calculated by use of eqns.(3) and (5), respectively. For purposes of comparison, the values of the slope at $f = \frac{1}{2}$ are also presented in Table 2 along with the corresponding values of $p(E - E^*)$ calculated from the previously[5] presented values of $p(E - E_2^{\circ\prime})$ at $f = \frac{1}{2}$. At $f = \frac{1}{2}$, $p\psi = -\frac{1}{2}p\delta + p(E - E_2^{\circ\prime})(F/RT)$, and the values of $p\psi$ so calculated were substituted into eqn.(5) to obtain the values of the slope at these points on the curve.

It is evident from Table 2 that the location of the point of minimum slope on the titration curve is *always subsequent* to the point at which $f = \frac{1}{2}$, although as $p\Delta E^{\circ\prime}$ increases, the location of this inflection point (corresponding to the minimum slope) approaches $f = \frac{1}{2}$ so that for $\Delta E^{\circ\prime} \geqslant 300$ mV the differences in location are negligible because even at $\Delta E^{\circ\prime} = 200$ mV, the difference is considerably less than the experimental error in locating these points. The magnitude of the slope at $f = \frac{1}{2}$ is always larger than it is at the value of f_i, although the difference becomes negligible for $\Delta E^{\circ\prime} \geqslant 200$ mV. When $p\Delta E^{\circ\prime} = 50$ mV, no point of minimum slope exists. As

may be recalled, for this value of $p\Delta E^{\circ\prime}$, there is no point of maximum slope. The first column of Table 2 lists values of $p\Delta E^{\circ\prime}$; the values in all succeeding columns have been calculated at 25°. Column 2 lists the corresponding values of k, and in the third column are listed the values of $p(E_i - E^*)$ corresponding to the point of minimum slope and calculated from eqn.(13). The fourth column lists the values of f_i, obtained *via* eqn.(3), at the inflection point where the slope has its minimum value which is listed in the fifth column and is calculated from eqn.(5). The sixth and seventh columns, respectively, list the value of pS at $f = \frac{1}{2}$, and the value of $p(E - E^*)$ at $f = \frac{1}{2}$. If $p = 2$, then for $\Delta E^{\circ\prime} = 50$ mV, the second entry in the first column must be used, and $E_i - E^*$ will be only -22.34 mV, f_i will occur at 0.593, and pS_i will be equal to 48.

TABLE 3

CHARACTERISTICS OF TITRATION CURVES OF SYMMETRICAL REDOX REACTIONS

$n_1 = n_2 = p$, 25°

$p\Delta E^{\circ\prime}$ (mV)		$E = E_2^{\circ\prime}$	Min. slope	Max. slope	Equivalence point
50					
f	$\frac{1}{2}$	0.572	no inflection points		1
$-p(E-E^*)$	30.4	25.00			0
pS	78.4	71.9			46.9
100					
f	$\frac{1}{2}$	0.5102	0.593	0.897	1
$-p(E-E^*)$	50.97	50.00	44.68	11.04	0
pS	97.1	96.8	96.07	108.1	102.7
150					
f	$\frac{1}{2}$	0.5015	0.507	0.9878	1
$-p(E-E^*)$	75.14	75.00	74.47	3.08	0
pS	101.84	101.82	101.4	252.5	252.1
200					
f	$\frac{1}{2}$	0.5002	0.5008	0.9983	1
$-p(E-E^*)$	100.02	100.00	99.90	1.104	0
pS	102.589	102.597	102.57	642.7	642.2
250					
f	$\frac{1}{2}$	0.50003	0.50008	0.9998	1
$-p(E-E^*)$	125.01	125.00	124.8	0.403	0
pS	102.70	102.689	102.678	1670.0	1669.7
300					
f	$\frac{1}{2}$	0.500004	0.50003	0.99998	1
$-p(E-E^*)$	150.005	150.00	149.95	0.150	0
pS	102.706	102.694	102.68	4425.2	4424.7

For each value of $p\Delta E^{\circ\prime}$, successive values of f are given, reading from left to right. Underneath each value of f is listed the corresponding value of $p(E - E^*)$ and below that the value of pS at that location.

There is yet another point of interest on these redox titration curves: the point at which $E = E_2^{\circ\prime}$, *viz.*, the potential is equal to the formal potential of the species *being* titrated. The values of f at this point have already been presented[3]. It may be easily verified that $\psi = -\frac{1}{2}\delta$ at $E = E_2^{\circ\prime}$ so that by use of eqn.(5), the values of the slope at this location on the curve may be readily calculated. In Table 3 is presented a comparison of these values with the values previously listed in Tables 1 and 2.

It is apparent from a consideration of Table 3 that a number of general statements may be made about titration curves for symmetrical redox reactions. At $f = \frac{1}{2}$, $p(E - E^*)$ is never exactly equal to $p\Delta E^{\circ\prime}/2$, or as previously[5] stated, at 50% titrated the value of E is *always less* than $E_2^{\circ\prime}$. The disparity decreases as the value of $p\Delta E^{\circ\prime}$ increases. At $f = \frac{1}{2}$, the slope increases with increasing values of $p\Delta E^{\circ\prime}$, and approaches a limiting value of 102.71; this value indicates that there is only a 23% increase in the magnitude of the slope accompanying a 500% increase in the value for $p\Delta E^{\circ\prime}$. In contrast, the equivalence-point slope (at $p\Delta E^{\circ\prime} = 300$ mV) is about one hundred times as large as it is at $p\Delta E^{\circ\prime} = 50$ mV, and the magnitude of the slope at this point does not approach a limiting value as $p\Delta E^{\circ\prime}$ increases.

The value of f at which $E = E_2^{\circ\prime}$ is never equal to $\frac{1}{2}$ but *always occurs subsequent* to it[3], the disparity decreasing as $p\Delta E^{\circ\prime}$ increases. The magnitude of the slope at $E = E_2^{\circ\prime}$ is *always less* than it is at $f = \frac{1}{2}$, but becomes less so as $p\Delta E^{\circ\prime}$ increases.

The general nature of a redox titration curve is readily discernible from Table 3. When $p\Delta E^{\circ\prime} = 50$ mV, there are no inflection points and hence no locations on the curve at which the slope is either a maximum or a minimum so that as the titration proceeds (increasing values of f) the slope continuously descreases throughout the entire titration. However, when $p\Delta E^{\circ\prime} = 100$ mV (or greater), the slope decreases to a *minimum* which always *occurs subsequent* to $f = \frac{1}{2}$, and then rises to a *maximum* which is located *prior* to the equivalence point. The minimum *always precedes* the maximum, whereas the minimum *always occurs subsequent* to the point at which $E = E_2^{\circ\prime}$, which in turn is always located subsequent to the point at which $f = \frac{1}{2}$. It is apparent from Table 3 that when $p\Delta E^{\circ\prime} \geqslant 300$ mV, the differences are negligible (and considerably less than experimental error) between the values predicted from the rigorous equations and those predicted from the customary and simpler equations.

It is evident that there must be some minimum value of $p\Delta E^{\circ\prime}$ in order that the titration has at least one inflection point. This minimum value of $p\Delta E^{\circ\prime}$ is 85.6 mV and corresponds to a value of k equal to 0.1888. For $k < 0.1888$, *i.e.*, $p\Delta E^{\circ\prime} > 85.6$ mV, the redox titration curve possesses two inflection points; the one corresponding to the minimum slope being located prior to the one corresponding to the maximum slope. When $k = 0.1888$, *only one* inflection point exists, that at $f = 0.707$ where $p(E_i - E^*) = -25.68$ mV (at $k = 0.1888$, there exists only one value of $p\psi_i$ that satisfies eqn.(13), *viz.*, $p\psi_i = -1$). For values of k such that $k > 0.1888$ (*i.e.*, $p\Delta E^{\circ\prime} < 85.6$ mV), the titration curve has no inflection points. NIGHTINGALE concluded from a mathematical treatment of the poising capacity[6] that in the titration of a solution initially containing two redox couples, the second end-point (corresponding to a minimum in the poising capacity, *i.e.*, where the slope of the titration curve has its maximum value) would not be observed if the difference between the formal potentials of the titrant redox couple and that of the couple initially present (containing the less readily oxidized species) was less than 85.6 mV.

It is instructive to compare the titration curves where $p\Delta E^{\circ\prime} = 85.6$ and 86.0 mV, respectively. From Table 4 it is apparent that even when $p\Delta E^{\circ\prime}$ is only 0.4 mV greater than the minimum value (necessary for the existence of an inflection point) of 85.6 mV, there is a considerable difference between the locations of the points of minimum and maximum slope although the magnitudes of these two slopes differ by only 0.1. It is seen that the redox titration curve even at this small value of $p\Delta E^{\circ\prime}$ (=86.0 mV) possesses the same general nature that is observed for much greater

TABLE 4

COMPARISON OF TITRATION CURVES FOR TWO SLIGHTLY DIFFERENT VALUES OF k AT 25°

		$E = E_2^{\circ\prime}$	*Inflection points*		*Equivalence point*
$p\Delta E^{\circ\prime} = 85.6$ mV; $k = 0.1888$					
f	$\frac{1}{2}$	0.5178	0.707		1
$-p(E-E^*)$	44.4	42.8	25.68		0
pS	93.6	92.8	90.0		80.85
			Min. slope	*Max. slope*	
$p\Delta E^{\circ\prime} = 86.0$ mV; $k = 0.187$					
f	$\frac{1}{2}$	0.5181	0.677	0.751	1
$-p(E-E^*)$	44.8	43.0	28.5	21.9	0
pS	93.9	92.9	90.2	90.3	81.5

TABLE 5

THE REDOX TITRATION CURVE FOR $p\Delta E^{\circ\prime} = 85.6$ mV AT 25°

f	$-p(E-E^*)$	$-p\psi$	pS	f	$-p(E-E^*)$	$-p\psi$	pS
0.500	44.4	1.729	93.6	0.712	25.2	0.980	89.9
0.509	43.7	1.700	93.2	0.721	24.4	0.950	89.9
0.5178	42.8	1.667	92.8	0.735	23.1	0.900	89.9
0.536	41.1	1.600	92.1	0.767	20.2	0.790	89.9
0.564	38.5	1.500	91.2	0.770	20.0	0.780	89.8
0.593	36.0	1.400	90.7	0.821	15.4	0.600	89.4
0.621	33.4	1.300	90.2	0.908	7.71	0.300	86.8
0.650	32.1	1.200	90.0	0.938	5.14	0.200	85.2
0.672	28.8	1.12	89.9	0.969	2.57	0.100	83.2
0.678	28.3	1.100	89.9	1	0	0	80.8
0.692	27.0	1.050	89.9	1.032	—2.57	—0.1	78.1
0.707	25.68	1.000	89.9	1.065	—5.14	—0.2	75.0

values of $p\Delta E^{\circ\prime}$, *viz.*, the slope of the titration curve decreases, as the value of f increases, until the point of minimum slope is reached—which occurs subsequent to the point at which $E = E_2^{\circ\prime}$ which, in turn, is subsequent to the point at which $f = \frac{1}{2}$. Thereafter, with progressively increasing values of f, the slope rises to a maximum occurring at a location prior to the equivalence point. From then on, the slope continually decreases.

It is only at one particular value of k that the slope exhibits neither a minimum nor a maximum value. Rather, the slope decreases as the titration proceeds until a

region is reached where the slope remains virtually constant as f progressively increases (see Table 5). Beyond this region, the slope then resumes its continually decreasing nature as the value of f increases. The existence of this region of constant slope may be considered to arise in the following manner. As the value of $p\Delta E^{\circ\prime}$ decreases (see Tables 3 and 4), the location of the point of minimum slope moves towards larger values of f whereas the point of maximum slope moves towards smaller values of f. Simultaneously, the magnitude of the minimum slope is decreasing somewhat and the magnitude of the maximum slope is greatly decreasing (as the value of $p\Delta E^{\circ\prime}$ decreases). Thus, at the critical value of $p\Delta E^{\circ\prime} = 85.6$ mV, the magnitudes of the two slopes have become essentially equal and their locations have merged into a single point of inflection located at $f = 0.707$. In the region of constant slope, the titration curve exhibits a linear (instead of a logarithmic) dependence of E upon f.

The behavior of titration curves for symmetrical redox reactions may be compared with the conclusions previously presented for other types of titration curves. All these titration curves, in general, may have two inflection points and whether or not they do, is dependent upon the quantitative relationships existing between the initial concentrations, the dilution occurring during the titration, and the magnitude of the equilibrium constant appropriate to the reaction under consideration.

For example, when a monobasic strong acid is titrated with a monoacidic strong base there are three apparently different types of titration curves possible: (a) no inflection points exist; (b) only the inflection point corresponding to the maximum slope exists, or(c) two inflection points exist. Under the usual conditions of titration, although both inflection points do exist on the titration curve, the one corresponding to the point of minimum slope is located virtually at $f = 0$, and therefore only the inflection point corresponding to the maximum slope exists at a non-zero value of f, which is virtually unity for solutions the concentration of which exceeds 10^{-4} F. As the initial concentration of the acid is decreased, the location of the point of minimum slope moves away from zero towards larger values of f—but never exceeds $f = \frac{1}{2}$ provided that the concentration of the base is not greater than that of the acid initially—and the location of the point of maximum slope moves towards smaller values of f. As we continue to decrease the initial concentration of acid, a concentration value is reached where the point of minimum slope *ceases* to exist although the point of maximum slope, located at a value of f considerably less than unity, still exists. When the initial acid concentration is allowed to decrease even further, the location of the maximum slope moves toward even smaller values of f until finally it too ceases to exist, and then throughout the titration, the slope of the curve decreases continuously from its initial value at $f = 0$. Thus, it is apparent that there is a similarity between these acid–base titration curves and the titration curves for symmetrical redox reactions in the existence of three different types of conditions which provide three apparently different types of curves. Furthermore, when the primary independent variable (the initial acid concentration in the acid–base titration; $p\Delta E^{\circ\prime}$ in the redox titration) has a value which is less than some minimal one, no inflection points exist.

In the titration of a monobasic weak acid of initial concentration C, with a monoacidic strong base[8] of concentration C, the value of f, at which $[H^+] = K_a$, is

equal to $\frac{1}{2}$ only when $pK_a = \frac{1}{2}\,pK_W$; the values of f are less than $\frac{1}{2}$ when $pK_a < \frac{1}{2}\,pK_W$, and greater than $\frac{1}{2}$ when $pK_a > \frac{1}{2}\,pK_W$. In contradistinction, for a symmetrical redox reaction, at $E = E_2{}^{\circ\prime}$, the value of f *always* exceeds $\frac{1}{2}$. Perhaps this difference in behavior may be attributed to the fact that there is not a point on the redox titration curve (in the region: $0 \leqslant f \leqslant 2$) where the value of K, and only K, directly determines the potential, *viz.*, $E - E^* = (RT/F) \ln K = p\Delta E^{\circ\prime}$. The variation of the location of the inflection point corresponding to the minimum slope on these acid–base titration curves, is similar to the behavior of values of f at which $[H^+] = K_a$, because it may occur at values of f greater or less than $\frac{1}{2}$. When $pK_a < \frac{1}{2}\,pK_W$, the point of minimum slope (when it exists) always occurs prior to the point at which $[H^+] = K_a$, which in turn precedes the "half-way point" (where $f = \frac{1}{2}$); whereas for $pK_a > \frac{1}{2}\,pK_W$, the point of minimum slope (when it exists) always follows the point at which $[H^+] = K_a$, which latter always occurs after the half-way point. The inflection point corresponding to the minimum slope always occurs before the inflection point corresponding to the maximum slope. In other words, the disparity between the location of the inflection point corresponding to the minimum slope and that of the half-way point is always greater than that between the point at which $[H^+] = K_a$ and the half-way point. However, in a symmetrical redox reaction, the location of the point of minimum slope always occurs after the point at which $E = E_2{}^{\circ\prime}$, which in turn always follows the half-way point, so that in a formal sense, this sequence resembles the acid–base titration where $pK_a > \frac{1}{2}\,pK_W$. Both for relatively large values of K_a, *e.g.*, $K_a \geqslant 0.1$, *and* for small values, *e.g.*, $K_a \leqslant 5 \cdot 10^{-12}$, the point of minimum slope ceases to exist, but it is *only* for the small values of K_a that the point of maximum slope may also cease to exist[9]. Essentially, this may be attributed to the fact that the location of the minimum slope may occur on either side of the half-way point, but the maximum slope can never occur before the half-way point, and indeed, ceases to exist before it ever reaches the half-way point. In contrast, for symmetrical redox reactions, the location of the minimum slope can only follow the half-way point. When neither a maximum nor a minimum slope exists ($K_a \leqslant 5 \cdot 10^{-12}$), the slope of the titration curve throughout the entire titration, continuously decreases from its initial value at $f = 0$, as it does in the redox titration where $p\Delta E^{\circ\prime} < 85.6$ mV.

SUMMARY

For titration curves of symmetrical ($n_1 = n_2 = p$) redox reactions, it has been demonstrated that there are always two inflection points whenever $p\Delta E^{\circ\prime} > 85.6$ mV at 25°; the location of the point of maximum slope is always prior to the equivalence point, whereas the point of minimum slope is always located subsequent to the half-way point. For practical titrations where $p\Delta E^{\circ\prime}$ is customarily greater than 300 mV, the differences between the locations of these points and the half-way point and the equivalence point, respectively, are considerably less than the experimental error incurred in the determination of their location. When $p\Delta E^{\circ\prime} = 85.6$ mV, the titration curve has neither a minimum nor a maximum slope but there is a region, in the vicinity of 71% titrated, wherein the slope remains constant as the titration progresses; whereas if $p\Delta E^{\circ\prime} < 85.6$ mV, no maximum nor minimum slope exists and throughout the titration the slope decreases continuously from its value at the start of the titration.

REFERENCES

1 I. M. KOLTHOFF AND N. H. FURMAN, *Potentiometric Titrations*, Wiley, New York, 1931, ch. III.
2 I. G. MURGULESCU AND C. DRAGULESCU, *Z. Physik. Chem.*, 185A (1940) 375.
3 J. A. GOLDMAN, *J. Electroanal. Chem.*, 11 (1966) 255.
4 E. BISHOP, *Anal. Chim. Acta*, 27 (1962) 253.
5 J. A. GOLDMAN, *J. Electroanal. Chem.*, 11 (1966) 416.
6 E. R. NIGHTINGALE, JR., *Anal. Chem.*, 30 (1958) 267.
7 L. MEITES AND J. A. GOLDMAN, *Anal. Chim. Acta*, 30 (1964) 200.
8 J. A. GOLDMAN AND L. MEITES, *Anal. Chim. Acta*, 30 (1964) 28.
9 L. MEITES AND J. A. GOLDMAN, *Anal. Chim. Acta*, 29 (1963) 472.

ELECTROANALYTICAL CHEMISTRY AND INTERFACIAL ELECTROCHEMISTRY
Elsevier Publishing Company, Amsterdam – Printed in The Netherlands

EVALUATION OF RIGHT-CYLINDER CONDUCTIVITY CELLS

RONALD A. SASSÉ, HERMANN J. DONNERT* AND RONALD I. BRANDLER
U.S. Army Nuclear Defense Laboratory, Edgewood Arsenal, Maryland 21010 (U.S.A.)
(Received October 28th, 1966)

INTRODUCTION

In certain types of research, measurements of electrolyte conductivity provide a convenient analytical tool. On occasions, practical application of conductimetric techniques requires that several virtually identical conductivity cells are available. In these instances, it is also desirable that such a set of reproducible conductivity cells should be easy to fabricate. Right-cylinder conductivity cells offer promise for meeting these requirements. To evaluate the feasibility of this approach, it was necessary to determine the effect of the geometric parameters on the cell constant; in particular, the variances induced by small errors in the positioning of the center electrode were assessed since this positioning is likely to be very critical.

Some relevant work was published by MUNSON[1] and KASPER[2]; their results are limited to the case of coaxial electrode arrangements. A related study of current-flow and potential distribution at any point between non-coaxial cylindrical electrodes was presented by KASPER[3]; however, his paper does not provide an easy means for obtaining a formula assessing the effects of electrode-axes displacement on the total resistance or cell constant, which is the object of the present investigation.

THEORY

The determination of the cell constant, K, for a right-cylinder conductivity cell can be reduced to solving a two-dimensional Dirichlet problem. The electrolyte is contained in a column of height h and volume V between two right-cylinder electrodes (Fig. 1A) with parallel axes displaced by the distance, δ; the contact surfaces, S' and S'', are circular cylinders with radii r' and r'', where $0 < r' \leq r' + \delta < r''$ is stipulated as the necessary limitation for the geometric configuration. Obviously, the geometry of this conductivity cell permits an essentially two-dimensional treatment of the problem.

The application of a constant electromotive force, E, between the electrodes causes a stationary electric current, I, to flow through the electrolyte; the resistance, R, is determined by Ohm's law, *i.e.*, $R = I^{-1}E$. For an electrolyte of concentration, c, and equivalent conductance, Λ, the electric conductivity, σ, is given by $\sigma = c\Lambda$. The cell constant K, defined as $K = c\Lambda R$, can then be expressed as

$$K = (\sigma^{-1} I)^{-1} E \qquad (1)$$

* New address: Department of Nuclear Engineering, Kansas State University, Manhattan, Kansas 66502, U.S.A.

For the volume-domain, V, filled by the electrolyte we can apply Ohm's law in the form[4]

$$\sigma^{-1} \boldsymbol{J} = -\nabla \Phi \tag{2}$$

where $\boldsymbol{J}$ is the electric-current density and Φ the electric potential. Boundary conditions are established by the requirement that the electrode surfaces must be at constant potential, say Φ' on S' and Φ'' on S'', so that $|\Phi'' - \Phi'| = E$. For the stationary-current problem at hand, the equation of continuity, given by[4] $\nabla \boldsymbol{J} = 0$, must hold; consequently, the Laplace equation

$$\nabla^2 \Phi = 0 \tag{3}$$

must be satisfied. Clearly, the stipulated conditions for Φ suffice to characterize a Dirichlet problem[5].

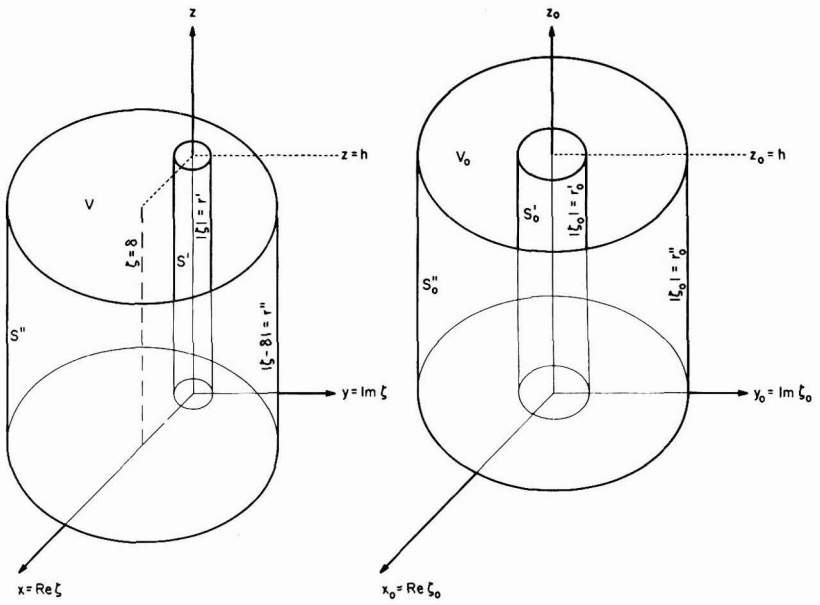

A B

Fig. 1. Geometric configuration of right-cylinder conductivity cells: (A), cell with displaced electrode axes; (B), cell with coincident electrode axes (denoted by zero subscripts). Dimensions in the figure are chosen so that both cells shown have equal cell constant.

The electric current, I, may be obtained from the current density, $\boldsymbol{J}$, by integration over any equipotential surface S within V as well as either S' or S''. Since $\nabla\Phi$ and, hence, $\boldsymbol{J}$ must be normal to S, the surface integration can be reduced to yield $\sigma^{-1} I = \iint_S |\nabla \Phi| \, \mathrm{d}^2 S$, where $\mathrm{d}^2 S$ denotes a surface element on S.

In the special case of coinciding electrode axes, *i.e.*, $\delta = 0$, (indicated, where necessary, by zero subscripts) the problem can be solved readily[6]. For this configuration (Fig. 1B), the potential Φ depends only on the radial distance r_0 from the axis of rotational symmetry. The equipotential surfaces S_0 are coaxial cylinders of height h with radii r_0 in the range $r_0' \leq r_0 \leq r_0''$; their areas are given by $\iint_{S_0} d^2 S_0 = 2\pi r_0 h$. In terms of cy-

lindrical coordinates, eqn. (3) becomes $\mathrm{d}/\mathrm{d}r_0[r_0(\mathrm{d}\Phi/\mathrm{d}r_0)]=0$; the solution $\Phi=\Phi'+\{(\Phi''-\Phi')[\ln(r_0/r_0')]/[\ln(r_0''/r_0')]\}$ satisfies the necessary boundary conditions. Differentiation of this expression yields $|\nabla_0\Phi|\equiv|\mathrm{d}\Phi/\mathrm{d}r_0|=Er_0^{-1}/[\ln(r_0''/r_0')]$; obviously, the value of $|\nabla_0\Phi|$ is a constant for any equipotential surface, S_0. The surface integration leads to $\sigma^{-1}I=2\pi hE/[\ln(r_0''/r_0')]$; substitution of this result into eqn. (1) renders the solution

$$K=(2\pi h)^{-1}\ln(r_0''/r_0') \tag{4}$$

In the general case of non-coinciding electrode axes, where $\delta\neq 0$, the relevant two-dimensional Dirichlet problem can be solved now by the conformal-mapping method[5]. To this end, we consider the coordinate plane normal to the electrode axes (Fig. 1A) as Gauss plane G for the complex variable ζ, so that the contact-surface contours are defined by the circles $|\zeta|-r'=0$ and $|\zeta-\delta|-r''=0$; similarly, we introduce the complex variable, ζ_0, for the coinciding-electrode configuration (Fig. 1B), so that the concentric circles $|\zeta_0|-r_0'=0$ and $|\zeta_0|-r_0''=0$ represent the contact-surface contours in a Gauss plane G_0. If we consider G_0 as the image plane, a conformal mapping of G on G_0 exists that induces suitable object-to-image correspondence of contact-surface contours. A simple calculation shows that an appropriate coordinate transformation is given by $\zeta_0=\lambda[(\zeta+u)/(\zeta+v)]$, where $u+v=+\delta^{-1}(r''^2-r'^2-\delta^2)$ and $u-v=-\delta^{-1}|\sqrt{(r''^2-r'^2-\delta^2)^2-(2r'\delta)^2}|$; λ is an arbitrary positive multiplier. With this transformation, the radii of the image circles in G_0 follow to be $r_0'=\lambda|\sqrt{u/v}|$ and $r_0''=\lambda|\sqrt{(u+\delta)/(v+\delta)}|$. Since it can be proven without great difficulty that $\iint_S|\nabla\Phi|\mathrm{d}^2S$ and, hence, K are invariants for the germane coordinate transformation, mere substitution of r_0' and r_0'' into eqn. (4) produces

$$K=(2\pi h)^{-1}\ln\{[(r''^2+r'^2-\delta^2)+|\sqrt{(r''^2+r'^2-\delta^2)^2-(2r''r')^2}|]/(2r''r')\}$$
$$=(2\pi h)^{-1}|\mathrm{Arcosh}[(r''^2+r'^2-\delta^2)/(2r''r')]| \tag{5}$$

as the desired expression for the cell constant. Application of this result for the special case of coinciding electrode axes, attained by setting $\delta=0$, reduces eqn. (5) to yield the cell constant

$$K_0=(2\pi h)^{-1}|\mathrm{Arcosh}[(r''^2+r'^2)/(2r''r')]|=(2\pi h)^{-1}\ln(r''/r') \tag{6}$$

which is in formal agreement with eqn. (4).

In the subsequent evaluation of changes in cell constant induced by variation of the electrode-axes displacement, the cell-constant ratio, $k=K/K_0$, is the quantity of principal interest. The form of eqns. (5) and (6) clearly suggests that K/K_0 is a function of two parameters, which define the proportion $r'':r':\delta$. The electrode-radii ratio, $\alpha=r'/r''$, appears to be a rather obvious choice for one parameter; the displacement fraction, $\xi=\delta/(r''-r')$, which represents a measure of the electrode-axes displacement, is introduced as the other variable. By use of eqns. (5) and (6) the explicit functional relationship

$$k=k(\xi,\alpha)\equiv\frac{|\mathrm{Arcosh}\{1+[(1-\alpha)^2/(2\alpha)](1-\xi^2)\}|}{|\mathrm{Arcosh}\{1+[(1-\alpha)^2/(2\alpha)]\}|} \tag{7}$$

is readily established; the previously stipulated condition $0<r'\leq r'+\delta<r''$ implies that the function $k(\xi,\alpha)$, defined by eqn. (7), shall be considered as physically meaningful for $0\leq\xi<1$ and $0<\alpha<1$.

A graphic presentation (Fig. 2) of the function $k(\xi,\alpha)$ illustrates several significant properties that can be deduced analytically from eqn. (7). A family of curves shows the relationship between k and ξ for selected values of α, the family parameter. This family of curves covers a region bounded by the functional limits (indicated in Fig. 2 by heavy lines) of eqn. (7) with respect to the family parameter, *i.e.*, $\lim_{\alpha\to 0+} k(\xi,\alpha) = 1$ and $\lim_{\alpha\to 1-} k(\xi,\alpha) = |\sqrt{1-\xi^2}|$. It is obvious that $k(\xi,\alpha)$ has a maximum at $\xi = 0$ given

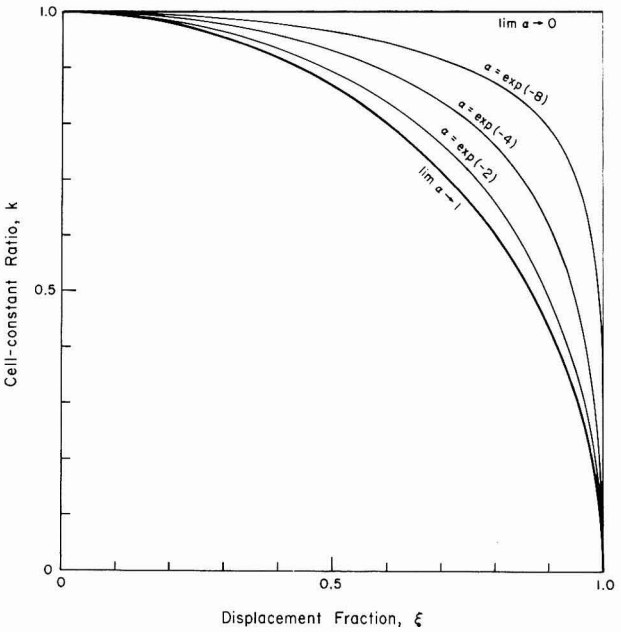

Fig. 2. Cell-constant ratio, k, as function of the displacement fraction, ξ, and the electrode-radii ratio, α.

by $k(0,\alpha) = 1$ and is monotone decreasing with increasing ξ in $0 < \xi < 1$ for any fixed value of α in $0 < \alpha < 1$; it can, furthermore, be seen that $|\sqrt{1-\xi^2}| < k = k(\xi,\alpha) < 1$ for any given value of ξ in $0 < \xi < 1$ and $0 < \alpha < 1$. From this, a general correlation between a maximum permissible error in electrode-axes alignment and the bounds impressed on the variation in cell-constant ratio can be inferred. If a particular displacement-fraction tolerance, $\hat{\xi}$, is stipulated, so that $0 \leq \xi < \hat{\xi} < 1$, then $\hat{k} = |\sqrt{1-\hat{\xi}^2}|$ represents the lower bound for the variation in cell-constant ratio, that is, $\hat{k} < k \leq 1$, which holds independent of the value of α, the electrode-radii ratio.

EXPERIMENTAL

An experiment was performed to demonstrate that eqn. (5) accurately describes the cell constant for right-cylinder configurations and to assess the experimental errors associated with various inner-electrode displacements. Inner electrodes of different radii were moved across the diameter of an outer electrode of fixed radius and the resistance was measured as a function of electrode-axes displacement. Based

on the known concentration and equivalent conductance of the electrolyte in the cell, experimental values for the cell constant were obtained from the measured resistance data and compared with theoretical values calculated from eqn. (5).

Apparatus and reagents

A Jones Bridge (Leeds and Northrup) and decade capacitors up to 0.1 μF (General Radio) were used to measure the resistance. Auxiliary equipment included an amplifier and null detector (General Radio, type 1231-B) with filter (type 1231-P5) and an audio oscillator (Hewlett-Packard, model 201).

The body of the conductivity cell (Fig. 3) was fabricated from a $\frac{1}{2}$-in. chrome-plated pipe nipple, 6.0 cm long with 15.90 mm inside diameter. The cell temperature was maintained by a constant-temperature bath (Haake, model F). The cell body was fixed on a movable microscope table (Bausch and Lomb) equipped with vernier calipers.

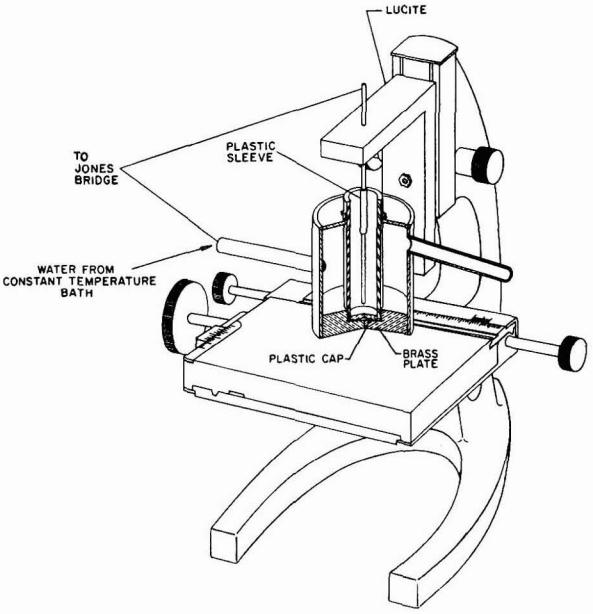

Fig. 3. Conductivity cell positioned on microscope table.

Stainless-steel plungers, 9.5 cm long, from Hamilton syringes were used as inner electrodes. These had radii of 0.362_5, 0.729_0, and 1.152_5 mm and were immersed in the electrolyte to depths of 4.42_0, 4.38_9, and 4.32_1 cm, respectively. The outer electrode had a fixed radius of 7.95 mm.

A solution of KCl, $1.46_6 \times 10^{-3}$ M, prepared with conductivity water ($7 \cdot 10^6$ Ω cm) was used as electrolyte.

PROCEDURE

The cell and glassware were washed with a 40-ml min^{-1} stream of conductivity water for 4 h before use. After cleaning, the cell was filled with KCl solution. The

electrodes were insulated with 2 cm of heat-shrinkable polyvinyl tubing such that 4 cm of exposed length was in contact with the electrolyte. The insulation was provided so that the effective length of the electrode, as it traversed the cell, would not be affected by the increasing solution height formed by the meniscus. This construction also facilitated measuring the effective electrode height which was not independent of the immersion depth. The electrodes were centered in the solution by adjusting the microscope table (which moved the outer cylinder) until the maximum resistance was obtained; this adjustment positioned the electrode within 0.2 mm of the center

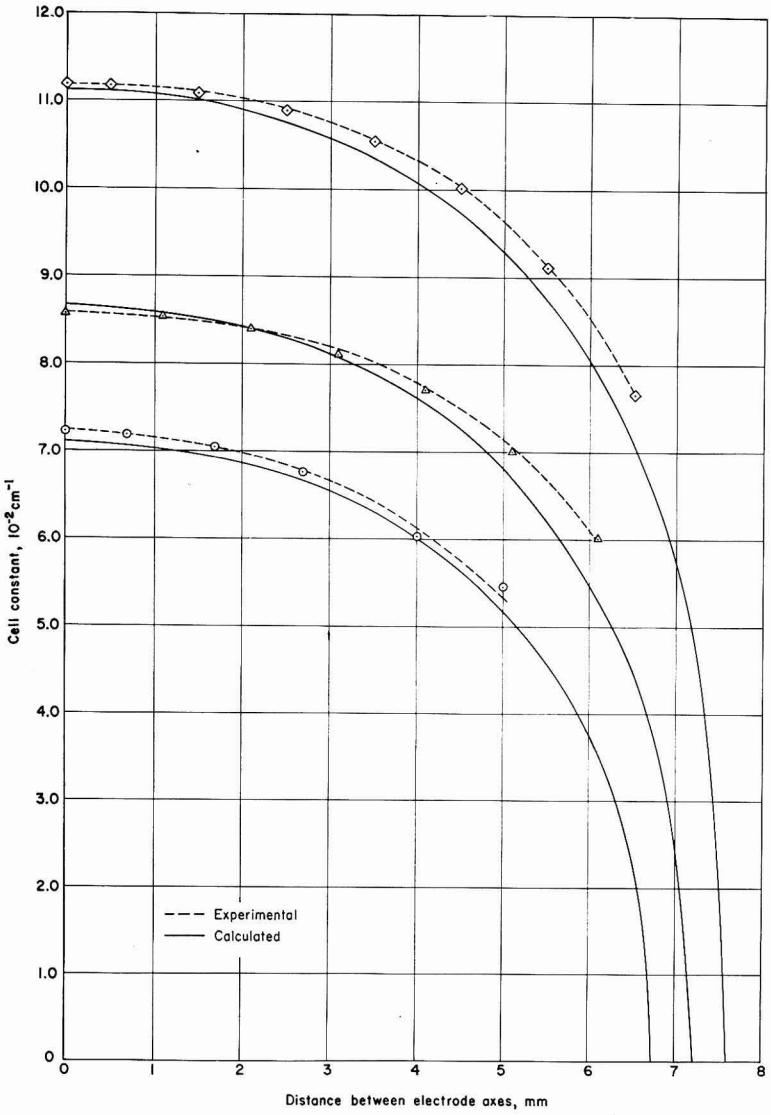

Fig. 4. Comparison of exptl. and calc. cell constants, $r'' = 7.95$ mm. (⊙), $r' = 0.3625$ mm and $h = 4.420$ cm; (△), $r' = 0.7290$ mm and $h = 4.389$ cm; (◈), $r' = 1.1525$ mm and $h = 4.321$ cm.

of the cell. The experiment was conducted by moving the outer electrode cylinder and measuring the resistance at various distances until the electrodes touched. The Bridge was operated at 10.0 V and 1 kHz while the cell was maintained at 25.00° ± 0.02°.

RESULTS AND DISCUSSION

The experimental results and the corresponding theoretical cell-constant values are shown in Fig. 4 and Table 1; in addition, Table 1 contains the per-cent differences between experimentally-determined and calculated cell constants. These differences are small enough to be judged as compounded experimental error, which can be accounted for by possible small uncertainties in electrolyte conductivity (due to the presence of dissolved gases such as CO_2), measured height of the electrolyte column, parallel alignment of the electrode axes, and positioning of the inner electrode. As may be seen from Table 1, the bulk of the experimental data is in very good agreement with the cell-constant values calculated from eqn. (5). In particular, differences

TABLE 1

CELL CONSTANT

Distance[a] *(mm)*	*Resistance*[b] *(Ω)*	$K_{exptl.}$ *(10⁻² cm⁻¹)*	$K_{calc.}$ *(10⁻² cm⁻¹)*	$\frac{K_{exptl.}-K_{calc.}}{K_{calc.}}$ *(%)*
$r' = 0.3625$ mm, $h = 4.420$ cm				
0.0	519.7	11.199	11.119	0.71
0.5	519.2	11.188	11.105	0.74
1.5	514.6	11.089	10.988	0.91
2.5	504.7	10.876	10.743	1.23
3.5	489.3	10.544	10.341	1.96
4.5	464.4	10.007	9.723	2.92
5.5	423.2	9.119	8.760	4.09
6.5	355.1	7.652	7.097	7.82
$r' = 0.7290$ mm, $h = 4.389$ cm				
0.0	397.9	8.574	8.664	−1.03
1.1	396.2	8.538	8.593	−0.64
2.1	389.8	8.400	8.400	0.00
3.1	376.7	8.117	8.060	0.70
4.1	357.6	7.706	7.527	2.37
5.1	324.9	7.001	6.704	4.43
6.1	279.4	6.021	5.329	12.98
$r' = 1.1525$ mm, $h = 4.321$ cm				
0.0	335.3	7.225	7.113	1.57
0.7	333.8	7.193	7.084	1.53
1.7	327.5	7.057	6.937	1.72
2.7	313.8	6.762	6.650	1.68
3.7	290.7	6.264	6.186	1.26
4.0	279.4	6.021	6.001	0.33
5.0	253.8	5.469	5.169	5.80

[a] Axial displacement distance of inner electrode from the center of right-cylinder cell with radius $r'' = 7.95$ mm.

[b] Resistance measured at 25° with KCl soln., $c = 1.466 \times 10^{-3}$ M and $\Lambda = 147$ cm² equiv.⁻¹ Ω^{-1}.

between experimental and theoretical results are extremely small for even moderate electrode-axes displacements (up to about 4 mm) substantially exceeding the range of practical interest. For larger displacements, discrepancies become more pronounced due to the drastically enhanced sensitivity of the theoretical cell-constant formula (eqn. (5) and Fig. 2) to minute errors in electrode positioning. In summary, it has been demonstrated that eqn. (5) provides cell-constant values for right-cylinder electrode configurations with adequate accuracy.

The right-cylinder cell design offers a number of advantages over the conventional parallel-plate type electrode arrangement. For instance, if the inner electrode were dislocated from the center of a cell (*i.e.*, deviating from the coaxial electrode configuration) as much as 30% of the electrode-radii difference (displacement fraction $\hat{\xi} \leq 0.3$), the theoretical limit of the cell-constant decrease from the maximum value would be only 5% (cell-constant ratio $\hat{k} \geq 0.95$ as obtained from Fig. 2); in the case of practically realistic electrode-radii ratios (α in the range from about 0.04 to 0.15) chosen for the experiment, this decrease (see Fig. 4) would amount to no more than about 2% (cell-constant ratio $K/K_0 \geq 0.98$). Thus, it would be a simple matter to fabricate reliably many cells having very similar cell constants. Furthermore, this cell design is inherently sturdy, a fact that could be exploited for on-stream measurements or even for simple dip-type conductivity cells. The right-cylinder type of conductivity cell would lend itself also to kinetic measurements in electrolyte-flow systems, since this design would not create any hold-up volume to produce turbulence and spoil an otherwise laminar flow.

SUMMARY

A theoretical equation, deduced from known physical principles, is presented for the cell constant of a right-cylinder conductivity cell as a function of the electrode radii and the electrode-axes displacement. Experimental data are compared with theoretical results and found in good agreement. In particular, the effects of changes in electrode-axes displacement are discussed. It is shown that small deviations from the coaxial electrode arrangement do not induce significant variations in cell constant.

REFERENCES

1 R. MUNSON, *Conductance of Electrolyte Solutions Studied with Concentric Cylindrical Electrodes*, Doctoral Dissertation, Northwestern University, 1959.
2 C. KASPER, *Trans. Am. Electrochem. Soc.*, 77 (1940) 353.
3 C. KASPER, *Trans. Am. Electrochem. Soc.*, 78 (1940) 147.
4 See for example: W. H. K. PANOFSKY AND M. PHILLIPS, *Classical Electricity and Magnetism*, Addison-Wesley Publishing Company, Inc., Reading, Mass., 1955.
5 See for example: W. KAPLAN, *Advanced Calculus*, Addison-Wesley Publishing Company, Inc., Reading, Mass., 1952.
6 See for example: F. SAUTER, *Differentialgleichungen der Physik*, Walter de Gruyter and Co., Berlin, 1950.

ELECTROANALYTICAL CHEMISTRY AND INTERFACIAL ELECTROCHEMISTRY
Elsevier Publishing Company, Amsterdam – Printed in The Netherlands

OPEN CIRCUIT ELECTRICAL DETECTION METHOD FOR TRANSPORT NUMBER MEASUREMENTS IN DILUTE SOLUTIONS BY THE MOVING BOUNDARY TECHNIQUE

EDUARDO PASSERON* AND ERNESTO GONZALEZ†
Electrochemical Laboratory, Facultad de Ciencias Exactas y Naturales, Universidad de Buenos Aires (Argentina)
(Received November 8th, 1966)

Since the experimental comparison of optical and conductometric techniques of boundary detection by LORIMER, GRAHAM AND GORDON[1], the greater sensitivity of the latter technique has prompted the development of other methods[2] based on the difference in the electrical properties of the solutions forming the boundary. In this paper a new electrometric technique is described which is believed to have some distinct advantages.

EXPERIMENTAL

Two electrodes of thin platinum foil are placed perpendicularly to the axis of the channel at about 0.3 mm from one another. They are connected externally through a 1 μF mica condenser and a current-sensitive device. The purpose of the condenser is to eliminate the possibility of electrolysis at the probe electrodes. When current is passing through the channel, the probe electrodes are subjected to a constant potential difference as long as they face only one kind of solution. When the boundary reaches the electrodes, this potential difference changes from the value characteristic of the leading solution to that in the following solution. The resulting readjustment of electrical charges on the plates of the condenser gives rise to a current peak which can be detected by a sensitive galvanometer or a registering microammeter in series with the probe electrode circuit.

The time elapsed between signals of such electrode pairs, conveniently placed along the channel, allows the transport number to be measured if the volume of solution contained between pairs is known from previous calibration[3].

Channel construction was as follows. Slits were carefully cut through the wall of a standard 4-mm Pyrex glass tube, as shown in Fig. 1. The tube was then annealed. Thin platinum foil was cut in rectangular pieces of approximately $0.1 \times 2 \times 10$ mm. These were folded at a right angle about 3 mm from one end and fixed in position through the slit with epoxy resin cement. When the cement had set, the ends of the

* Present address: Pueyrredón 1445, Buenos Aires (Argentina).
† Present address: Department of Physical Chemistry, School of Chemistry, The University, Bristol 8.

foils protruding inside the tube were ground down to the wall with a cylindrical file. The internal diameter of the channel at the electrode site was thus unaffected. Polypropylene tube channels were also constructed. These have the advantage of being less fragile than their glass equivalents. Shielded wire leads, passing through rubber tubing, were then soldered to the free foil ends. The rubber tubing was finally sealed to the glass wall with epoxy resin cement.

Self-generation of the boundary[4] with cadmium and silver anodes was used. Copper was also employed in the preliminary experiments. Silver–silver chloride or platinum electrodes were used as cathodes. The finished apparatus is shown in Fig. 2. Water held at $25° \pm 0.1°$ was circulated through the glass jacket. The wiring diagram

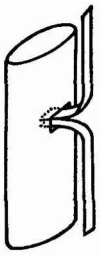

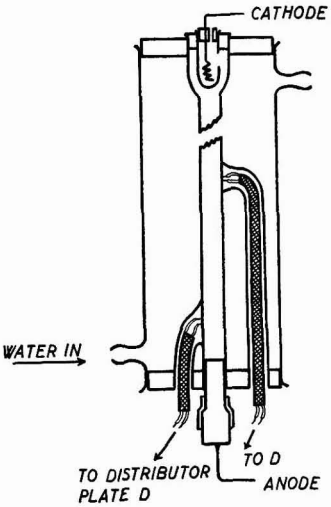

Fig. 1. Channel construction. Platinum-foil electrodes are fitted into the slit in the glass wall.

Fig. 2. Finished apparatus showing two pairs of probe electrodes connected to shielded wire leads fitted into rubber tubings.

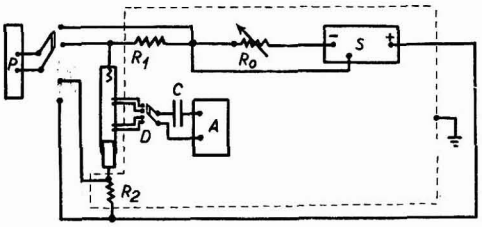

Fig. 3. Schematic wiring diagram.

is given in Fig. 3. The whole circuit was carefully shielded. A distributor plate, (D), was used to switch from one electrode pair to the next after the boundary had passed. A registering microammeter, (A), Kipp Micrograph BD-2, on the 0.1 μA scale, was used to time the boundary. Alternatively, in a preliminary run, a chronometer and a Tinsley galvanometer of 10 Ω internal resistance and a period of 2 sec were used for

the same purpose. The error in the estimation of the time interval between signals from two pairs of electrodes was about 1 sec for sharp signals such as those shown in Fig. 4. For flatter signals, corresponding to lower boundary velocities, the indetermination was greater, but as the time interval was longer the relative error in the timing

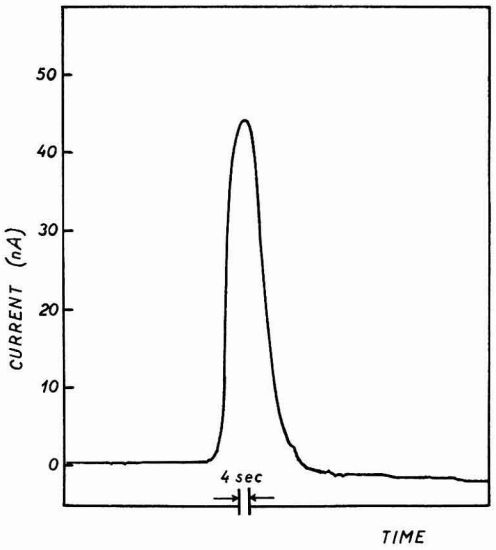

Fig. 4. Trace obtained with a registering microammeter as the boundary passes a probe electrode pair.

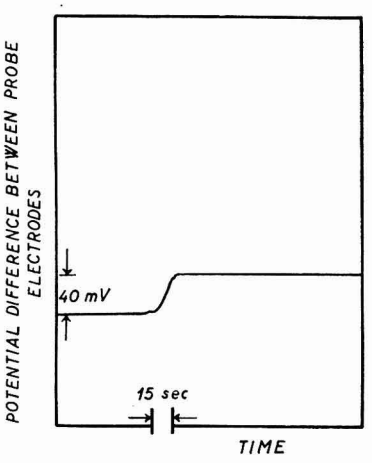

Fig. 5. Potential variation at a probe electrode pair at the moment of boundary passage.

was kept approximately constant. A Tacussel ASA 4/60 potentiostat, (S), working as a constant-current device served as a current source. The value of the current was fixed through the ohmic drop on the variable resistor, R_0. The current was measured to one tenth of a microampere immediately before the anode and immediately after the cathode, at 5-min intervals, using a potentiometer, (P), and two standard resistors, (R_1) and (R_2). The absolute value of the resistance was known to one part in a thousand. Differences greater than 0.2 μA between the two readings were taken as indication of current leakage. The tube was discarded in such a case. The mean current was obtained from a graph of the readings. Solutions were prepared from reagent-grade chemicals. In the case of the hydrochloric acid solutions, the twice-distilled azeotrope was conveniently diluted.

Preliminary experiments

A typical trace of the current peak is shown in Fig. 4. The smallest division of the abscissae corresponds to a 4-sec interval. The time axis runs from left to right. Peak height is 0.045 μA. The leading solution in this experiment is 0.01 M H_2SO_4 followed by $CuSO_4$. The current through the channel is 0.6 mA. Similar signals were obtained with a $HCl/CdCl_2$ boundary using concentrations as low as $5 \cdot 10^{-5}$ M HCl. Current peaks are flatter the lower the boundary velocity.

A series of experiments were run to establish whether or not the electrical

signal was actually due to the boundary passage. For this purpose a 0.1 M H_2SO_4/$CuSO_4$ boundary was formed and its position observed visually[5]. The electrical signal was detected with the galvanometer mentioned above. The peak of the galvanometer current was found to be simultaneous to within about 0.5 sec with the boundary passage through a point approximately midway between the electrodes. Additional information on the origin of the current peak was obtained by registering the potential difference between the microelectrodes at the moment of boundary passage in a similar experiment. A cathode follower as an impedance adapter and a Metrohm registering voltmeter were used for this purpose. The trace obtained is shown in Fig. 5. The potential step is approximately 40 mV. Comparison of Figs. 4 and 5 suggests that the two double-layer capacities of the probe electrode–solution interfaces[6] act approximately as a differentiating circuit[7] on the potential variation. Furthermore, a higher capacitance of the condenser increases the peak current of the boundary signal. This is to be expected since the condenser C and the two double layers form a series circuit. The total capacity, to which the peak current is proportional, increases with C until C^{-1} becomes much smaller than the reciprocal capacity of the double layer. Above 10 μF there was no further effect. During the actual measurements of Table 1 a 1-μF mica Sullivan condenser was used. It should be realized, however, that the detector system is not a simple differentiating circuit since there must be a contribution to the current peak due to the change in the double-layer capacities when the leading solution is replaced by the indicator.

TABLE 1

Leading soln.	*Indicator soln.*	*Concn. of leading soln. (M)*	t_+ *in leading solns.*	*Current (mA)*	*Volume (ml)*
HCl	$CdCl_2$	0.01211	0.8254[a]	0.2969	0.3963
				0.2485	0.3970
				0.2970	0.3957
				0.2474	0.3947
				0.2217	0.3956
				0.3477	0.3951
		0.006156	0.8241[a]	0.1314	0.3946
KNO_3	$AgNO_3$	0.01116	0.5084[b]	0.1992	0.3965
				0.2205	0.3967
				0.2208	0.3958
				0.2202	0.3947

Mean: 0.3957±0.0002 ml
Standard deviation of a single measurement: 0.0008 ml
Geometrical volume (see text): 0.36±0.04 ml

[a] Values interpolated from data in ref. 8.
[b] From data ref. 9.

Precision of the method

As a criterion of the feasibility of the method for transport-number measurements, the volume between two pairs of electrodes was calculated from experiments using known transport numbers. The measurements in Table 1 show the calculated volume to be independent of current strength, concentration and the nature of the leading or following solution, to within five parts in ten thousand. The value quoted

is the probable error of the mean. The calculated volume was compared with the geometrical volume between the lower electrodes of each pair assuming a cylindrical channel. Both values were found to be identical within the experimental errors.

DISCUSSION, ADVANTAGES AND LIMITATIONS

In common with the conductometric and potentiometric detection, the open circuit technique can be used well below the concentrations accessible to optical methods for following the boundary. The latter technique is, in the authors' opinion, relatively simpler from an experimental point of view, mainly because of the absence of high impedance apparatus in the recording circuit. Indeed, under favourable circumstances, the boundary can be timed using the maximum deflection of a simple galvanometer as a signal.

A requirement of all moving boundary techniques is that Joule heating be kept at a minimum. The maximum admissible value under the conditions used in these experiments was found to be about 10 mW for glass tubes. This should undoubtedly depend strongly on tube diameter, wall thickness and thermal conductivity, and water flow rate through the jacket, but the point was not investigated further.

In principle, the best asset of the technique under discussion is the *open* character of the registering circuit. This feature, alone, should make the sensitivity of the boundary detection independent of the resistance of the solution under study. It should therefore be useful for measurements in solutions of very low ionic concentrations. Once the channel current giving an adequate signal has been found, the signal peak height can be held practically constant in magnitude over a wide range of concentrations by keeping the linear velocity of the boundary at the same value. Nevertheless, it was not found possible to keep the precision at 0.2% in $1 \cdot 10^{-3}$ M HCl solutions, although good signals had been obtained down to much lower concentrations, *e.g.*, $5 \cdot 10^{-5}$ M. It is however doubtful whether the boundary method itself can give accurate results at such low concentrations[1].

ACKNOWLEDGEMENTS

The authors are grateful to Dr. CARLOS V. D'ALKAINE and Mr. EMILIO MASSA, for helpful discussions and assistance in the performance of some of the preliminary experiments. They also wish to thank Dr. ROGER PARSONS of Bristol University for suggestions and encouragement.

SUMMARY

Two microelectrodes inserted at different closely spaced heights in the channel of a conventional moving boundary apparatus, are externally connected through a current-sensitive device and a condenser. At the moment of the boundary passage, the abrupt change in the ohmic drop between the two electrode sites causes a readjustment of the charges on the capacities of the electrode circuit involving a small transient current peak of a few hundredths of a microampere. This provides a sensitive signal for the timing of the boundary. The boundary velocity may be determined using pairs of microelectrodes conveniently placed along the channel. The method

has been tested by calibration of the volume between two such electrode pairs. The standard deviation in a series of eleven measurements was 0.2%. The technique can be used at high dilutions. Although it has been tested only in aqueous solution it should be adequate for measurements in non-aqueous solvents.

REFERENCES

1 J. W. LORIMER, J. R. GRAHAM AND A. R. GORDON, *J. Am. Chem. Soc.*, 79 (1957) 2347.
2 J. E. SMITH AND E. L. DISMUKES, *J. Phys. Chem.*, 67 (1963) 1160; 68 (1964) 1603.
3 R. A. ROBINSON AND R. H. STOKES, *Electrolyte Solutions*, Butterworths, London, 1959, p. 104.
4 H. P. CADY AND L. G. LONGSWORTH, *J. Am. Chem. Soc.*, 51 (1929) 1656.
5 D. A. MACINNES AND T. B. SMITH, *J. Am. Chem. Soc.*, 45 (1923) 2246.
6 R. PARSONS, *Equilibrium Properties of Electrified Interfaces* in *Modern Aspects of Electrochemistry*, No. 1, edited by J. O'M. BOCKRIS, Butterworths, London, 1959.
7 P. DELAHAY, *New Instrumental Methods in Electrochemistry*, Interscience Publishers, New York, 1954, p. 363.
8 R. A. ROBINSON AND R. H. STOKES, *Electrolyte Solutions*, Butterworths, London, 1959, p. 158.
9 B. E. CONWAY, *Electrochemical Data*, Elsevier, Amsterdam, 1952.

ELECTROANALYTICAL CHEMISTRY AND INTERFACIAL ELECTROCHEMISTRY
Elsevier Publishing Company, Amsterdam – Printed in The Netherlands

PROPRIÉTÉS ÉLECTROCHIMIQUES ET PHOTOÉLECTROCHIMIQUES DES ÉLÉMENTS SEMICONDUCTEURS DU QUATRIÈME GROUPE IX. L'INFLUENCE DE LA COMPOSITION CHIMIQUE DE L'ÉLECTROLYTE SUR LE PROCESSUS DE LA POLARISATION ANODIQUE DU SILICIUM ET DU GERMANIUM

ANDRZEJ WOLKENBERG
Institut Télé et Radiotechnique, Varsovie (Pologne)
(Reçu le 15 septembre, 1966)

Le germanium et le silicium sont des éléments chimiques du type semiconducteur, appartenant au groupe IV du classement périodique. Leurs propriétés fondamentales physiques et chimiques sont bien connues[1-3] et nous avons donné un aperçu des propriétés électrochimiques spécifiques des éléments semiconducteurs[4], qui est fondé sur les travaux de BRATTAIN ET GARRETT[5], GERISCHER[6], PLESKOV[7] et BODDY[8].

Nous essayerons de présenter, sur la base de l'effet de dressage sur les électrodes semiconductrices découvert par BRATTAIN[5], l'interprétation physique simple du processus de polarisation anodique et cathodique du germanium et du silicium.

PARTIE THÉORIQUE

On peut diviser les courbes de polarisation anodiques en trois groupes. Le premier groupe se caractérise par un courant relativement important qui croît rapidement avec l'augmentation de la polarisation inverse, mais ne possède pas de limite de tension bien definie. Si on fait croître la tension davantage, on peut provoquer une augmentation rapide et illimitée du courant à cause des effets thermiques (Fig. 1, courbe I)[9,10].

Le deuxième groupe se caractérise par le début des courbes exponentielles, et provient du fait q'une génération a lieu dans la région de la charge d'espace, se transformant plus loin en une zone dite "de transition molle" dans la zone de claquage pour le potentiel maximal (Fig. 1, courbe II).

Le troisième groupe englobe les courbes encore plus rapprochées des courbes théoriques (Fig. 1, courbe III). Le potentiel de l'électrode pour lequel la densité du courant commence à croître rapidement s'appelle potentiel de claquage. La valeur maximale du potentiel de claquage est définie par la disruption de jonction par suite de l'action d'un champ électrique très important sur la zone de la charge d'espace. Le mécanisme de claquage en volume, correspond au troisième groupe des courbes de polarisation décrit çi-dessus.

L'accroissement de la densité de courant de conduction près du potentiel de claquage résulte de la multiplication en avalanche des porteurs dans la zone de la charge d'espace, dans la double couche au voisinage de l'électrode (Fig. 2).

Les opinions de TURNER[11] et FLYNN[12], sur la dépendence du courant de saturation de la corrosion et de la vitesse de diffusion des trous, que nous avons exposées en ref. 4, semblent être verifieés, surtout si nous supposons en outre que les réactions chimiques ont une influence négligeable en comparaison du phénomènes physiques.

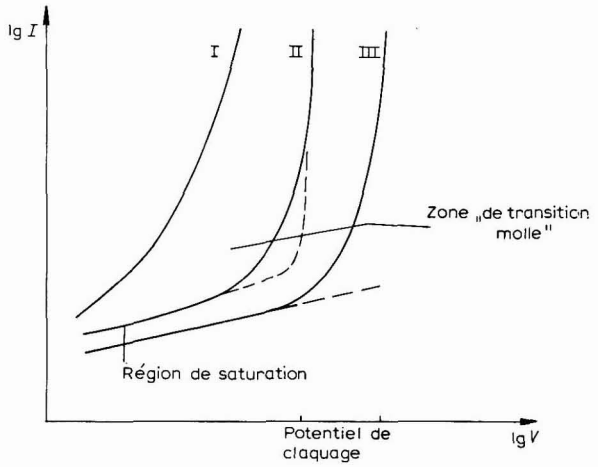

Fig. 1. Augmentation de l'intensité (I) en fonction de la tension.

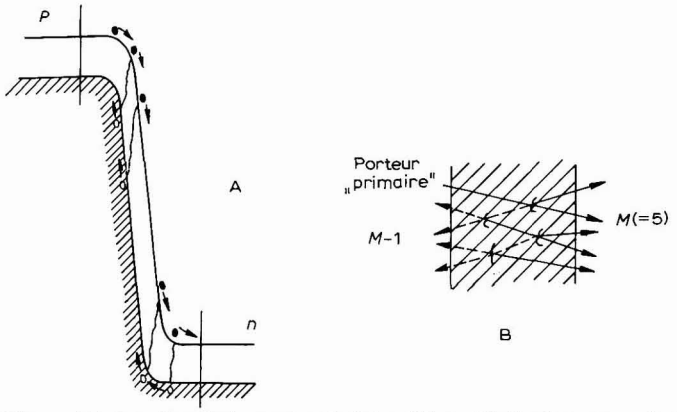

Fig. 2. (A) Jonction fortement polarisée; (B) multiplication en avalanche des porteurs.

Le coefficient de multiplication de courant, M, résultant du processus décrit çi-dessus peut être ramené à une formule du type[13]:

$$M = \frac{1}{1 - \left(\frac{\phi}{\phi_p}\right)^m}$$

où ϕ = potentiel de l'électrode
ϕ_p = potentiel de claquage
m = 3 pour le germanium de type n, 6 pour le germanium de type p, 2.5 pour le silicium de type n et p

Quand $M=1$, la multiplication ne s'effectue pas il en est de même quand le potentiel de l'électrode tend vers l'infini. Quand un champs électrique suffisament puissant excite les électrons de la bande de conduction le claquage inverse de la jonction peut avoir lieu. On suppose que le claquage de ce type, qu'on appelle souvent perçage, peut se présenter seulement dans les jonctions avec un semiconducteur fortement dopé de deux cotés, car c'est seulement alors que le champ électrique peut atteindre des valeurs assez importantes (10^6 V/cm), ce qui, dans notre cas, correspond aux électrodes d'une résistivité faible.

PARTIE EXPÉRIMENTALE

Pour effectuer les mesures nous avons utilisé le récipient représenté sur la Fig. 3 en utilisant de l'argon dépourvu d'oxygène pour mélanger la solution étudiée. Nous avons mesuré le potentiel de l'électrode etudiée (Fig. 4) par rapport à une électrode au calomel, à l'aide d'un pH-mètre "Radiometer" ou bien d'un milivoltmètre à lampe d'une résistance d'éntrée de 40 MΩ.

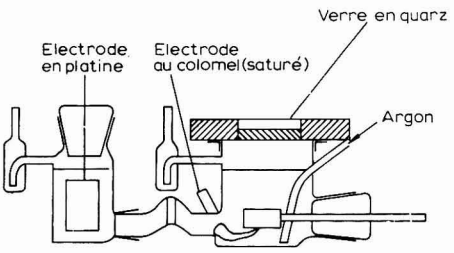

Fig. 3. Coupe longitudinale du récipient pour effectuer les mesures.

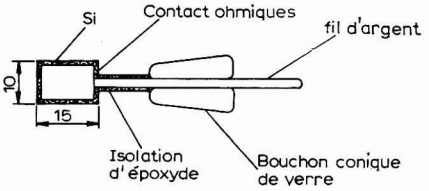

Fig. 4. Coupe de l'électrode.

Les électrodes étudiées, en silicium ou en germanium (de 2 cm² de surface), étaient polarisées par rapport à une électrode en platine (6 cm² de surface) en utilisant la méthode au courant continu.

Les solutions étaient effectuées avec des réactif p.a. dans de l'eau bidistillée.

Les courbes de polarisation cathodique du germanium et du silicium de type *n* (Fig. 5) montrent leur similitude. La jonction *p–n* formée par la surface de l'électrode de type *n* et l'électrolyte de type *p*, a des propriétés physiques analogues aux jonctions *p–n* dans les sémiconducteurs (Figs. 5, 6 et 7). On obtient la valeur la plus importante du rapport courant direct–courant inverse dans le cas du silicium de type *n* ($\varrho=0.3$ Ωcm) et avec potentiel d'électrode de l'ordre de -1.55 V (Fig. 5).

Pour les valeurs plus élevées de la résistance des électrodes, les courbes de polarisation cathodique se redressent (Figs. 5 et 6) pour devenir dans certains cas linéaires.

Les courbes de polarisation anodique du germanium et du silicium se ressemblent et démontrent, que dans les deux cas il s'agit d'une jonction *p–n* polarisée dans la direction de blockage.

Le courant inverse de saturation peut être observé sur toutes les courbes

de polarisation anodique, des Figs. 7 et 8, qui peuvent être comparées à la courbe théorique.

Pour le germanium il est difficile de déceler cet effet sur les courbes de polarisation de la Fig. 7 par suite d'une échelle trop serrée sur l'axe des potentiels, mais on peut facilement voir cet effet en étendant l'échelle, comme on l'a fait pour une courbe de la Fig. 7.

Les études que nous avons effectuées permettent de dire que la valeur du

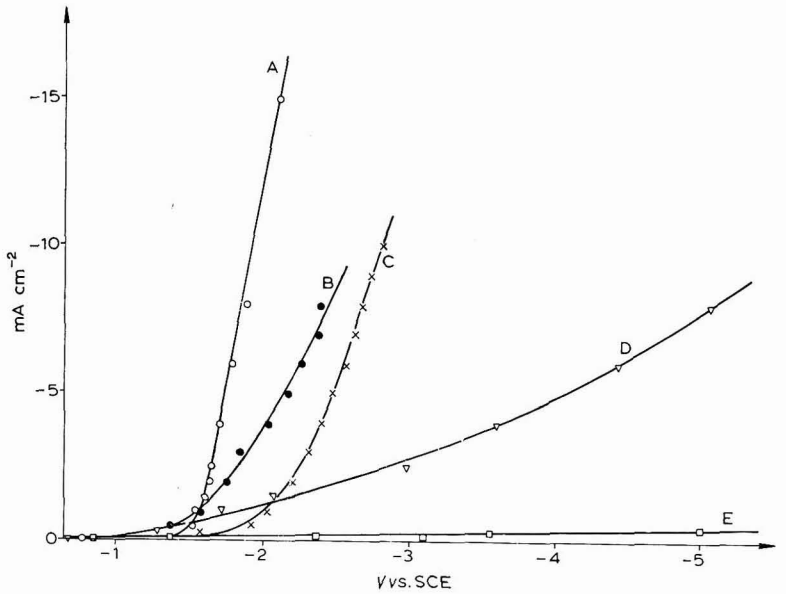

Fig. 5. (A) Si-*n*, $\varrho = 0.3$ Ωcm, 0.1 *M* $NaNO_3$; (B) Ge-*n*, $\varrho = 0.3$ Ωcm, 0.1 *M* $NaNO_3$; (C) Ge-*p*, $\varrho = 0.7$ Ωcm, 0.1 *M* $NaNO_3$; (D)-(E), Si-*p*; (D) $\varrho = 1.15$ Ωcm, 0.1 *M* $FeCl_2 + FeCl_3$, (E) $\varrho = 470$ Ωcm, 0.1 *M* $FeCl_3 + FeCl_2$, 0.1 *M* $Fe(NO_3)_2 + Fe(NO_3)_3$.

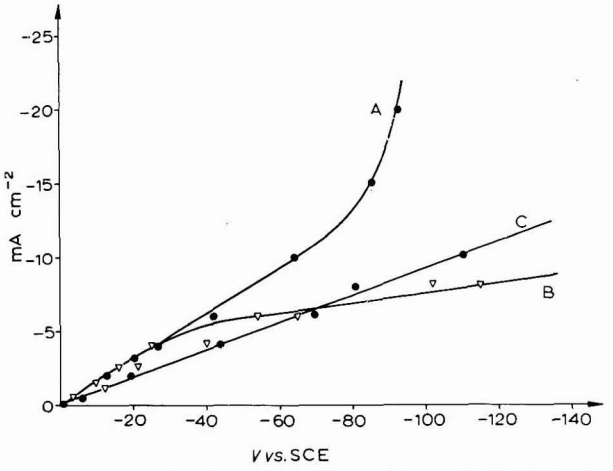

Fig. 6. (A) et (B), Si-*n*, $\varrho = 255$ Ωcm; (A) 0.1 *M* $Fe(NO_3)_2 + Fe(NO_3)_3$, (B) 0.1 *M* $FeCl_2 + FeCl_3$. (C) Si-*p*, $\varrho = 470$ Ωcm, 0.1 *M* $Fe(NO_3)_2 + Fe(NO_3)_3$ et 0.1 *M* $FeCl_2 + FeCl_3$.

courant de saturation dépend de la nature du semiconducteur, du type de conduction et de la composition chimique de l'électrolyte[14].

Le courant de saturation apparaissant pendant la polarisation anodique est relativement plus important dans le cas des électrodes en germanium que pour des électrodes en silicium (Fig. 7). La zone dans laquelle le courant de saturation ne dépend pas du potentiel de polarisation est pour une électrode de 0.3 Ω relativement plus étroite que pour une électrode en semiconducteur dont la résistivité est plus grande.

Aux trois groupes de courbes de polarisation anodique representées sur la

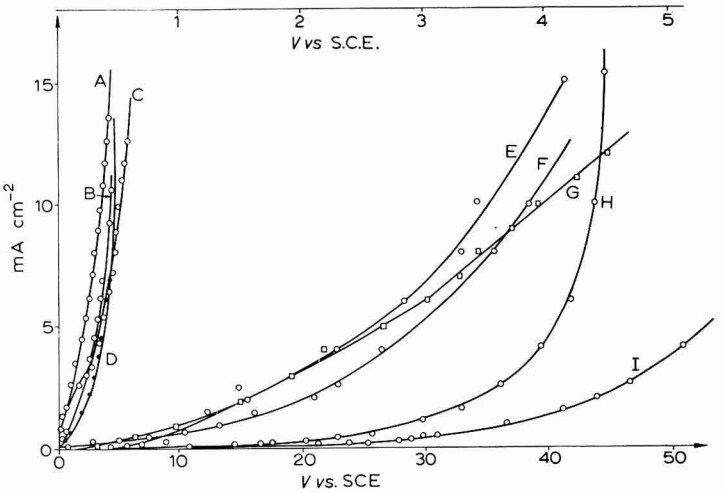

Fig. 7. (A), (C), (D) et (G), Ge-*n*, $\varrho = 0.3$ Ωcm; (A) 0.1 *M* $FeCl_2 + FeCl_3$; (C) 0.1 *M* $FeSO_4 + Fe_2(SO_4)_3$; (D) 0.1 *M* $NaNO_3$; (G) 0.1 *M* $NaNO_3$ (haute scale). (B) Ge-*p*, $\varrho = 0.7$ Ωcm; (B) 0.1 *M* $NaNO_3$. (E), (H) et (I), Si-*n*, $\varrho = 0.3$ Ωcm; (E) 0.1 *M* $NaNO_3$; (H) 0.1 *M* $FeCl_2 + FeCl_3$; (I) 0.1 *M* $FeSO_4 + Fe_2(SO_4)_3$, (F), Si-*p*, $\varrho = 1.15$ Ωcm, 0.1 *M* $NaNO_3$.

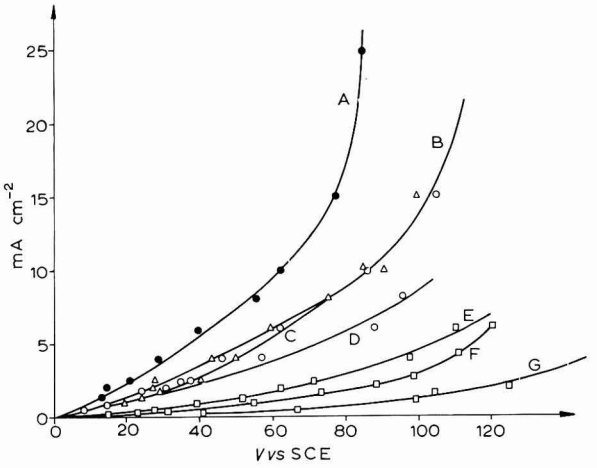

Fig. 8. (A), (B) et (E), Si-*p*, $\varrho = 470$ Ωcm; (A) 0.1 *M* $Fe(NO_3)_2 + Fe(NO)_3$; (B) 0.1 *M* $FeCl_2 + FeCl_3$ et 0.1 *M* $FeSO_4 + Fe_2(SO_4)_3$; (E) 0.1 *M* $NaNO_3$. (C), (D), (F) et (G), Si-*n*, $\varrho = 225$ Ωcm; (C) 0.1 *M* $FeCl_2 + FeCl_3$; (D) 0.1 *M* $FeSO_4 + Fe_2(SO_4)_3$; (F) 0.1 *M* $NaNO_3$; (G) 0.1 *M* $Fe(NO_3)_2 + Fe(NO_3)_3$.

Fig. 1, le germanium appartient au premier groupe (Fig. 7); au second le silicium de type p (Figs. 7 et 8); et le troisième groupe englobe les courbes de polarisation du silicium de type n (Figs. 7 et 8).

Le potentiel de claquage pour une électrode de 0.3 Ωcm en germanium en 0.1 M $FeCl_2+FeCl_3$ (Fig. 7) est égal à 4 V environ et pour le silicium a environ 44 V.

Dans le cas étudié, on peut distinguer une différence entre les potentiels de claquage du germanium et du silicium (Fig. 7). Ces différences sont pour les semiconducteurs de type n ($\varrho=0.3$ Ωcm) de l'ordre de 35 V, dans l'électrolyte 0.1 M $NaNO_3$, de l'ordre de 40 V dans l'électrolyte redox 0.1 M $FeCl_2+FeCl_3$ et de 50 V environ dans 0.1 M $FeSO_4+Fe_2(SO_4)_3$ pour un courant de polarisation inverse de 5 mA/cm². Pour un semiconducteur de type p (Fig. 7) cette différence est de l'ordre de 25 V. Le courant de saturation est beaucoup plus grand pour le germanium, que pour le silicium, parce que il depend de la quantité totale des porteurs minoritaires. La mobilité des porteurs minoritaires, c'est à dire des trous, est dix fois plus grande dans le germanium que dans le silicium.

Ces phénomènes expliquent bien la différence entre le processus de polarisation anodique des électrodes en germanium et en silicium. On peut supposer, qu'en diminuant la densité des additions, c'est à dire en faisant croître la résistivité du sémiconducteur, on fait en même temps croître la tension de disruption et diminuer le courant de saturation. Cela était confirmé par l'éxpérience (Fig. 8). Par example, la tension de claquage pour une électrode en silicium n de resistivité $\varrho=255$ Ωcm est égale à 120 V environ, dans l'électrolyte 0.1 M $NaNO_3$, tandis que pour une électrode en silicium n de résistivité 0.3 Ωcm, dans le même électrolyte elle est égale à 30 V seulement. La polarisation anodique des électrodes en sémiconducteur de type p (Figs. 7 et 8) a une allure similaire, avec la seule différence, que le courant de saturation est plus important et la tension de perçage plus faible, à cause d'une densité plus grande des porteurs minoritaires, c'est à dire des trous.

L'influence de la composition chimique de l'électrolyte sur le processus de polarisation anodique est representée sur le Fig. 8. Pour des concentrations différentes du même électrolyte (HNO_3 par exemple) l'accroissement du courant de saturation est proportionnel à l'augmentation de la concentration de HNO_3[11].

Pour les électrolytes différents, le processus de polarisation anodique dépend du genre de cation et de l'anion. On peut expliquer ces phénomènes en comparant les propriétés physico-chimiques du système électrode–électrolyte aux jonctions p–n semiconducteur–métal.

L'analyse montre que ces différences sont dues aux valeurs différentes des constantes qui caractérisent les jonctions p–n dans les différents électrolytes ou aux différentes concentrations du même électrolyte.

Le coefficient de multiplication de courant M (éqn. (1)) calculé pour les électrodes semiconductrices soumises aux essais montre l'abaissement du coefficient de multiplication d'avalanche dans 0.1 M $NaNO_3$, en fonction de l'augmentation de la résistivité du semiconducteur (Tableau 1) et de la composition chimique de l'électrolyte (Tableau 2).

Pour le germanium, le coefficient M est plus grand que pour le silicium. Un phénomène analogue se présente dans les transistors et diodes.

La polarisation cathodique du germanium et du silicium, dont les résistivités sont faibles, est une polarisation dans la direction de conduction de la jonction p–n

TABLEAU 1

LE COEFFICIENT DE MULTIPLICATION DE COURANT M POUR LES ÉLECTRODES DE LA RESISTIVITÉ DIFFÉRENT

0.1 M $NaNO_3$, $\phi = 3$ V

	Ge_n	Si_n	Ge_p	Si_p	Si_n	Si_p
$\varrho(\Omega cm)$	0.3	0.3	0.7	1.15	255	470
	1.3	1.0002	1.04	1.0002	1.00002	1.00002

TABLEAU 2

LE COEFFICIENT DE MULTIPLICATION DE COURANT M POUR LES DIFFÉRENTES ÉLECTROLYTES

Si_p, $\phi = 30$ V

0.1 M $Fe(NO_3)_2$ + $Fe(NO_3)_3$	0.1 M $FeCl_2$ + $FeCl_3$	0.1 M $FeSO_4$ + $Fe_2(SO_4)_3$	0.1 M $NaNO_3$
1.2	1.03	1.03	1.009

dans laquelle la surface du sémiconducteur est du type n. Les électrodes en germanium et en silicium du type p se caractérisent par les densités plus faibles des électrons que les électrodes du type n, et grâce à cela montrent une résistance de polarisation plus importante.

La polarisation des électrodes dans les sémiconducteurs dont les résistivités sont importantes (matériaux purs) par example Si de type n, $\varrho = 255$ Ωcm, ou Si de type p, $\varrho = 470$ Ωcm, se caractérise par un processus (Fig. 7) qui cesse d'être linéaire seulement pour les intensités importantes de champ électrique (Fig. 6). L'interprétation des propriétés électrochimiques d'une électrode en germanium, donnée précédemment[14], à l'aide de l'équation généralisée de Tafel, semble être verifiée parce que cette équation relie les valeurs mesurables du courant de polarisation et du potentiel de l'électrode, résultant des propriétés physico-chimiques de l'électrode et de l'électrolyte.

L'interprétation physique de ces phénomène doit cependant être basée sur les thèses exposées çi-dessus.

CONCLUSIONS

La polarisation des électrodes en sémiconducteur, appartenant au IV groupe dans des électrolytes différents, s'effectue d'une façon analogue que la polarisation des jonctions p–n, réalisées avec les mêmes semiconducteurs. L'application des thèses essentielles de la théorie des jonctions p–n dans les sémiconducteurs pour la compréhension de ces phénomènes, permet l'explication logique de plusieurs phénomènes, qui jusqu'à présent semblaient provenir d'erreurs expérimentales ou simplement ne pouvaient pas être expliqués. Il semble que nos propres mesures et l'analyse des travaux publiés par d'autres auteurs soutiennent cette hypothèse.

REMERCIEMENTS

Je tiens à remercier Monsieur le Professeur S. MINC pour tout l'intérêt qu'il a temoigné à ce travail et les discussions sur les sujets traités.

Les expériences ont été faites dans le laboratoire de Chimie Physique de l'Université de Varsovie.

RÉSUMÉ

En se basant sur nos propres mesures et les travaux publiés par d'autres auteurs nous proposons une interprétation physique du processus de polarisation anodique et cathodique des électrodes semiconductrices en germanium et en silicium dans des électrolytes différents.

L'analyse est basée sur la supposition, que le processus de polarisation anodique ou cathodique d'une électrode sémiconductrice est le processus de polarisation d'une jonction *p–n* existante à la limite des phases électrolyte–semiconducteur.

SUMMARY

On the basis of our own measurements and the work published by other authors, we propose a physical interpretation of the process of anodic and cathodic polarisation of semiconductor electrodes of Ge and Si in different electrolytes. The analysis is based on the assumption that this process is the polarisation of a *p–n* junction existing at the electrolyte–semiconductor interface.

BIBLOGRAPHIE

1 N. KRASIUK ET A. J. GRIBOV, *Les Semiconducteurs Germanium et Silicium*, Goschimizdat, Moscou, 1962.
2 H. GERISCHER, *Z. Phys. Chem. NF.*, 26 (1960) 223; 26 (1960) 325; 27 (1961) 48.
3 P. J. HOLMES (ed.), *The Electrochemistry of Semiconductors*, Academic Press, Londres, 1962, p. 155.
4 A. WOLKENBERG, *Wiadomości Chemi.*, 20 (1966) 201.
5 W. BRATTAIN ET C. GARRETT, *Bell System. Tech. J.*, 34 (1955) 129.
6 H. GERISCHER, dans P. DELAHAY (ed.), *Advances in Electrochem. Electrochem. Eng.*, Vol. 1, Interscience, New York, 1961, p. 139.
7 J. W. PLESKOV, *Electrochemistry of Semiconductors*, Moscou, 1965.
8 P. J. BODDY, *J. Electroanal. Chem.*, 10 (1965) 199.
9 A. K. JONSCHER, *Principles of Semiconductor Device Operation*, Bell and Sons, Londres, 1960.
10 J. SHIVE, *The Properties, Physics and Design of Semiconductor Devices*, Van Nostrand Co., Princeton, N.J., 1959.
11 D. TURNER, *J. Electrochem. Soc.*, 108 (1961) 561.
12 J. FLYNN, *J. Electrochem. Soc.*, 105 (1958) 715.
13 S. L. MILLER, *Phys. Rev.*, 99 (1955) 1234.
14 A. WOLKENBERG, *Ann. Soc. Chim. Polonorum*, 39 (1965) 291.

ELECTROANALYTICAL CHEMISTRY AND INTERFACIAL ELECTROCHEMISTRY
Elsevier Publishing Company, Amsterdam – Printed in The Netherlands

A STUDY OF INTERMEDIATES ADSORBED ON PLATINIZED-PLATINUM DURING THE STEADY-STATE OXIDATION OF METHANOL, FORMIC ACID, AND FORMALDEHYDE

M. W. BREITER
General Electric Research & Development Center, Schenectady, New York (U.S.A.)
(Received October 31st, 1966)

INTRODUCTION

In recent years, charging curves[1,2,4,6,7,9] and different potentiostatic techniques[1,3,5,8,10] have been used for the study of adsorbed intermediates that were formed during the anodic oxidation of organic species on smooth[1-5] and platinized[6-9] electrodes and miniature versions[10] of Teflon fuel cell electrodes with platinum-black catalyst. The charge, Q_a, due to the oxidation of adsorbed intermediates is obtained by anodic pulses. Cathodic pulses serve to determine the charge, Q_H, due to the co-deposition of hydrogen atoms on sites that are not covered by intermediates. However, this information is not sufficient for the identification of the intermediate. It appears desirable to know the number, N_c, of adsorbed intermediates besides Q_a and Q_H. This number may be determined[3] under certain conditions from measurements of the rate of adsorption as a function of time on a surface which was free of intermediates at the start. The rate of adsorption has to be diffusion-controlled and the net formula for the conversion of the species in the electrolyte to the intermediates has to be known. In the simplest case (CO for instance[3]) the composition of the intermediate and of the species in the electrolyte is the same.

A combination of radiometric measurements[11] and pulse techniques should allow the simultaneous determination of Q_a and N_c if (a) each of the species in the electrolyte and each of the intermediates contains only one carbon atom or if (b) only H-atoms and OH-radicals are split off by dissociative adsorption in the case of organic species with more than one carbon atom in the electrolyte. Both cases can be studied by a combination of gas chromatography[12] and pulse techniques in conjunction with electrodes of large surface area[6,7,9] since the anodic oxidation of most intermediates occurs according to eqn. (1):

$$C_sH_pO_q + (2s-q)\ H_2O = s\ CO_2 + (4s+p-2q)\ H^+ + (4s+p-2q)\ e^- \qquad (1)$$

Here, $C_sH_pO_q$ designates the net composition of the intermediates in a general way; s,p,q are integers. For simplicity, the intermediates are assumed to be neutral species. The consideration of charged intermediates would require the introduction of one more integer. Since the total amount of CO_2 evolved according to reaction (1) has to be measured, the technique is restricted to acidic solutions. Let us define:

$$Q_{CO_2} = sN_cF/N_0 \qquad (2)$$

where F = Faraday constant and N_0 = Avogadro number.

Then it follows:

$$Q_a/Q_{CO_2} = 4 + (p - 2q)/s \quad (3)$$

Equation (3) shows that only the ratio $(p-2q)/s$ is accessible to an experimental determination by a combination of pulse techniques with gas chromatography, in the general case. A similar statement applies to the interpretation of results obtained by a combination of pulse techniques and radiometric measurements.

Charging curves and gas chromatography were applied to the investigation of adsorbed intermediates that had been formed on platinized-platinum in sulphuric acid solutions during the steady-state oxidation of methanol, formic acid, and formaldehyde, respectively. The oxidation of adsorbed CO was studied to test the accuracy of the technique. Finally, the shape of the four charging curves for the oxidation of the intermediates formed in the presence of different species in the electrolyte are compared. These curves were taken at the same charging rate on the same electrode.

EXPERIMENTAL

The experiments were carried out at 20° in a Pyrex vessel of standard design with three compartments. The platinized-platinum electrode with 50 cm^2 of geometric surface area was in the large compartment having a volume of about 200 cm^3. The electrolytic solution in this compartment was continuously stirred by a stream of purified helium bubbling through a frit at 0.50 ± 0.01 cm^3 sec^{-1}. The electrolytic solutions were prepared from AR-grade chemicals and double-distilled water. Pre-electrolysis of the sulfuric acid solutions (0.05 M and 0.5 M H_2SO_4) before the addition of the organic species did not affect the results. At the beginning of every experiment, an anodic charging curve was taken at 50 mA in the absence of fuel to verify that oxidizable impurities were not adsorbed on the test electrode. The charge equivalent, ${}_sQ_H$, of the hydrogen layer was determined approximately from the charge consumed between 0.07 and 0.4 V. As reported previously[8], a gradual decrease of ${}_sQ_H$ with the number of experiments was observed when the measurements were started on a freshly platinized electrode. However, the subsequent conclusions are independent of this decrease since the ratio Q_a/Q_{CO_2} was obtained for the same surface roughness during each run. The electrode potential is referred to a hydrogen electrode in the same solution as the test electrode.

After the addition of the desired amount of fuel, a constant current was maintained between test electrode and counter electrode for 20–30 min to assure steady-state conditions. After the interruption of the current, the electrolytic solution was pushed out of the large compartment through the frit and gas inlet by applying nitrogen pressure to the gas outlet. Then sulfuric acid solution from which oxygen had been removed by extensive nitrogen bubbling was added through the gas outlet under nitrogen pressure. Air did not have access to the large compartment during this "washing" procedure which had already been used in other work[6,7,9]. It was found that the length of the arrest that results from the anodic oxidation of the intermediates at a current of 50 mA (1 mA cm^{-2}, referred to geometric area) did not further decrease for $n > 4$ at fuel bulk concentrations ${}_0c \leq 0.1$ M. Here, n designates the number of

repetitions of the washing procedure. A current of 50 mA and four washings were used in the following experiments. It is conceivable that "weakly bonded" intermediates are removed by the washing procedure if the heat of adsorption of the intermediates decreases considerably with coverage. Such an effect will not influence the subsequent conclusions if the removable intermediates are of the same type (net composition) as the remaining intermediates, since Q_a and Q_{CO_2} correspond to the same number of adsorbed species. About equal values were obtained for ${}_sQ_a/{}_sQ_H$ by direct pulse techniques on smooth platinum[1] and by charging curves with preceding washing procedure on platinized-platinum[9] for saturation coverage with intermediates formed during the anodic oxidation of methanol. This suggests a small loss of intermediates during the washing procedure, but does not eliminate the possibility that a small amount of weakly-bonded intermediates plays an important role in the oxidation reaction. Thirty minutes of bubbling with helium were sufficient to remove the CO from the electrolytic solution in the studies of CO-adsorption.

The potential of the test electrode was brought in the vicinity of 0.07 V after the four washings. Then a constant flow of helium was maintained at 0.50 ± 0.01 $cm^3\ sec^{-1}$ through the large compartment and the sampling coil (25 cm^3) of the gas chromatograph. It took 20–30 min to remove the air from the connecting tubing and the coil after the hook-up of the gas chromatograph to the gas outlet of the large compartment. A negligible height of the CO_2-peak of the gas chromatogram of the gas mixture from the cell was taken as the criterion.

The gas chromatograph (Perkin-Elmer, Model 154, with silica gel column) was calibrated as follows. Electrolysis of 0.1 *M* $C_2H_2O_4$ was carried out on the test electrode in 0.5 *M* H_2SO_4 at different anodic currents. The net reaction for this process is:

$$\tfrac{1}{2}\, C_2H_2O_4 \rightarrow CO_2 + H^+ + e^- \qquad (4)$$

The reaction occurs with 100% efficiency[13–15] on platinized-platinum between 0.8 and 1.0 V. One electron is required for the production of one CO_2-molecule. A constant flow rate (0.50 ± 0.01 $cm^3\ sec^{-1}$) of helium was maintained through the large compartment and the sampling coil of the gas chromatograph. The height of the CO_2-peak of the GC analysis of the gas mixtures was determined as a function of the anodic current, I, under steady-state conditions with respect to the CO_2-content of the mixtures. The achievement of the latter condition was verified experimentally by measuring the height of the peak as a function of time after turning on or changing the current until the peak height no longer increased. The large solubility of CO_2 in sulfuric acid solutions leads to a considerable time lag. The plot of the peak height *versus* the current was linear between 0.05 and 100 mA. The same straight line was obtained under equivalent conditions for the anodic oxidation of 0.1 *M* HCOOH in 0.05 *M* H_2SO_4 when plotting double the peak height *versus* the current since two electrons are required/CO_2-molecule in this case.

Curves (a) and (b) in Fig. 1 are examples of charging curves in 0.05 *M* H_2SO_4 at 50 mA. Curve (a) exhibits a short hydrogen branch and an arrest between about 0.55 and 0.60 V. The arrest is due to the oxidation of intermediates that were formed previously during methanol oxidation at 50 mA in 0.1 *M* $CH_3OH + 0.05$ *M* H_2SO_4 for 40 min. The transition to the oxygen region occurs between about 0.6 and 0.8 V. The shape of curve (a) is similar to the shape of corresponding charging curves in

recent communications[9,16]. Curve (b) was taken after curve (a). It coincides practically with the charging curve taken in 0.05 M H_2SO_4 before methanol was added and the electrolysis started. Curve (b) represents the charging curve of the test electrode free of organic intermediates. The starting potential is nearly the same for both curves. As pointed out[7,9,16], the two curves coincide at potentials corresponding to the arrest. Therefore, the transition time, τ, for the oxidation of the intermediates is easily determined as demonstrated in Fig. 1. In the case of curve (a), the anodic current was stopped at a potential of about 0.9 V and the electrode remained at open circuit until the end of the gas analysis.

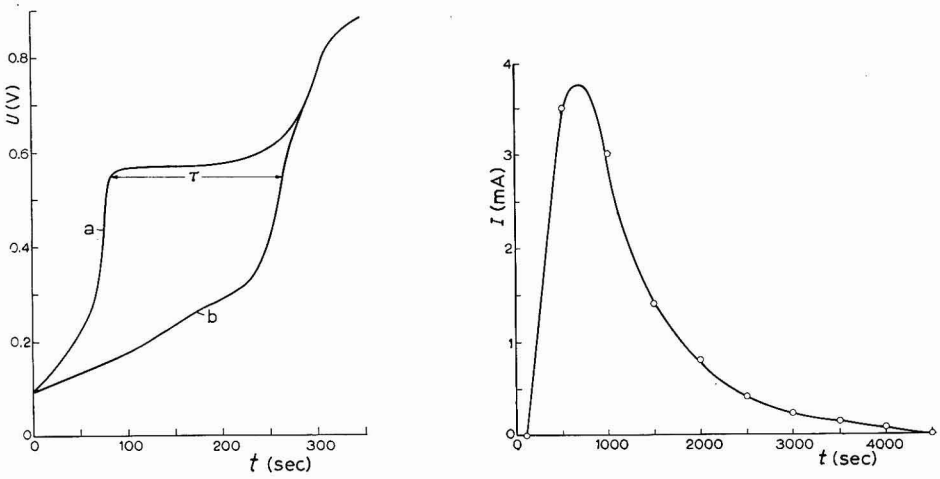

Fig. 1. Charging curves in 0.05 M H_2SO_4 at 50 mA: (a), intermediates formed during electrolysis in 0.1 M CH_3OH + 0.05 M H_2SO_4; (b), electrode free of intermediates.

Fig. 2. CO_2-content of the gas mixture in electrical units after the oxidation of adsorbed intermediates as a function of time. Intermediates were formed during methanol oxidation.

The GC analysis of the gas mixtures could be carried out in intervals of about 500 sec after the start of curve (a) in Fig. 1. Up to 100 sec, the analysis showed only an air peak corresponding to a partial pressure (nitrogen + oxygen + argon) of less than $3 \cdot 10^{-3}$ atm. The height of the air peak remained practically constant during all the GC analysis. The height of the CO_2-peak increased rapidly after 100 sec, passed through a maximum and then decreased slowly. Other peaks besides the air- and CO_2-peak were not observed in the GC analysis of the gas mixtures during and after the oxidation of intermediates formed previously in the presence of CH_3OH, HCOOH, or CH_2O, respectively. After the peak heights had been converted into currents with the aid of the calibration curve, the plot in Fig. 2 was made. It takes 60–90 min to remove the CO_2 from the solution. From plots of the type in Fig. 2, Q_{CO_2} may be computed:

$$Q_{CO_2} = \int_0^{t_0} I\,(t-25)\,dt \qquad (5)$$

The time is counted in seconds. The time, t_0, of the upper integration limit corresponds to 4500 sec in the case of curve (a) in Fig. 1. Since it takes 50 sec for the gas mixture to flow through the 25-cm^3 coil at a rate of 0.50 ± 0.1 cm^3 sec^{-1}, an

average value, I, which corresponds to $(t-25)$ is measured at the time, t, when the sampling coil is separated from the cell by the valve. The accuracy of the procedure was checked by evolving CO_2 for 35 sec at 100 mA on a small platinized-platinum electrode (8 cm^2 of geometric surface) in 0.1 M HCOOH + 0.05 M H_2SO_4, and determining Q_{CO_2} according to eqn. (5). The values of $Q_a = 3.5$ C and $4\,Q_{CO_2} = 3.7$ C agreed within 6%. If an uncertainty of 5% is estimated for the determination of τ, the error in the determination of Q_a/Q_{CO_2} (≈ 2) will be 10–20%.

RESULTS AND DISCUSSION

The maximum and minimum vales of Q_a/Q_{CO_2} that were obtained during five experiments for each of the four cases, are compiled in Table 1.

The adsorbed layers of CO had been formed by bringing the test electrode to 0.1 V, opening the circuit and bubbling with a mixture of 90% Ar + 10% CO for 1–3 h.

As to be expected on the basis of the error estimate, the numerical values for the ratio Q_a/Q_{CO_2} scatter considerably. The average values are close to 2. This result was to be expected for the oxidation of CO_{ad}. It follows:

$$(p-2q)/s = -2$$

An infinite number of net compositions is compatible with these results. However, it is considered unlikely that $s > 2$, $p > 2$, $q > 3$, in the cases of simple organic species studied. Possible compositions are put together in Table 2.

TABLE 1

MAXIMUM AND MINIMUM VALUES OF Q_a/Q_{CO_2}

Initial species	*CO*	*CH_3OH*	*HCOOH*	*CH_2O*
Q_a/Q_{CO_2}, max.	2.2	2.5	2.2	2.2
Q_a/Q_{CO_2}, min.	1.9	1.7	2.0	1.8

TABLE 2

POSSIBLE NET COMPOSITIONS OF INTERMEDIATES

	$s=1$		$s=2$	
p	0	2	0	2
q	1	2	2	3
Composition	CO	H_2CO_2	C_2O_2	$H_2C_2O_3$

Charging curves for the oxidation of the intermediates in the four cases are compared in Fig. 3. The U–t curves, (a), (b), (c), and (d), were chosen such that the length of the arrest is not too different. The curves (a), (b), and (c) coincide within the experimental error within a certain region starting at the beginning of the arrest. If it is assumed that the plateau of the charging curves appears at various potentials for the oxidation of the possible intermediates in Table 2 because of different kinetic hindrance, the coincidence of curves (a), (b), and (c) within a certain region means that the same intermediate is formed during the oxidation of CH_3OH, HCOOH, and CH_2O. The preceding assumption is likely, but lacks experimental verification.

The arrest of the charging curve for the oxidation of CO is located at slightly more anodic potentials. Besides, the presence of CO_{ad} hinders the co-deposition of H-atoms more strongly than the other adsorbed intermediates. This may be interpreted as an indication that CO is not the intermediate. A similar conclusion was

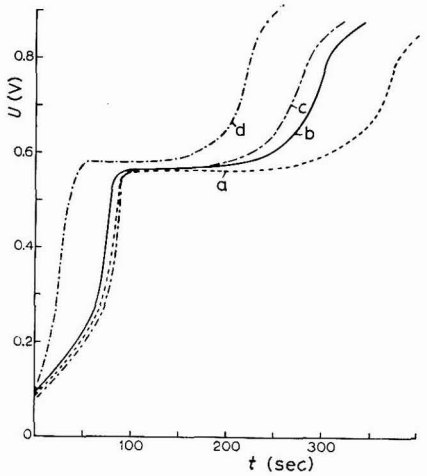

Fig. 3. Charging curves at 50 mA for the oxidation of intermediates formed in: (a), 0.1 *M* HCOOH +0.05 *M* H_2SO_4; (b), 0.1 *M* CH_3OH+0.05 *M* H_2SO_4; (c), 0.1 *M* CH_2O+0.05 *M* H_2SO_4; (d), bubbling with 90% A+10% CO.

arrived at previously[17] by the comparison of charging curves for the oxidation of CO_{ad} and the intermediate of the formic acid oxidation on smooth platinum. However, the author does not consider the results in Fig. 3 and in ref. 17 as sufficient evidence for a distinction between CO_{ad} and other intermediates.

The above results will require a re-interpretation of previous voltammetric studies of methanol oxidation on smooth platinum. It had been assumed[1], that methanol molecules are adsorbed. The results are not in agreement with the postulation[18] of HCO as the intermediate of methanol oxidation on smooth platinum. Work is in progress to check the conclusion[9,16] that HCO is formed as an intermediate during the open-circuit decay of the potential of platinized-platinum after the addition of methanol. The previous conclusion[2,19] ($s=1$, $p=2$, $q=2$) on the intermediate during the anodic oxidation of formic acid is compatible with the results in Table 2, but the other possibilities in Table 2 cannot be ruled out with certainty[20].

It should be emphasized that the preceding considerations are based on the simplifying assumption that the net composition of the intermediate can be described with s, p, and q as integers. This assumption is generally made in the fuel cell literature. If different types of intermediates exist simultaneously or if a bonding occurs between adsorbed intermediates of one type, s, p, q need no longer be integers. The error in the determination of Q_a/Q_{CO_2} is too large to allow a distinction in the present study. For this reason, the simple interpretation of integers has been used.

SUMMARY

A combination of charging curves and gas chromatography was used in

conjunction with platinized-platinum electrodes of large real surface, to study the intermediates that are formed under steady-state conditions during the anodic oxidation of methanol, formic acid, and formaldehyde in sulfuric acid solutions. It appears that the composition of the adsorbed intermediates is very similar in the three cases. On the average, the oxidation of one intermediate requires two electrons. The behavior of adsorbed CO is slightly different from that of the intermediates.

REFERENCES

1 M. W. BREITER AND S. GILMAN, *J. Electrochem. Soc.*, 109 (1962) 622.
2 M. W. BREITER, *Electrochim. Acta*, 8 (1963) 447.
3 S. GILMAN, *J. Phys. Chem.*, 66 (1962) 2657; 67 (1963) 78.
4 S. B. BRUMMER AND A. C. MAKRIDES, *ibid.*, 68 (1964) 1448.
5 O. A. KHAZOVA, YU. B. VASIL'EV AND V. S. BAGOTSKII, *Elektrokhimiya*, 1 (1965) 84.
6 T. O. PAVELA, *Ann. Acad. Sci. Fennicae, Ser. A. II*, (1954) 59.
7 A. N. FRUMKIN AND B. I. PODLOVCHENKO, *Dokl. Akad. Nauk SSSR*, 150 (1963) 349.
8 J. GINER, *Electrochim. Acta*, 9 (1964) 63.
9 B. I. PODLOVCHENKO AND E. P. GORGONOVA, *Dokl. Akad. Nauk SSSR*, 156 (1964) 673.
10 L. NIEDRACH, S. GILMAN AND I. WEINSTOCK, *J. Electrochem. Soc.*, 112 (1965) 1161.
11 H. DAHMS, M. GREEN AND J. WEBER, *Nature*, 195 (1962) 1310.
12 W. T. GRUBB AND L. W. NIEDRACH, *Proc. Ann. Power Sources Conf., 17, Atlantic City, New Jersey*, (1963) p. 69.
13 T. AKERBERG, *Z. Anorg. Allgem. Chem.*, 31 (1902) 161.
14 D. N. GRAIG AND I. H. HOFFMAN, *Nat. Bur. Std. (U.S.), Circ.*, (1953) 524.
15 J. GINER, *Electrochim. Acta*, 4 (1961) 42.
16 O. A. PETRY, B. I. PODLOVCHENKO, A. N. FRUMKIN AND H. LAL, *J. Electroanal. Chem.*, 10 (1965) 253.
17 S. B. BRUMMER, *J. Phys. Chem.*, 69 (1965) 1363.
18 O. A. KHAZOVA, YU. B. VASIL'EV AND V. S. BAGOTSKII, *Elektrokhimiya*, 2 (1966) 267.
19 M. W. BREITER, *Electrochim. Acta*, 10 (1965) 503.
20 S. B. BRUMMER, *J. Electrochem. Soc.*, 113 (1966) 1043.

ELECTROANALYTICAL CHEMISTRY AND INTERFACIAL ELECTROCHEMISTRY
Elsevier Publishing Company, Amsterdam – Printed in The Netherlands

INVESTIGATION OF THE KINETICS AND MECHANISM OF THE ELECTROREDUCTION OF NICKEL(II) IN THIOCYANATE AND THIOCYANATO–PYRIDINE MEDIA

Z. GALUS AND LJ. JEFTIC*
Department of Inorganic Chemistry, University of Warsaw, Warsaw (Poland)
(Received September 24th, 1966)

The mechanism and kinetics of the electroreduction of nickel(II) in thiocyanate-containing solutions have not been investigated to any great extent. A few papers[1–5] deal mainly with analytical problems, the determination of the stability constants of the complexes, and the kinetics of chemical reactions preceding charge transfer.

The reduction of nickel(II) in mixed (thiocyanate and pyridine)-containing solutions has not been investigated at all.

In this paper, the kinetic parameters of the electrode process and its mechanism are given and discussed.

Two methods for the determination of the rate constant of the electrode process were used. The first was based on the theory of irreversible polarographic waves given by KOUTECKY[6], and the second on the theory of cyclic voltammetry curves elaborated by NICHOLSON[7].

The first method is undoubtedly more precise but to determine standard rate constants, standard potentials have to be known. Owing to the instability of nickel amalgam[8], its preparation by the prolonged electroreduction of nickel(II) on a mercury pool electrode, followed by measurements of the potential of this amalgam in contact with the solution of nickel(II) salts, appeared impossible. Measurements must be performed under conditions of relative stability of the amalgam, which were determined earlier[9], using other methods. The determination of these potentials using the method proposed by KORYTA[10] is not precise because of the significant deviation of this system from reversibility. Standard, or rather formal, potentials especially at low thiocyanate concentrations were determined from the curves obtained using the hanging mercury drop electrode method proposed by RANDLES[11] for the determination of standard potentials from anodic–cathodic polarographic curves.

In the calculation of the rate constants, by the comparison of experimental curves showing larger or smaller deviations from reversibility with the theoretically reversible curve, the parameter, χ, for different potentials was obtained from the table of $F(\chi)$ functions given by KOUTECKY. This parameter is related to the reduction rate constant (k_1) at the potential, E, by the following:

$$\chi = \left(\frac{12t_1}{7D_1}\right)^{\frac{1}{2}} k_1 \left\{1 + \left(\frac{D_1}{D_2}\right)^{\frac{1}{2}} \exp \frac{nF(E-E_0)}{RT}\right\} \qquad (1)$$

* On leave of absence from the "Ruder Boskovic" Institute, Zagreb, Yugoslavia.

where t_1 is the drop time, E_0 the standard potential and D_1 and D_2 the diffusion coefficients of oxidized and reduced forms, respectively.

Formal rate constants were obtained from the plot of the logarithm of the reduction rate constant *vs.* potential. Transfer coefficients were calculated from the slope of the resulting lines.

The method proposed by NICHOLSON[7] is perfectly suitable in this case, since the calculation of the standard potential is unnecessary.

On the basis of peak potential separations, the parameter ψ was determined; this is related to the standard rate constant by the equation:

$$\psi = (D_1/D_2)^{\alpha} k_s/\sqrt{\pi n F V D_1/RT} \qquad (2)$$

where α is the transfer coefficient and V the rate of polarization. The disadvantage in this method is that the determination of a transfer coefficient is not possible.

EXPERIMENTAL

Reagents

$Ni(ClO_4)_2$ was obtained by neutralization of nickel carbonate with perchloric acid followed by crystallization.

Chemically pure KCNS was recrystallized from triple-distilled water.

All solutions were prepared with triple-distilled water, the third distillation being carried out in an all-quartz still.

Mercury was chemically purified and then twice-distilled in vacuum.

Apparatus

All polarographic and chronovoltammetric curves were recorded with the Radiometer PO4 polarograph. Potentials were measured with respect to the saturated calomel electrode. Experiments were performed at $25 \pm 0.2°$.

RESULTS

1. Nickel(II)–thiocyanate system

This system was investigated polarographically and the results (half-wave potentials and slopes of recorded curves) were similar to those reported in the literature.

At low concentrations of thiocyanate up to 0.01 M (with $5 \cdot 10^{-4}$ M Ni) three waves were observed, the magnitude of which was dependent on the drop time; the potential of the most negative agrees with that of hydrated nickel ions. The two more positive waves are evidently associated with the reduction of nickel–thiocyanate complexes. From the slope of the curves it could be supposed that this system is quasi-reversible in the polarographic condition, and that the polarographic determination of standard rate constants would be possible.

We also determined the half-peak potentials and the anodic and cathodic peak potentials from the curves recorded using the hanging mercury drop electrode. These results (mean values of four determinations) are given in Fig. 1 as a function of thiocyanate concentration. At low concentrations of SCN^-, the half-peak and peak

potentials are definitely negative, and the shift of these values to more positive potentials is observed with increase of thiocyanate concentration up to 0.2 *M*. A further increase in the concentration leads to a potential shift towards more negative values. The potential change in this region was linearly dependent on the logarithm of the concentration.

The magnitude of $\Delta E_{p/2.c.}/\Delta \log C_{SCN^-}$ or $\Delta E_{p.c.}/\Delta \log C_{SCN^-}$ was equal to 95 mV suggesting that the principal complex in this region of concentration has three thiocyanate ions bound to a nickel ion.

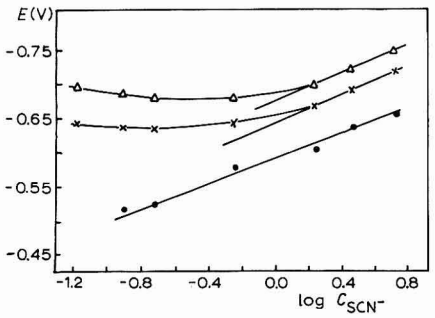

Fig. 1. The dependence of: (×), $E_{p/2.c.}$; (△), $E_{p.c.}$; (●), $E_{p.a.}$ on log C_{SCN^-}.

An inspection of the slope of the line representing the potential change of the peak of anodic oxidation of nickel from the amalgam *vs.* the logarithm of thiocyanate concentration, $\Delta E_{p.a.}/\Delta \log C_{SCN^-} = 90$ mV, indicates that the anodic process is not different from the cathodic process and that the final product of anodic oxidation is identical with a substrate of cathodic reduction.

The change of rate of charge transfer in a quasi-reversible system can be followed by an investigation of the separation between the potentials of the anodic and cathodic peaks.

In Fig. 2, the slope of the cathodic curves in terms of $(E_{p/2.c.} - E_{p.c.})$ is given, together with the difference between anodic and cathodic peak potentials, $E_{p.a.} - E_{p.c.}$. These data also represent the mean values of four measurements.

At low thiocyanate concentrations, these differences are strongly dependent on the thiocyanate concentration, suggesting that there is a change in the rate of the electrode process.

On the basis of the difference, $E_{p.a.} - E_{p.c.}$, the rate constants at formal potential were determined with the use of eqn. (2). Mean values obtained for various thiocyanate concentrations are given in Table 1.

The kinetics of the electrode process were investigated more extensively, by applying KOUTECKÝ's theory of polarographic irreversible curves. This was possible because even in chronovoltammetric conditions (where the rate of the transport of the depolarizer to the electrode was lower than under polarographic conditions) some deviations from reversibility were observed (Fig. 2).

Two sets of experiments for the calculation of standard rate constants were made, one with constant ionic force and varying concentrations of thiocyanate and the other with different concentrations of thiocyanate. The calculated mean values of rate constants and transfer coefficients are presented in Table 2.

Standard rate constants obtained from the curves recorded for the solutions containing different concentrations of thiocyanate (greater than 0.2 M) are similar. An insignificant decrease of the standard rate constants with increase of thiocyanate concentration from 0.6–5.5 M is visible. At concentrations of thiocyanate below

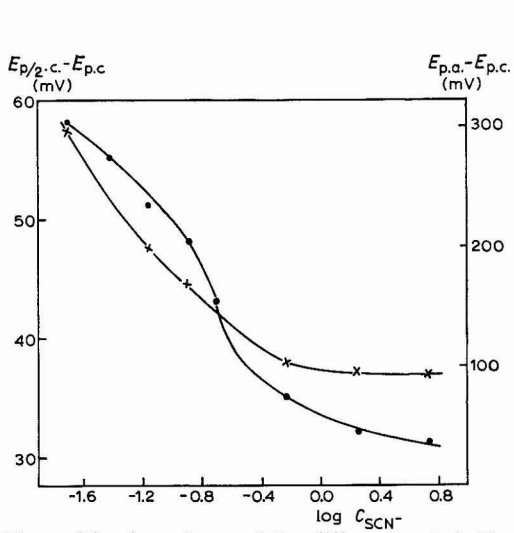

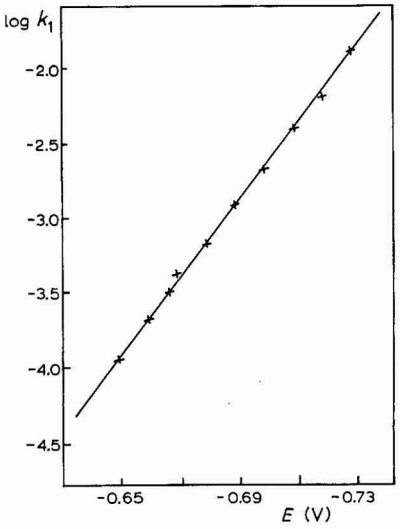

Fig. 2. The dependence of the differences: (•), $E_{p/2.c.}-E_{p.c.}$; (×), $E_{p.a.}-E_{p.c.}$, on log C_{SCN^-}.

Fig. 3. The dependence of the logarithm of the reduction rate constant on the potential.

TABLE 1

RATE CONSTANTS AT FORMAL POTENTIAL FOR THE Ni^{2+}–SCN^-/Ni(Hg) SYSTEM

KSCN concn. *(M)*	ψ	k_s *(cm sec^{-1} · 10^4)*
0.2	0.051	1.5
0.6	0.108	3.2
1.8	0.127	3.8
5.5	0.141	4.2

TABLE 2

KINETIC PARAMETERS OF THE ELECTRODE REACTION OF NICKEL(II) IN SOLUTIONS OF KSCN

Composition of soln.	*Standard rate constant* *(cm sec^{-1} · 10^4)*	*Transfer coefficient* *(α)*
0.2 M KSCN; 0.18 M $NaClO_4$	0.25	0.49
0.04 M KSCN; 0.16 M $NaClO_4$	0.63	0.50
0.07 M KSCN; 0.13 M $NaClO_4$	2.3	0.51
0.13 M KSCN; 0.07 M $NaClO_4$	2.7	0.53
0.2 M KSCN	2.9	0.60
0.6 M KSCN	3.4	0.66
1.8 M KSCN	3.1	0.73
5.5 M KSCN	2.5	0.75

0.2 M, the values of the standard rate constants decrease with decrease of thiocyanate ion concentration.

In all cases, the dependence of the reduction rate constant on the potential was linear. An example of this dependence is given in Fig. 3 for nickel(II) reduction in 1.8 M KSCN.

2. Nickel(II)–thiocyanate–pyridine (picolines) system

The kinetics of these systems were not investigated by us in detail. Application of KOUTECKÝ's method for standard rate constant calculations appeared impossible because a maximum was observed on all polarographic curves recorded for solutions containing nickel, thiocyanate and some amount of pyridine or picolines.

However, the kinetics could be estimated with good approximation on the basis of our chronovoltammetric experiments. The difference between cathodic and anodic peak potentials was assumed to be a measure of the rate of charge transfer. We started our experiments with an investigation of the behaviour of nickel(II) in 0.1 M KSCN. The difference between cathodic and anodic peak potentials was equal to 0.205 V, and the slope of the cathodic curves in terms of $(E_{p/2.c.} - E_{p.c.})$ was equal to 0.051 V. The standard rate constant for such a system determined by Koutecký's method was $2.5 \cdot 10^{-4}$ cm sec^{-1}. This experiment was followed by an investigation of a series of solutions containing the same quantity of nickel(II) and thiocyanate with the addition of varying amounts of pyridine or γ-picoline.

TABLE 3

THE EFFECT OF DIFFERENT CONCENTRATIONS OF PYRIDINE OR γ-PICOLINE ON THE CYCLIC VOLTAMMETRIC CURVES OF $5 \cdot 10^{-4}$ M Ni(II) IN 0.1 M KSCN

V = 0.8 V/min

Concn. ($\times 10^3$)		$E_{p.c.}$ *(V)*	$E_{p.a.} - E_{p.c.}$ *(V)*	$E_{p/2.c.} - E_{p.c.}$ *(V)*
pyridine	*γ-picoline*			
0		−0.695	0.205	0.051
1		−0.680	0.190	0.054
2		−0.685	0.190	0.052
4		−0.685	0.195	0.048
16		−0.730	0.260	0.012
	1	−0.675	0.190	0.057
	2	−0.720	0.235	0.029
	4	−0.770	0.375	0.018

The differences, $E_{p.a.} - E_{p.c.}$ and $E_{p/2.c.} - E_{p.c.}$, for these solutions are summarized in Table 3. All the data represent mean values of four experiments. It can be seen that the addition of small quantities of pyridine to the solution of nickel(II) in 0.1 M KSCN causes almost no change in the chronovoltammetric behaviour of nickel(II).

A small decrease of the difference, $E_{p.a.} - E_{p.c.}$, with respect to the difference for the solution without pyridine, suggests a slightly higher value of the standard rate constant then $2.5 \cdot 10^{-4}$ cm sec^{-1} found for the nickel(II)–0.1 M KSCN system. A considerable increase in this difference was noticed when the concentration of pyridine was increased to $1.6 \cdot 10^{-2}$ M; but a precipitate of a complex of nickel(II)

with thiocyanate and pyridine was already visible in the solution and this system could not, therefore, be investigated at higher concentrations of pyridine.

Similar behaviour was observed in the case of the nickel(II)–thiocyanate–γ-picoline system, but in this case the phenomenon of hindering of the rate of electrode reaction was observed even at lower γ-picoline concentration.

With increase of the difference, $E_{p.a.}-E_{p.c.}$, the slope of the curves increased. This slope was so great that it can be assumed that the reduction process under such conditions is adsorption-controlled.

DISCUSSION

The results presented in the experimental part enabled the rate constants of the charge transfer of the Ni(II)–SCN^-/Ni(Hg) system to be calculated. The experiments carried out also enabled us to identify the species reduced on the mercury electrode at different concentrations of thiocyanate ions in the solution.

From the dependence of $E_{p.c.}$, $E_{p/2.c.}$ and $E_{p.a.}$ on the logarithm of the SCN^- concentration one can assume that at concentrations exceeding 1.0 M (concentration of nickel(II) was $5\cdot10^{-4}\,M$) there exists in the solution mainly the $[Ni(SCN)_3]^-$ complex.

The dependence of $E_{p.c.}$, $E_{p/2.c.}$, and $E_{p.a.}$ on the SCN^- concentration is equivalent to $E_{1/2}=f(\log[SCN^-])$, because $E_{1/2}$ differs only by a constant from these potentials, assuming that the process is diffusion-controlled. This assumption was justified in our case, since the electrode process is moderately rapid and the rate of mass transport in our experiments was rather low.

KOUTECKÝ's theory was applied to determine the complexes reduced at low concentrations of SCN^-, when three waves are observed.

Assuming that the middle wave is associated with the reduction of the complex, MeX_m, than the first wave will be due to complex MeX_p which is formed from MeX_m in the transformations

$$MeX_m + X \rightleftharpoons MeX_{m+1} \tag{3}$$

$$MeX_{m+1} + X \rightleftharpoons MeX_{m+2} \tag{4}$$

$$MeX_{p-1} + X \underset{k_b}{\overset{k_f}{\rightleftharpoons}} MeX_p \tag{5}$$

which precede the electrode process.

The current of the first wave (i_k) will than be related to the concentration of X as follows:

$$i_k/(i_d - i_k) = 0.886\,(k_b t_1)^{\frac{1}{2}}\,[X]^{p-m} K_m \ldots K_p \tag{6}$$

where K_m and K_p are equilibrium constants, t_1 the drop time and i_d the current of the three waves.

Our experimental conditions do not fulfil exactly the conditions of applicability of such a relation, since three waves were observed at low SCN^- concentrations and the assumption that the concentration of thiocyanate does not change on the surface of the electrode in the course of the electrode process was only approximate.

However, this should have no significant effect on the result obtained by us

which indicates that two SCN^- ions are transferred in the chemical reaction preceding the charge transfer in the first wave.

This result was obtained on the basis of the log $\{i_k/(i_d-i_k)\}$–log[SCN^-] plot; the slope of $\Delta\log\{i_k/(i_d-i_k)\}/\Delta\log[SCN^-]$ was equal to 1.9. Since the $[Ni(SCN)_4]^{2-}$ complex does not exist at low concentrations of thiocyanate, it follows from these calculations that at low thiocyanate concentrations the complex $[Ni(H_2O)_5(SCN)]^+$ is reduced in the middle wave.

The wave at the most positive potentials is then—as we found—preceded by the reactions

$$[Ni(H_2O)_5(SCN)]^+ + SCN^- \rightleftharpoons [Ni(H_2O)_4(SCN)_2] + H_2O \quad (7)$$

$$[Ni(H_2O)_4(SCN)_2] + SCN^- \underset{k_b}{\overset{k_f}{\rightleftharpoons}} [Ni(H_2O)_3(SCN)_3]^- + H_2O \quad (8)$$

with a slow reaction (8). The complex $[Ni(H_2O)_3(SCN)_3]^-$ is reduced in this wave. This mechanism resembles that suggested, by TURYAN AND SEROVA[3].

The rate constants of the electrode process calculated using the two different methods are similar, but the results obtained using Koutecky's approach seem to be more precise. The decrease in the rate at higher thiocyanate concentrations may be due to a double-layer effect since an anion is discharged on a rather negatively-charged electrode. Since the cyclic voltammetry technique for the determination of the rate constant is rapid and gives results similar to those obtained by polarography, it should be widely applied especially to systems for which the standard potentials are not known.

Experiments performed with solutions containing nickel(II) ions and both pyridine and thiocyanate, indicate that at low concentrations of the organic compound, the nickel–thiocyanate complex predominates in the solution because the standard rate constant is almost identical to that obtained in nickel–thiocyanate solution. At higher concentrations of pyridine or picolines close to the critical point at which a precipitate begins to form, the slope of the chronovoltammetric curves increased and the rate of the electrode process decreased.

From an analysis of the slope of the curves recorded, it can be assumed that the reduction process under such conditions is adsorption-controlled. Two possible explanations for this behaviour can be considered.

First, the formation at higher pyridine (picolines) concentration of a mixed complex composed of pyridine and thiocyanate ions. This complex could be adsorbed on the surface. It is also possible that it could interact with an adsorbed layer of pyridine on the surface of the electrode. In this case the shape of the recorded i–V curves should indicate an adsorption-controlled process.

The second possibility is a change occurring only in the double layer of the electrode (in the solution of nickel(II)–thiocyanate complex). The substitution of the adsorbed layer of thiocyanate ions by pyridine molecules could also produce the observed phenomena. It seems, however, that the first of these possibilities is the more probable because the changes in electrochemical behaviour are observed at a concentration at which a clathrate is formed; this is a sparingly-soluble compound containing thiocyanate and pyridine or picoline molecules. The existence in solution of such a compound in equilibrium with the solid, seems probable.

ACKNOWLEDGEMENT

The authors are greatly indebted to Professor W. KEMULA for helpful discussions.

SUMMARY

The mechanism and kinetics of nickel(II) reduction in thiocyanate solutions have been investigated using polarography and cyclic voltammetry.

The process was found to be moderately rapid, and the rate constants determined by two methods for higher thiocyanate concentrations varied between 2 and $3 \cdot 10^{-4}$ cm sec^{-1}.

Three waves observed at low thiocyanate concentrations are associated with the reduction of $[Ni(H_2O)_3(SCN)_3]^-$, $[Ni(H_2O)_5(SCN)]^+$ and hydrated nickel(II) ions (at the first wave, middle wave, and the wave at the most negative potential, respectively).

In addition, studies were carried out on the mechanism of nickel(II) reduction in (thiocyanate and pyridine)-containing solutions.

REFERENCES

1 J. J. LINGANE AND H. KERLINGER, *Ind. Eng. Chem. Anal. Ed.*, 13 (1941) 77.
2 YA. I. TURYAN, *Zh. Fiz. Khim.*, 31 (1957) 2423.
3 YA. I. TURYAN AND T. F. SEROVA, *Zh. Fiz. Khim.*, 34 (1960) 1009.
4 YA. I. TURYAN AND T. F. SEROVA, *Dokl. Akad. Nauk SSSR*, 140 (1959) 125.
5 YA. I. TURYAN, *Dokl. Akad. Nauk SSSR*, 140 (1961) 416.
6 J. KOUTECKÝ, *Chem. Listy*, 47 (1953) 323.
7 R. S. NICHOLSON, *Anal. Chem.*, 37 (1965) 1351.
8 W. KEMULA AND Z. GALUS, *Bull. Acad. Polon. Sci. Classe* III, 7 (1959) 729.
9 Z. GALUS, *Bull. Acad. Polon. Sci., Ser. Sci. Chim.*, 14 (1966) 167.
10 J. KORYTA, *Electrochim. Acta*, 6 (1962) 67.
11 J. E. B. RANDLES, *Progress in Polarography*, Vol. 1, Interscience Publishers Inc., New York, 1962, p. 123.

ELECTROANALYTICAL CHEMISTRY AND INTERFACIAL ELECTROCHEMISTRY
Elsevier Publishing Company, Amsterdam – Printed in The Netherlands

POLAROGRAPHIC BEHAVIOUR OF IRON 2,2′-BIPYRIDINE COMPLEXES AT A PLATINUM MICROELECTRODE WITH PERIODIC RENEWAL OF THE DIFFUSION LAYER

FRANCESCO PANTANI AND GIULIANO CIANTELLI
Institute of Analytical Chemistry, University of Florence (Italy)
(Received July 25th, 1966; revised October 24th, 1966)

It is well known that 2,2′-bipyridine (Bip) yields a deep red complex, $[FeBip_3]^{2+}$, with Fe(II), which in acidic medium is oxidized giving the corresponding pale blue Fe(III) complex; the red complex is used as a reversible indicator with high standard oxidation potential (formal potential)[1,2]. A direct mixing of Fe^{3+} and 2,2′-bipyridine solutions results in a yellow instead of the blue complex, as with 1,10-phenanthroline and similar complexing agents, which have usually received greater attention than 2,2′-bipyridine, owing to the higher stability of the iron(II) complexes.

As BAXENDALE AND BRIDGE[3] have recently pointed out, the blue iron(III) complex is as easily photoreducible as, although to a less extent, the yellow complex. The formal potential for the $[FeBip_3]^{2+}$–$[FeBip_3]^{3+}$ redox couple in 0.01–12 M H_2SO_4 has been determined by SCHILT[4]; the data, corrected for the dissociation rate of the complex, are higher than those reported by SMITH AND RICHTER[5]. In a recent paper, ANDEREGG[6] described the determination of the structure and stability constants of the yellow iron(III) complexes with 1,10-phenanthroline and 2,2′-bipyridine, by potentiometric, magnetic and spectrophotometric measurements. In the case of 2,2′-bipyridine he reports log $K = 16.29$ and the more probable formula proposed for the yellow complex is

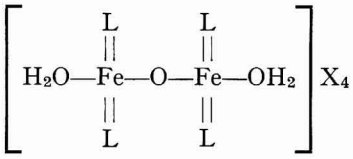

where L is the bidentate ligand and X is a monovalent ion. According to ANDEREGG such a structure is in a fair agreement with the behaviour of the complex and it must be preferred to the formula

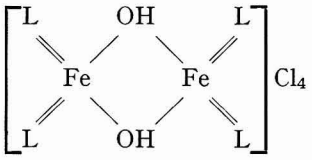

proposed by GAINES, HAMMETT AND WALDEN[7] for the yellow complex of 1,10-phenanthroline.

The present work contributes to the knowledge of the behaviour of iron complexes with 2,2′-bipyridine, by using the polarographic technique recently developed by COZZI, RASPI AND NUCCI[8] which is based on the use of a platinum microelectrode with periodic renewal of the diffusion layer (DLPRE).

REAGENTS AND INSTRUMENTATION

A 0.02 *M* solution of the $[FeBip_3]^{2+}$ red complex was obtained by mixing weighed amounts of iron(II) sulphate and 2,2′-bipyridine. The corresponding blue complex was always prepared immediately before the measurements, avoiding any excess of the oxidizing agent. The yellow complex of Fe^{3+} with 2,2′-bipyridine was also prepared immediately before the measurements, by mixing standard iron(III) nitrate and ligand solutions. Polarographic measurements were carried out with a Sargent model XV polarograph at 25° with a saturated calomel reference electrode. For the description and the use of the polarographic cell the reader is referred to the original paper[8].

A double-beam Tektronix 502 B cathode-ray oscillograph and a Metrohm Präzisionmodell E 187 potentiometer were also employed. All chemically pure reagents were assayed, if necessary, by standard analytical methods.

RESULTS AND DISCUSSION

The red iron(II) complex

The well known red complex, $[FeBip_3]^{2+}$, yields a well-developed anodic wave with DLPRE; no pre-treatement of the electrode such as pre-anodization or platinum black deposition is required and the recorded limiting current is proportional to the complex concentration. The logarithmic analysis of the current–potential curve gives

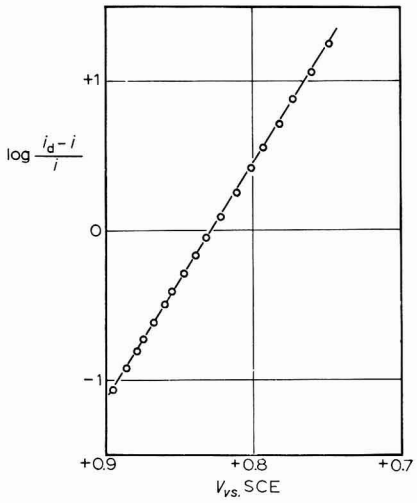

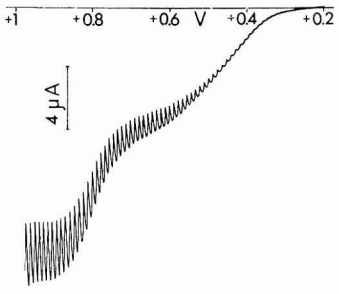

Fig. 1. Log. analysis of the anodic wave of 0.6 m*M* $[FeBip_3]^{2+}$ in 0.1 *M* K_2SO_4 at pH 5.7.

Fig. 2. Anodic wave of 1 m*M* $[FeBip_3]^{2+}$ + 1 m*M* Fe^{2+} in 0.1 *M* K_2SO_4, pH ~ 3.

a straight line with a 63-mV slope (Fig. 1). As expected, the oxidation involves one electron and the electrode process is reversible (see below).

The polarographic investigation is better performed in an almost neutral medium as it is known that $[FeBip_3]^{2+}$ undergoes dissociation in alkaline medium (resulting in a slow formation of the brown iron(III) hydroxide) as well as in acidic medium[4]; in fact, when a high concentration of H^+ ions is present there is a consistent protonation of 2,2′-bipyridine as a Brønsted base. Oxidimetric titrations with Ce(IV) have been performed in order to determine the amount of the complex which dissociates in a given time, producing free Fe^{2+}; within 1–2 days the solutions almost reach the composition corresponding to the competitive protonation and complexation equilibria (Table 1). The values given in the last column of this table have been calculated using data found in the literature ($pK_a = 4.34$ and $\log \beta_3 = 17.41$ at μ 0.01). A satisfactory agreement results and protonation should therefore be the only competitive reaction.

TABLE 1

CERIMETRIC DETERMINATION OF FREE Fe^{2+} IN AGED SOLUTIONS OF 0.8 mM $[FeBip_3]^{2+}$

pH	*Free* $[Fe]^{2+}$ *(mM)*		
	Found after 48 h	*Found after 2 weeks*	*Calcd.*
1.68	0.252	0.250	0.290
2.12	0.120	0.122	0.145
2.60	0.055	0.056	0.065
3.10	0.029	0.024	0.029

The polarographic investigation of identical solutions also gave concordant results. It can be seen in Fig. 2 that the anodic steps of the free Fe^{2+} and 2,2′-bipyridine complex are largely separated. The half-wave potential of the step of the complex examined is slightly dependent on the medium composition; at pH 5.7, the measured value of $E_{\frac{1}{2}}$ is +0.824 V (SCE), which corresponds to the $E°$-value determined by potentiometric titrations[4]. When the acidity increases, $E_{\frac{1}{2}}$ shifts towards less positive potentials (*e.g.* +0.750 V in 1 M H_2SO_4); however, owing to the fact that the solutions are not stabilized (in 1 M H_2SO_4 stabilization would correspond to a complete dissociation) the meaning of the reported shift is still open to question.

No visible influence is exerted on $E_{\frac{1}{2}}$ by a 2,2′-bipyridine excess, in agreement with a reaction scheme where the ligand concentration is not apparent

$$[FeBip_3]^{2+} \rightleftharpoons [FeBip_3]^{3+} + e$$

An average increase of about 1.5%/degree for the limiting current ($E_{\frac{1}{2}}$ remaining constant) is recorded with a temperature variation from 20–50°, which is consistent with a diffusion-controlled reversible electrode process. This property is established by following the value of the limiting current as t_{tot} (the period between two successive renewals) is varied. Under the conditions of the present work t_p, the time in which the diffusion layer is renewed, exerts a large influence on the value of the measured current; the limiting current, corrected for this contribution is

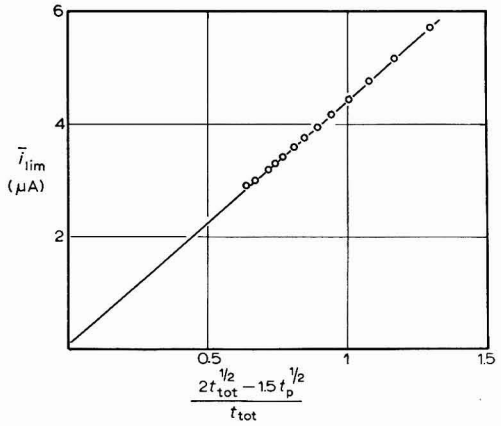

Fig. 3. Average limiting current of 0.6 mM $[FeBip_3]^{2+}$ in 0.1 M K_2SO_4 as a function of the corrected renewal period.

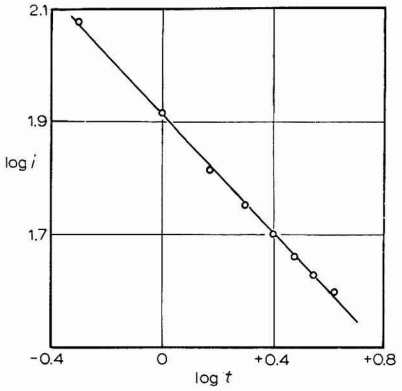

Fig. 4. Log. analysis of the oscillographic curve on 1 mM $[FeBip_3]^{2+}$ in 0.1 M K_2SO_4.

$$\bar{i} = a + b\,\frac{2t_{tot}^{\frac{1}{2}} - 1.5t_p^{\frac{1}{2}}}{t_{tot}}$$

where $a = nFADC/r$ is the contribution of the spherical diffusion and $b = nFAD^{\frac{1}{2}}C/\pi^{\frac{1}{2}}$ is that of planar diffusion. Setting $(2t_{tot}^{\frac{1}{2}} - 1.5t_p^{\frac{1}{2}})/t_{tot}$ as variable, a previous oscillographic evaluation of t_p is necessary; t_p, under the conditions of the present work, was 23 msec. A plot if $\bar{i}$ against $(2t_{tot}^{\frac{1}{2}} - 1.5t_p^{\frac{1}{2}})/t_{tot}$ results in a straight line (Fig. 3) for t_{tot} in the usual polarographic range of 2–8 sec; beyond 8 sec, the diffusion process is disturbed and measurements are unreliable. From the slope of the straight line one can obtain $b = 4.5 \times 10^{-6}\ A$; and from the intersection with the ordinate axis $a = 0.1 \times 10^{-6}\ A$. Such data, in principle, could enable the diffusion coefficient, D, to be calculated if the electrode surface area, A, is known; but a microscopical examination of the platinum microelectrode revealed a rough surface the area of which, therefore, could not be optically measured.

More detailed information about the electrode process and the electrochemically efficient electrode surface has been obtained from the oscillographic recording of the i–t curve at a constant applied potential between two renewals of the diffusion layer, according to the technique described by MARK AND REILLEY[9]. The platinum microelectrode behaves as stationary between two successive renewals of the diffusion layer; if such a condition is fulfilled in a polarographically-reversible process, the instantaneous current at fixed potential varies with time according to the well known relation for spherical diffusion

$$i_t = a + bt^{-\frac{1}{2}}$$

where a and b have the meanings previously reported. A typical plot of log i *vs.* log t (Fig. 4) is practically a straight line with a slope of -0.52, which is in satisfactory agreement with the value -0.50 which would result from a negligible contribution by a. Identical results were obtained at any point along the wave, confirming the previous conclusions on the reversibility of the electrode process reported on the basis

of the measurements of the average currents. In the values of a and b obtained from the plot of Fig. 4, the surface area, A, is the electrochemically efficient one; this value, different from that obtained by optical measurements, can be indirectly calculated through comparison with a reversibly-oxidized substance the diffusion coefficient of which is known, *e.g.*, cyanoferrate(II) ion for which STACKELBERG *et al.*[10] give $D = 6.50 \times 10^{-6}$ cm^2 sec^{-1} at 25° in 0.1 M KCl. Once the effective surface area has been found in this way, from a measure of the instantaneous current on the limiting plateau of $[FeBip_3]^{2+}$, the diffusion coefficient of the complex has been evaluated as $D = 4.6 \times 10^{-6}$ cm^2 sec^{-1} at 25° in 0.1 M K_2SO_4.

The blue iron(III) complex

The red complex can be chemically oxidized to give the well known blue complex. Suitable oxidizing agents usually require an acidic medium which, however, does not represent the best conditions for investigations as the range for reasonable stability of the blue complex is fairly critical. In practice, in acidic medium the competition of the hydrogen ion produces a considerably fast dissociation as for the iron(II) red complex. On the other hand, by increasing the pH to about 3, the blue complex is transformed in a short time into the yellow complex, the behaviour of which is discussed below. Furthermore, the possibility of photoreduction[3] requires operations in the dark. Once the blue complex is obtained, a very fast polarographic measurement is necessary or, better, a sequence of measurements with extrapolation to zero time. The extent of dissociation may be measured by potentiometric titrations: the results for various H^+ concentrations are shown in Fig. 5.

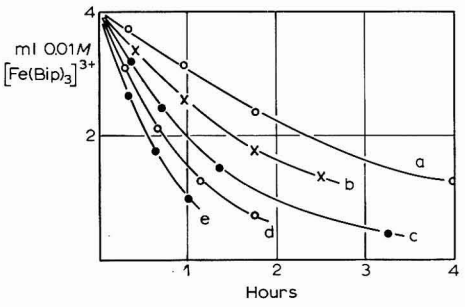

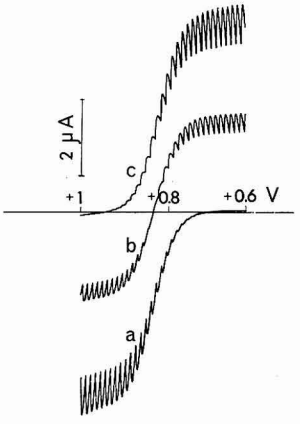

Fig. 5. Decrease of $[FeBip_3]^{3+}$ concn. with time at 18° in: (a), 0.02; (b), 0.07; (c), 0.25; (d), 0.75; (e), 2 M H_2SO_4 (from iodometric titrations).

Fig. 6. Polarographic waves obtained from (a) 0.8 mM red $[FeBip_3]^{2+}$; (b), 0.4 mM $[FeBip_3]^{2+}$ + $[FeBip_3]^{3+}$; (c), 0.8 mM blue $[FeBip_3]^{3+}$.

Nevertheless, the polarographic examination reveals a well-developed cathodic wave for the blue solutions (Fig. 6) in the same range of applied potential as for the red complex. The logarithmic analysis of the current *vs.* potential yields a linear plot with a slope corresponding to a one-electron exchange, and a cathanodic wave is recorded from solutions containing a mixture of the two complexes; these facts

confirm that the electrode reduction

$$[FeBip_3]^{3+} + e \rightleftharpoons [FeBip_3]^{2+}$$

is a reversible process.

In the 0.2–2 mM range, the wave height is proportional to the blue complex concentration, so that it is possible to follow its dissociation polarographically. The results in Fig. 7 show the influence of acidity: when the acidity is increased, the limiting current is lowered and $E_{\frac{1}{2}}$ shifts toward less positive values of the applied potential (*e.g.*, in 5 M H_2SO_4 $E_{\frac{1}{2}} = +0.64$ V); the dissociation rate increases even if solutions are kept in the dark. When the H_2SO_4 concentration is raised to 8 M, the

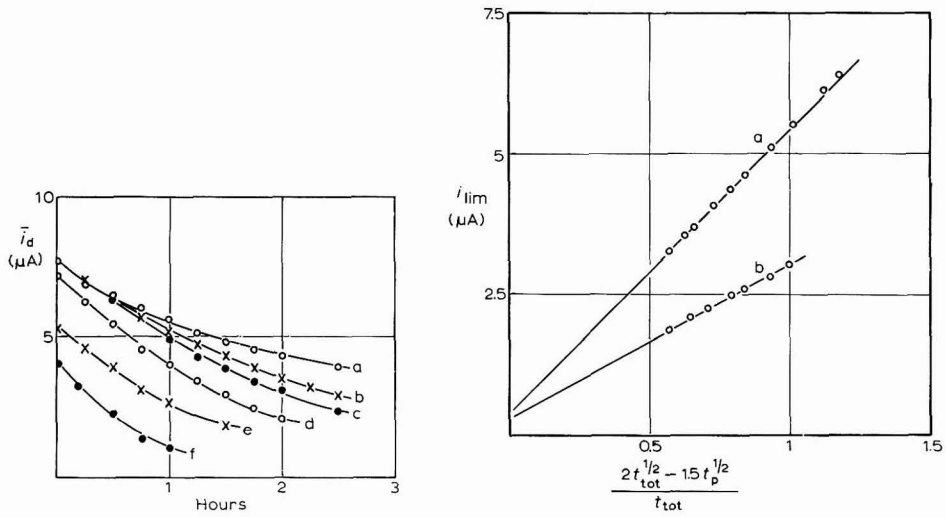

Fig. 7. Decrease of $[FeBip_3]^{3+}$ concn. with time at 18° and pH: (a), 2.6; (b), 1.95; (c), 1.8 and in (d), 1; (e), 2; (f), 5 M H_2SO_4.

Fig. 8. Average limiting current of 0.8 mM $[FeBip_3]^{3+}$ in (a), 0.2 M; (b), 4 M H_2SO_4 as a function of the corrected renewal period.

limiting current further decreases, $E_{\frac{1}{2}}$ is shifted toward less positive values (+0.48 V) and, usually, the wave appears to be poorly defined. In such a medium, no longer to be considered a truly aqueous one, the dissociation rate of the blue complex is considerably lowered, contrary to the behaviour of the red complex the dissociation of which is very fast. Therefore, by adding a small amount of Fe^{2+} to a blue complex solution, a fast dissociation can be observed, since the mechanism is no longer in agreement with the scheme

$$[FeBip_3]^{3+} + 3\,H^+ \xrightarrow{\text{slow}} Fe^{3+} + 3\,HBip^+$$

but it may possibly occur according to the following reactions which are in agreement with the polarographically observed behaviour

$$\begin{array}{ccc} Fe^{2+} + [FeBip_3]^{3+} & \xrightarrow{\text{fast}} & Fe^{3+} + [FeBip_3]^{2+} \\ \uparrow & & \downarrow \\ Fe^{2+} + 3\,HBip^+ & \xleftarrow{\text{fast}} & 3\,H^+ + [FeBip_3]^{2+} \end{array}$$

The cyclic mechanism accounts for the high rate of the dissociation process. Nevertheless, at any acidity, the average limiting current follows the spherical diffusion law, as tested by the data in Fig. 8, which is very similar to the Fig. 3 for the red complex.

Oscillographic measurements in 0.1 M K_2SO_4 + 0.5 N H_2SO_4 as in the previously reported procedure, gave a slope for the log i_t–log t plot almost identical with the theoretical value, −0.50, thus confirming control by diffusion also for the blue complex reduction. A diffusion coefficient, $D = 3.6 \times 10^{-6}$ cm^2 sec^{-1}, has been calculated for the blue complex, but, owing to the rapid dissociation of the complex itself, a higher uncertainty must be attributed to this datum in comparison with the analogous result for the red complex.

The yellow iron(III) complex

When the red iron(II) complex is electrochemically oxidised using a platinum anode, coulometric measurements are in agreement with the previous data, as the anodic wave disappears with an amount of electricity corresponding to 1 F/mole. The formation of the blue iron(III) complex is not easily followed, since in acidic medium it partially dissociates during its electrolytic generation; in a slightly acidic medium a fast transformation into a yellow complex occurs. On the other hand, it must be taken into account that several minutes are required before the polarogram can be recorded even with an electrolysis at relatively high current density (in any case with a 100% current efficiency). For example, after a 60% oxidation of the red complex (10 min were required, see Fig. 9) a composite cathodic–anodic wave appears

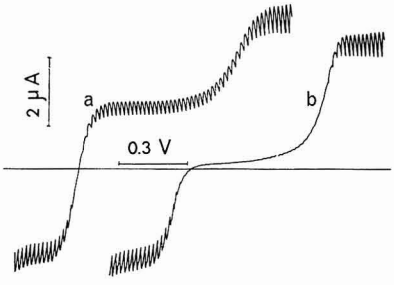

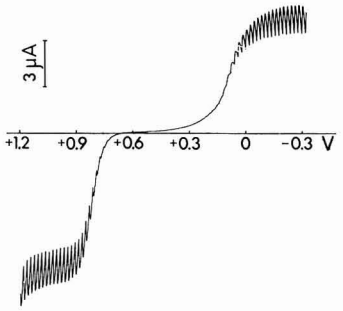

Fig. 9. Polarographic waves on 60% electrolytically-oxidized red complex in the presence of an excess of 2,2′-bipyridine: (a), immediately after electrolysis; (b), after about 30 min.

Fig. 10. Polarographic wave from a soln. containing 1 mM $[FeBip_3]^{2+}$ and 1 mM Fe^{3+} + 7 mM 2,2′-bipyridine in 0.1 M KNO_3 (*i.e.*, equiv. amounts of the red and the yellow complex in the presence of an excess of ligand).

the anodic branch of which is due to the residual red complex and the cathodic branch to a part of the electrolytically generated blue complex, while at less positive applied potentials the cathodic wave relative to the yellow iron(III) complex is clearly observed. On aging, a complete transformation of the blue form into the yellow form occurs and a sharp separation into a cathodic and an anodic step is polarographically recorded. This transformation is progressively more easy as the pH of the solution is increased.

The yellow iron(III) complex obtained by aging of the blue solutions possesses

the same properties as the complex obtained when 2,2′-bipyridine is added to an iron(III) solution, the dimeric formula of which has been elucidated by ANDEREGG[6]; therefore the study of this complex has been performed on solutions prepared directly by mixing iron(III) and ligand solutions. The separation between the wave of the red complex and the wave of the yellow complex obtained in such a way is reported in Fig. 10. The height of the reduction wave of the yellow complex is proportional to the analytical iron(III) concentration, but its shape varies with electrode pretreatments. Two limiting curves are reported in Fig. 11 relative to a strong reduction (electrochemical evolution of hydrogen for 1 min) and to a strong oxidation (electrochemical evolution of oxygen for 1 min) of the electrode. By keeping the solutions in the dark in order to avoid photoreduction, results do not show any variation after a several days aging.

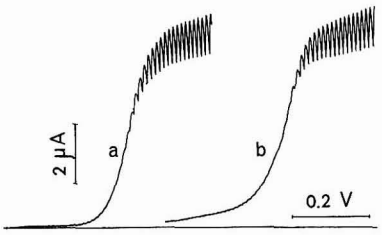

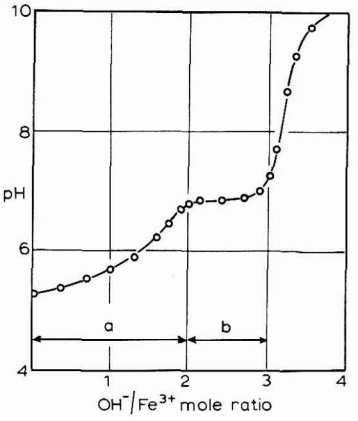

Fig. 11. Polarographic waves of the yellow complex, obtained from 1 mM Fe^{3+} + 7 mM 2,2′-bipyridine, in 0.1 M KNO_3 on (a), pre-reduced; (b), pre-oxidized DLPRE.

Fig. 12. Alkalimetric titration of 1 mM Fe^{3+} + 2,2′-bipyridine in excess (yellow complex): (a), neutralization of $HBip^+$; (b), precipitation of iron(III) hydroxide.

The stability of the yellow complex is not maintained in alkaline medium; the alkalimetric titration of a solution with a Fe^{3+}/2,2′-bipyridine ratio of 1:10 results (Fig. 12) in a consumption of 2 OH^-/mole of iron(III), (in agreement with ANDEREGG) after which the solution becomes turbid, owing to the precipitation of iron(III) hydroxide. An electrolysis using a platinum electrode results in the complete reduction to the red complex, but the separation of the two waves indicates that this is not a reversible process.

When the pH or the 2,2′-bipyridine concentration is increased, the half-wave potential shifts towards less positive values. For example, with a 0.01 M 2,2′-bipyridine analytical concentration, $E_{\frac{1}{2}}$ is found at +0.138 V for pH 3.4 and +0.082 V for pH 5.1, which indicates a progressively more difficult reduction when the concentration of the complexing species (*i.e.*, OH^- and 2,2′-bipyridine) increases. However, no quantitative conclusions can be drawn from this shift owing to an overlapping of the ligand protonation with the complexation in this pH range, and the irreversibility of the electrode process.

In fact, a small pre-wave is present at the beginning of the polarographic cathodic curve, and is more evident the higher the temperature, as shown in Fig. 13. According to the data in Table 2, an increase of 6.7%/degree is found for the pre-wave height, indicating that it is of kinetic nature, while the height of the true cathodic step increases in the usual way of a diffusion-controlled wave. The half-wave potential shifts 3.3 mV/degree towards more positive values as a consequence of the irreversible

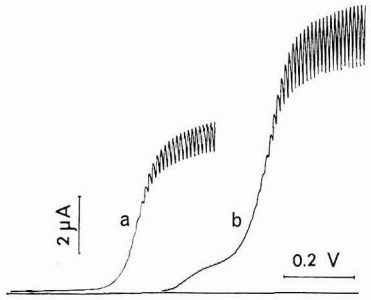

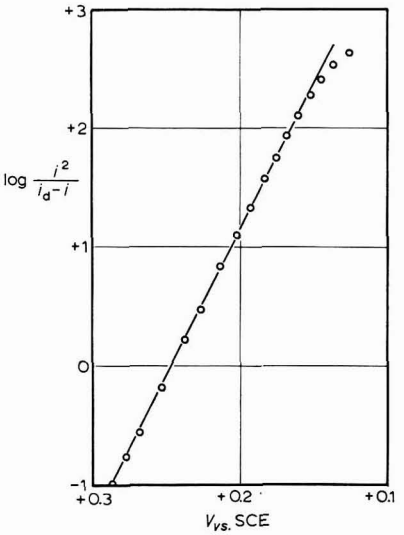

Fig. 13. Polarographic waves of the yellow complex, obtained from 1 mM Fe^{3+} + 5 mM 2,2′-bipyridine, in 0.1 M KNO_3: (a), at 15°; (b), at 50°.

Fig. 14. Log. analysis of the polarographic wave of the yellow complex.

TABLE 2

POLAROGRAPHIC CHARACTERISTICS AT VARIOUS TEMPERATURES FOR THE YELLOW COMPLEX (AS IN FIG. 13) ON PRE-REDUCED DLPRE

Temp. (°C)	*Limiting current* (μA)		$E_{\frac{1}{2}}$ (*V vs. SCE*)
	1st step	*2nd step*	
25	0.24	5.36	+0.140
30	0.35	5.75	+0.156
35	0.44	6.28	+0.168
40	0.56	6.72	+0.184
45	0.76	7.24	+0.198
50	1.01	7.50	+0.222

nature of the electrode process. The log plot of the wave (Fig. 14) clearly confirms this irreversibility; since the yellow complex is binucleate[6], a possible reaction scheme is

$$[Fe^{III}Bip_x]_2 + 2\,(y-x)\,Bip + 2e \rightarrow 2\,[Fe^{II}Bip_y]$$

so that in the logarithmic term the second power of the reduced form concentration must be considered. A plot of $\log i^2/(i_d - i)$ *vs.* E results in a straight line with a 41-mV slope, very far from the theoretical 29.5 mV for a reversible process.

If the limiting current is recorded at various renewal times, when the pre-wave is not apparent, the usual linear plot of the diffusion-controlled currents results (Fig. 15); on the contrary at 50°, the height of the pre-wave does not change in the range of 2.55–8 sec renewal times. This kinetic nature of the pre-wave is better demonstrated by means of oscillographic measurements.

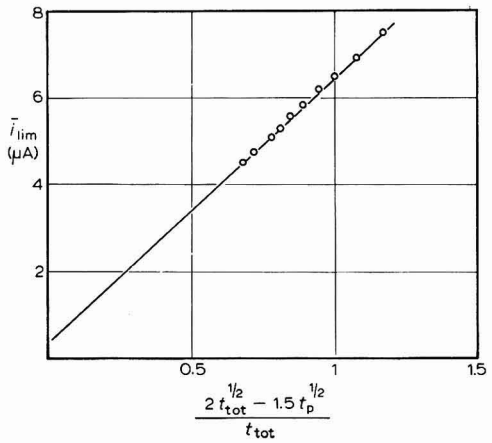

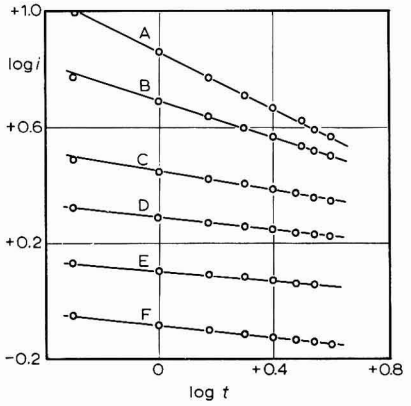

Fig. 15. Average limiting current of 0.5 mM yellow complex in 0.1 M KNO_3 as a function of the corrected renewal period.

Fig. 16. Log. analysis of the instantaneous currents oscillographically recorded at constant potential along the polarographic wave of the yellow complex. Ratio i/i_{lim}: (A), 1.00; (B), 0.667; (C), 0.333; (D), 0.191; (E), 0.103; (F), 0.065.

For a completely irreversible cathodic electrode process occurring at a plane electrode, the instantaneous current at the beginning of the polarographic wave is[11]

$$i_t = nFAk_1C,$$

typical of a kinetically-controlled current, independent of t and D. When the applied potential becomes more negative (upper portion of the wave), the limiting current is given by

$$i_{lim} = nFACD^{\frac{1}{2}}/(\pi t)^{\frac{1}{2}},$$

typical of a diffusion-controlled polarographic wave; it is apparent by a transition from a purely kinetic current to a purely diffusion-controlled one. Research in progress in this laboratory[12] on electrochemically irreversible systems, has demonstrated that the previous theoretical deductions are suitable for the DLPRE. The electrode is here considered plane, but such an assumption does not constitute a serious restriction owing to the partially kinetic nature of the process, being a kinetic current independent of the electrode shape. According to this treatment, in a log i_t *vs.* log t plot there is a transition from a straight line with zero slope to a straight line with a slope, −0.50. Experimental results (Fig. 16) substantiate this conclusion; however, a slope nearly

equal to zero is observed for a larger region along the wave than one could expect for a purely irreversible process. This behaviour can be explained by assuming the presence of a kinetic process (different from that responsible for the limiting current) which contributes to keep the current constant. As has been pointed out, this kinetic pre-process is better revealed at high temperature when a small ill-defined step appears; nevertheless, oscillographic data clearly show that the process has a sensible effect also when a single nearly regular polarographic wave appears. The kinetic contribution to the total current is not easily and certainly distinguished, thus preventing a reliable evaluation of the diffusion coefficient of the yellow complex according to the previously reported method.

The average polarographic current at DLPRE can be computed by dividing the total amount of electricity by the electrolysis time[8]. In the case of a completely irreversible electrode process[12]:

$$\frac{\bar{\imath}}{\bar{\imath}_d} = \frac{\pi^{\frac{1}{2}}}{(2-1.5x)} \cdot \frac{1}{\lambda} \left\{ \exp(\lambda^2)\, \mathrm{erfc}(\lambda) + \right.$$

$$\left. + \frac{2}{\pi^{\frac{1}{2}}}\, \lambda(1-x) + \exp(\lambda^2 x^2)\, \mathrm{erfc}(\lambda x) \left(\frac{\lambda^2 x^2}{2} - 1 \right) \right\} \quad (1)$$

where

$$x = t_p^{\frac{1}{2}} / t_{tot}^{\frac{1}{2}} \,. \quad (2)$$

When (1) is plotted against log λ, several curves are obtained, corresponding to the various x-values. In any single case the experimental determination of $\bar{\imath}$ and $\bar{\imath}_d$ allows the evaluation of λ. Since

$$\log \lambda = \frac{\log t_{tot}^{\frac{1}{2}} k_0}{D^{\frac{1}{2}}} - \frac{\alpha n F}{2.3\, RT}\, E \quad (3)$$

a plot of log λ *vs.* E gives a straight line of slope $= -\alpha n F / 2.3\, RT$, as has been confirmed by using the irreversible system thallium(III)–thallium(I) on a smooth platinum DLPRE.

The log λ *vs.* E plot from the polarographic data of the yellow complex is reported in Fig. 17 where two slopes are clearly observable; this fact confirms the oscillographic data for the instantaneous currents, again suggesting that two different processes are present along the polarographic wave.

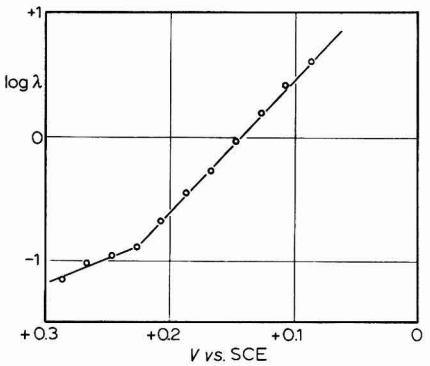

Fig. 17. Variation of log λ as a function of the applied potential along the polarographic wave of the yellow complex.

ACKNOWLEDGEMENT

The financial support by the Italian National Research Council (CNR) is gratefully acknowledged.

SUMMARY

The red tris(2,2′-bipyridine)iron(II) complex is oxidized at a platinum electrode with periodic renewal of the diffusion layer, yielding a well-developed wave the limiting current of which is found to be diffusion-controlled. Also, the blue tris-(2,2′-bipyridine)iron(III) complex undergoes a reversible electrode process. On aging, the blue complex is transformed into a yellow complex, identical to that obtained by a direct mixing of iron(III) and 2,2′-bipyridine solutions. The irreversible reduction wave of this complex shows a small pre-wave, the current of which appears to be kinetically controlled. The characteristics of the instantaneous currents have also been investigated oscillographically.

REFERENCES

1 D. N. HUME AND I. M. KOLTHOFF, *J. Am. Chem. Soc.*, 65 (1943) 1895.
2 F. W. CAGLE AND G. F. SMITH, *Ind. Eng. Chem., Anal. Ed.*, 19 (1947) 384.
3 J. H. BAXENDALE AND N. K. BRIDGE, *J. Phys. Chem.*, 59 (1955) 783.
4 A. A. SCHILT, *Anal. Chem.*, 35 (1963) 1599.
5 G. F. SMITH AND F. P. RICHTER, *Ind. Eng. Chem., Anal. Ed.*, 16 (1944) 580.
6 G. ANDEREGG, *Helv. Chim. Acta*, 45 (1962) 1643.
7 A. GAINES, L. P. HAMMETT AND G. H. WALDEN, *J. Am. Chem. Soc.*, 58 (1936) 1668.
8 D. COZZI, G. RASPI AND L. NUCCI, *J. Electroanal. Chem.*, 12 (1966) 36.
9 H. B. MARK AND C. N. REILLEY, *J. Electroanal. Chem.*, 3 (1962) 54.
10 M. VON STACKELBERG, M. PILGRAM AND V. TOOME, *Z. Elektrochem.*, 57 (1953) 342.
11 P. DELAHAY, *New Instrumental Methods in Electrochemistry*, Interscience, New York, 1954.
12 D. COZZI, G. CIANTELLI AND R. GUIDELLI, unpublished work.

ELECTROANALYTICAL CHEMISTRY AND INTERFACIAL ELECTROCHEMISTRY
Elsevier Publishing Company, Amsterdam – Printed in The Netherlands

THE NATURE AND ORIGIN OF THE MULTIPLE POLAROGRAPHIC WAVE OBSERVED DURING THE ONE-ELECTRON REDUCTION OF AQUATED BIS(ETHYLENEDIAMINE)COBALT(III) IONS

ROBERT C. HENNEY, HENRY F. HOLTZCLAW, JR. AND ROBERT C. LARSON
Department of Chemistry, University of Nebraska, Lincoln, Nebraska (U.S.A.)
(Received August 25th, 1966)

In a previous study of the polarographic behavior of cobalt(III) coordination compounds[1], two waves were noted for the one-electron reduction of diacidobis-(ethylenediamine)cobalt(III) ions. The second of these waves had a half-wave potential common to all of the species exhibiting the two waves and it was postulated that it was due to a common species in all of the solutions. This common electroactive species was believed to be an aquated bis(ethylenediamine)cobalt(III) ion arising from hydrolysis of the parent compound.

MAKI *et al.*[2] observed two waves for the polarographic reduction of the dibromo- and dichloro-bis(ethylenediamine)cobalt(III) ions and attributed the second of the waves to an aquated species. They also reported some data on the reduction of the aquohydroxobis(ethylenediamine)cobalt(III) ion. MASON AND WHITE[3] have recently investigated the nature of the double wave observed in the reduction of the dinitrobis-(ethylenediamine)cobalt(III) ion.

Diacidobis(ethylenediamine)cobalt(III) ions have been of much interest in recent years in the study of solvolysis. It has been found that one or both of the acido ligands can frequently be replaced by solvent molecules, leaving the solvated bis-(ethylenediamine)cobalt(III) substrate. In preparation for studies of hydrolysis, an investigation was made of the polarographic characteristics of several aquated bis(ethylenediamine)cobalt(III) ions, the products of hydrolysis.

EXPERIMENTAL

Reagents and solutions

Trans-dithiocyanato- and *trans*-aquothiocyanato-bis(ethylenediamine)co-balt(III) nitrate, aquopentamminecobalt(III) perchlorate, aquoammine- and *cis*- and *trans*-aquohydroxo-bis(ethylenediamine)cobalt(III) bromide and tris(ethylene-diamine)cobalt(III) chloride were prepared by standard methods found in the literature[4–7].

The cell solutions were made 0.10 M in potassium nitrate and 1.00×10^{-3} M in cobalt complex by dissolving the weighed solid compounds and diluting to volume. Nitric acid or potassium hydroxide solution was added to adjust the pH to the desired level. In the case of the halide salts, an equivalent amount of silver nitrate was added to the solutions and the silver halide filtered off. Since all bis(ethylenediamine)-cobalt(III) ions are known to isomerize in solution to reach a *cis–trans* equilibrium,

the solutions were allowed to stand for 2–3 days before recording the polarograms. Previous work has indicated that no significant differences are to be expected in the polarographic behavior between the *cis*- and *trans*-isomers used in this study[1]. Polarograms of basic fresh solutions (about 6 min were required for dissolution, filtering, and recording) of both isomers of the aquohydroxobis(ethylenediamine)-cobalt(III) ions were compared and found to be identical at comparable pH-values. For the dithiocyanatobis(ethylenediamine)cobalt(III) ion, the *trans*-isomer was used and since it is believed to undergo slow aquation, only fresh solutions (less than 24 h old) were used. Reproducible results were obtained.

Nitrogen was bubbled through the cell solution for 10–15 min before each polarogram was recorded, and a nitrogen atmosphere was maintained above the solution during the recording. The cell was immersed in a water bath thermostatically controlled at $25.0 \pm 0.1°$.

Maximum suppressors were not used.

Apparatus

A Leeds and Northrup Electrochemograph, Type E, was used to obtain the current–voltage curves. The electromotive force recorded by the instrument was checked periodically with a potentiometer. The standard H-type cell (No. 7733-D) supplied with the Electrochemograph was used with the dropping mercury electrode. Both arms of the cell were filled with the electrolysis solution. The saturated calomel reference electrode was placed in one side-arm with the tip of the calomel electrode well below the fritted disk, and maintained there only while the polarograms were being run. In this manner, chloride ion from the calomel was prevented from diffusing into the polarographic compartment. The resistance of the cell solution was checked with a conductance bridge and all potentials were corrected for iR-drop.

pH-measurements were made immediately before and after each recording with a Leeds and Northrup Model 7401 pH meter standardized at pH-values of 4.01 and 6.86.

RESULTS

Unbuffered solutions

In acidic ($pH < 3$) unbuffered 0.10 M potassium nitrate solution, the one-electron reduction from the cobalt(III) to the cobalt(II) state of all the aquated bis(ethylene-diamine)cobalt(III) ions studied and also the aquopentaamminecobalt(III) ion takes place in a single irreversible wave at half-wave potentials between 0.08 and −0.08 V *vs.* the saturated calomel electrode (SCE). At pH 3, a second irreversible wave appears at *ca.* −0.4 V *vs.* SCE, the height of which increases with increasing pH accompanied by an almost corresponding decrease in the height of the first wave. At high pH, the second wave replaces either half or all of the first wave, depending upon the ion involved. At pH-values between 3 and 10, both waves are observed. In the case of the aquoamminebis(ethylenediamine)cobalt(III) ion, a third, intermediate wave is observed between pH 3.0 and 3.3 at a half-wave potential *ca.* −0.25 V *vs.* SCE; above pH 3.3, it is believed to be merged with the last (most negative) wave. This accounts for the more positive half-wave potential of the most negative wave at low pH as compared with the most negative wave of the other ions. With aquo-

hydroxobis(ethylenediamine)cobalt(III) ion, as the pH is raised above 3, an intermediate wave of half-wave potential of *ca.* −0.06 V *vs.* SCE becomes discernible with a maximum height at pH 3.3 of *ca.* 0.44 of the total wave height; it disappears at *ca.* pH 10.

The half-wave potentials of the first waves appear to be virtually independent of pH, an exception being that of the aquothiocyanatobis(ethylenediamine)cobalt(III) ion, which shifts to more negative potentials with increasing pH (see Table 1).

The half-wave potentials of the most negative waves of the aquoammine- and aquothiocyanatobis(ethylenediamine)cobalt(III) ions and of the aquopentamminecobalt(III) ion change only slightly with pH. The half-wave potential of the most

TABLE 1

POLAROGRAPHIC DATA FOR THE FIRST (MOST POSITIVE) WAVE OF THE ONE-ELECTRON REDUCTION OF *trans*-AQUOTHIOCYANATOBIS(ETHYLENEDIAMINE)COBALT(III) ION IN UNBUFFERED, 0.10 *M* POTASSIUM NITRATE SOLUTION

pH	$E_{\frac{1}{2}}$	i_{d_1}/i_{d_T}	*Slope*
2.48	0.08	1.00	0.21
3.30	0.04	0.94	0.19
4.29	0.01	0.82	0.18
5.37	−0.01	0.81	0.17
6.41	−0.05	0.77	0.16
7.13	−0.07	0.74	0.14
8.52	−0.07	0.71	0.12
9.29	−0.11	0.68	0.11
9.71	−0.14	0.61	0.10
9.97	−0.16	0.59	0.11
10.65	−0.20	0.5	0.11
10.83	−0.21	0.5	0.10

TABLE 2

POLAROGRAPHIC DATA OF THE FIRST (MOST POSITIVE) AND LAST ONE-ELECTRON REDUCTION WAVES OF AQUATED m*M* COBALT(III) IONS IN UNBUFFERED 0.10 *M* POTASSIUM NITRATE SOLUTION

Ion	*First wave at pH 2.5*	*Last wave*			
		pH	$E_{\frac{1}{2}}$	*Slope*	i_d/i_{d_T}
Aquoamminebis(ethylenediamine)cobalt(III)	$E_{\frac{1}{2}} = -0.08$ V Slope = 0.08	2.71			0.02
		3.38	−0.26	0.17	0.56
		5.81	−0.37	0.13	0.83
		9.95	−0.42	0.089	0.97
Aquopentamminecobalt(III)	$E_{\frac{1}{2}} = -0.03$ V Slope = 0.090	2.85			0.03
		3.54	−0.36	0.13	0.69
		9.88	−0.38	0.11	0.99
Aquothiocyanatobis(ethylenediamine)cobalt(III)	See Table 1	3.30	−0.36		0.06
		6.41	−0.38	0.070	0.23
		10.83	−0.41	0.069	0.50
Aquohydroxobis(ethylenediamine)cobalt(III)	$E_{\frac{1}{2}} = +0.02$ Slope = 0.070	3.60	−0.40	0.070	0.31
		5.89	−0.40	0.092	0.77
		9.79	−0.44	0.120	0.94
		10.60	−0.48	0.120	1.00

negative wave of the aquohydroxobis(ethylenediamine)cobalt(III) ion appears to become more negative with increasing pH; however, the slope of the already irreversible wave increases in basic solution, making it difficult to draw firm conclusions about the pH-dependence. A summary of representative data obtained in unbuffered solution is presented in Table 2.

For comparison purposes, one non-aquated ion (the dithiocyanatobis(ethylenediamine)cobalt(III) ion), was studied. The polarogram consists once again of a single early wave in acidic solution, somewhat distorted because of an irrepressible maximum and the insolubility of mercury(I) thiocyanate. At pH 3, the wave common to bis(ethylenediamine)cobalt(III) ions appears at *ca.* −0.37 V *vs.* SCE and increases in relative height as the pH is raised, reaching an apparent maximum of one-half of the total height at a pH *ca.* 11. Data for this last wave are reported in Table 3.

TABLE 3

POLAROGRAPHIC DATA FOR THE MOST NEGATIVE WAVE OF THE ONE-ELECTRON REDUCTION OF m*M* DITHIOCYANATOBIS(ETHYLENEDIAMINE)COBALT(III) NITRATE IN 0.10 *M* POTASSIUM NITRATE

pH	$E_{\frac{1}{4}}$ (*V*)	*Slope*	i_a/i_{a_r}
7.92	−0.37	0.066	0.25
9.20	−0.39	0.064	0.31
10.00	−0.39	0.069	0.36
10.28	−0.40	0.068	0.40
11.50	−0.41	0.068	0.50

The total diffusion current was nearly the same for all the bis(ethylenediamine)-cobalt(III) ions, using the same electrode and mercury head, and about 10% higher for the aquopentamminecobalt(III) ion. The variation of the wave height with pH was only slightly in excess of the experimental error, but it was estimated that the wave heights of all of the ions were 3 ±1.5% higher in basic solution than in acidic solution. This difference is probably due either to a shift in the electrocapillary curve of mercury or to small changes of the diffusion coefficients of the electroactive species with changes in pH.

Buffered solutions

Because of the known complicating effects of pH changes at the electrode surface, further studies were made in buffered solutions, in spite of complexing and other disadvantages of buffering agents.

When phosphate ion was used as a buffering agent, deleterious effects were noted only with the aquohydroxobis(ethylenediamine)cobalt(III) ion. With this ion, results were reproducible only in freshly buffered solutions; if the solutions aged for a few hours or if they were made basic and then reacidified, anomalous reduction waves appeared. No evidence of formation of any cobalt(II) phosphate on the electrode surface was detected, nor has any been reported by other investigators working in this medium[3].

The important consequence of buffering with phosphate ion is, as expected, a simplification of the polarograms engendered by the maintenance of constant pH at the electrode surface. In 0.10 *M* phosphate solution the two waves observed in un-

buffered solution for the aquopentaamminecobalt(III) ion are replaced by a single wave with a slope of 0.10 and a half-wave potential that varies regularly from −0.06 V *vs.* SCE at pH 2.53 to −0.48 V at pH 10.08.

With solutions of millimolar aquoamminebis(ethylenediamine)cobalt(III) ion buffered with 0.10 *M* potassium dihydrogen phosphate, only one reduction wave, of slope 0.09, is evident below pH 7; the half-wave potential varies from −0.12 V at pH 2.18 to −0.19 V at pH 6.12. Slightly above pH 7.0, the wave common to all the bis(ethylenediamine)cobalt(III) ions appears at about −0.40 V *vs.* SCE and grows in height as the pH is raised, reaching a maximum of about half of the total height at a pH *ca* 9. Inasmuch as the first wave is shifting to more negative potentials, it merges with the second wave slightly above pH 9 and only one wave can then be observed.

In the case of the diaquobis(ethylenediamine)cobalt(III) ion, solutions freshly buffered with 0.10 *M* phosphate ion show only one reduction wave, of slope 0.09, the half-wave potential becoming more negative as the pH is raised. Above pH 6, the reduction wave common to the bis(ethylenediamine)cobalt(III) ions appears at −0.40 V *vs.* SCE and increases in magnitude at the expense of the earlier wave as the pH is raised further.

Because of the problems associated with the use of phosphate ion, borate was also used as a buffer with the diaquobis(ethylenediamine)cobalt(III) ion in its effective buffering range of *ca.* 8.4–10.5. In 0.10 *M* boric acid, well-defined waves of slope 0.08–0.09 were obtained, the half-wave potential varying from −0.35 V *vs.* SCE at pH 8.39 to −0.48 V at pH 10.92.

The effects of freshly added ethylenediamine on the most negative reduction wave of the aquohydroxobis(ethylenediamine)cobalt(III) ion are tabulated in Table 4.

TABLE 4

EFFECT OF ETHYLENEDIAMINE ON THE THIRD (MOST NEGATIVE) ONE-ELECTRON REDUCTION WAVE OF AQUATED BIS(ETHYLENEDIAMINE)COBALT(III) ION IN 0.10 *M* POTASSIUM NITRATE SOLUTION

Sample	*pH*	*Concn. of en (mM)*	*Free en (mM)*	$E_{\frac{1}{4}}$ *(V)*	*Slope*
1	8.46	2.0	0.038	−0.42	0.069
2	9.20	5.0	0.51	−0.44	0.065
3	10.72	1.0	0.79	−0.52	0.126
4	9.21	10	1.0	−0.45	0.061
5	8.32	50	1.3	−0.45	0.061
6	10.70	2.0	1.6	−0.47	0.083
7	9.21	50	5.2	−0.46	0.058
8	9.25	100	11	−0.46	0.058
9	10.71	20	16	−0.48	0.077
10	9.03	500	35	−0.48	0.063
11	9.21	500	52	−0.48	0.059
12	9.39	500	75	−0.48	0.063
13	11.30	100	97	−0.50	0.103
14	9.68	500	130	−0.48	0.068
15	10.00	500	210	−0.49	0.073
16	10.38	500	320	−0.51	0.073
17	10.71	500	390	−0.53	0.096
18	11.12	500	450	−0.57	0.113
19	11.58	500	480	−0.60	0.125

Ethylenediamine, in addition to fulfilling the role of ligand, is also an effective buffer in the pH range 6–11. The concentration of free ethylenediamine for each sample is calculated from the relationship

$$[\text{Ethylenediamine}] = \frac{C_{en} K_{a_1} K_{a_2}}{K_{a_1} K_{a_2} + K_{a_1}[H^+] + [H^+]^2}$$

where C_{en} is the analytical or total concentration of ethylenediamine. The values of the ionization constants employed are $10^{-7.42}$ and $10^{-10.14}$, as determined by NYMAN, MUHRBACH AND MILLARD[8] for solutions 0.1 *M* in potassium nitrate.

Since it might reasonably be expected that the presence of ethylenediamine in the same solution as aquated bis(ethylenediamine)cobalt(III) ion would result in the formation of the very stable tris(ethylenediamine)cobalt(III) ion, a means of detecting this was necessary. It was found that in an acidic solution (pH < 3) of diaquobis-(ethylenediamine)cobalt(III) ion, any tris(ethylenediamine)cobalt(III) ion present can be detected to polarographic limits as a separate wave at *ca.* −0.38 V *vs.* SCE. All of the $[Co(en)_2(H_2O)_2]^{3+}$ appears as the first wave near zero volts *vs.* SCE and hence does not interfere. This means of detection was used to check the solutions of aquohydroxobis(ethylenediamine)cobalt(III) ion in excess ethylenediamine after the polarograms were recorded. The solutions were immediately made acidic and the polarograms re-recorded; no evidence of any tris(ethylenediamine)cobalt(III) ion was found in the solutions. In one experiment, a solution 0.50 *M* in ethylenediamine and 1.00×10^{-3} *M* in $[Co(en)_2(H_2O)(OH)]^{2+}$ was allowed to stand at room temperature at a pH of 10.7 for a period of 52 h, after which the solution was made acidic and the polarogram recorded. No evidence of any $[Co(en)_3]^{3+}$ was observed.

The effects of excess ethylenediamine on the cathodic waves of aquohydroxobis-(ethylenediamine)cobalt(III) ion below pH 8 were insignificant and are not reported in Table 3.

At a pH level above 8, where the third wave of the aquohydroxobis(ethylene-diamine)cobalt(III) ion accounts for most of the reduction current in unbuffered solution (see Table 1) and the second wave accounts for less than one-sixth of the total height, the addition of ethylenediamine to the solution causes a further decrease of the second wave and a corresponding increase in the third wave. At a pH of 8.7, for example, if the solution is made 0.01 *M* in ethylenediamine, the second wave disappears entirely and the third wave accounts for all of the reduction current. The significance of this will be taken up in the discussion section.

Added ethylenediamine causes an analogous diminution of the wave height of the first reduction waves of the aquoammine-, the aquothiocyanato-, and the dithiocyanatobis(ethylenediamine)cobalt(III) ions and a corresponding increase in the height of the last (most negative) waves. Quantitative data for the dithiocyanatobis(ethylenediamine)cobalt(III) ion are reported in Table 5. Since the waves are close together at the pH-levels under investigation and since the ethylenediamine further accentuates the merging of the waves, it is not possible to treat the two waves separately. It is more revealing to treat them as a single wave (which they rapidly become as free ethylenediamine is formed) and to note the effect of the ethylene-diamine on the slope. When the slope falls to the value specified for a reversible one-electron reduction, *i.e.*, 0.059, merging of the waves can be considered to be

TABLE 5

EFFECT OF 0.010 *M* ETHYLENEDIAMINE ON LAST (MOST NEGATIVE) ONE-ELECTRON REDUCTION WAVE OF m*M* DITHIOCYANATOBIS(ETHYLENEDIAMINE)COBALT(III) NITRATE IN 0.10 *M* POTASSIUM NITRATE

pH	*Concn. of free en (mM)*	$E_{\frac{1}{2}}$ *(V)*	*Slope*
8.78	0.40	−0.42	0.067
8.88	0.52	−0.42	0.065
9.07	0.77	−0.43	0.064
9.18	0.97	−0.44	0.061
9.28	1.20	−0.44	0.059

complete. A glance at Table 5 indicates that this occurs when the concentration of free ethylenediamine reaches the level of approximately one millimolar.

As the polarographic waves just reported will frequently be compared with the polarographic reduction wave of the tris(ethylenediamine)cobalt(III) ion, it was deemed advisable to investigate the behavior of this ion with the dropping mercury electrode. Data relating the half-wave potential and the slope of the single observed wave to the concentration of added ethylenediamine are presented in Table 6. The oxidation–reduction potential of the tris(ethylenediamine)cobalt(III)–tris(ethylenediamine)cobalt(II) system in excess ethylenediamine was investigated earlier by KONRAD AND VLČEK[9] using platinum electrodes.

TABLE 6

CHANGE OF HALF-WAVE POTENTIAL AND SLOPE OF THE ONE-ELECTRON REDUCTION WAVE OF m*M* TRIS(ETHYLENEDIAMINE)COBALT(III) NITRATE WITH CONCENTRATION OF ADDED ETHYLENEDIAMINE

pH	*Concn. of en (mM)*	*Free en (mM)*	$E_{\frac{1}{2}}$ *(V)*	*Slope*
7.23	0.00	0.00	−0.38	0.086
12.0	0.00	0.00	−0.38	0.089
8.25	1.00	0.011	−0.39	0.082
8.71	1.00	0.034	−0.39	0.077
9.17	1.00	0.095	−0.40	0.070
9.73	1.00	0.28	−0.42	0.063
10.18	1.00	0.52	−0.43	0.063
9.44	10.0	1.60	−0.44	0.058
10.29	10.0	5.80	−0.45	0.059
10.70	10.0	7.80	−0.46	0.057
11.50	200	190	−0.46	0.061
10.39	500	320	−0.46	0.060
11.60	500	480	−0.46	0.061

An examination of Table 6 shows that the reduction is irreversible in the absence of excess ethylenediamine but becomes reversible as soon as the concentration of free ethylenediamine reaches a minimum value of *ca.* 0.5 m*M*, giving a half-wave potential of *ca.* −0.42 V *vs.* SCE.

KONRAD AND VLČEK[9] have shown that the oxidation–reduction potential of the system depends upon the concentration of free ethylenediamine present and is independent of the pH of the solution (except insofar as the pH determines the

concentration of free ethylenediamine). An examination of Table 6 confirms this, as it can be observed that the half-wave potential decreases (becomes more negative) regularly with increasing concentration of free ethylenediamine, regardless of the pH. In 0.10 *M* potassium nitrate solution, the half-wave potential shifts from −0.38 V *vs.* SCE with no added ethylenediamine to a limiting value of −0.46 V at concentrations of free ethylenediamine of 10 m*M* or more. This compares closely with the findings of KONRAD AND VLČEK.

DISCUSSION

Consideration of the reduction of bis(ethylenediamine)cobalt(III) ions must take into account the so-called *ligand exchange* mechanism of LAITINEN AND KIVALO[10]. These authors observed that the half-wave reduction potential of the hexaamminecobalt(III) ion in 0.1 *M* ethylenediamine occurs at the half-wave potential of the tris(ethylenediamine)cobalt(III) ion, about 0.2 V more negative than the half-wave potential of the hexamminecobalt(III) ion in 1.0 *M* sodium nitrate without added ethylenediamine. They reasoned that the reduction of the hexamminecobalt(III) ion is taking place at the expected half-wave potential, followed by a replacement of the ammine ligands on the labile cobalt(II) ion by three ethylenediamine molecules. At the reduction potential of hexamminecobalt(III), tris(ethylenediamine)cobalt(II) is immediately oxidized and cancels any observable reduction of the hexamminecobalt(III) ion. When the potential reaches the reduction potential of the tris(ethylenediamine)cobalt(III) ion, this oxidation of tris(ethylenediamine)cobalt(II) can no longer take place and one then observes the reduction wave of the tris(ethylenediamine)-cobalt(III) ion.

MASON AND WHITE[3] have since attributed the double wave[1] observed in the reduction of the dinitrobis(ethylenediamine)cobalt(III) ion to the ligand exchange mechanism. They propose a preliminary reduction of the *trans*-dinitrobis(ethylenediamine)cobalt(III) ion at a half-wave potential of −0.26 V *vs.* SCE followed by a rearrangement of ligands:

$$2\,[Co(en)_2(NO_2)_2]^+ + 2e \rightarrow [Co(en)_3]^{2+} + [Co(en)]^{2+} + 4\,NO_2^-$$

Theoretically, two tris(ethylenediamine)cobalt(II) ions could be formed from the reduction of three bis(ethylenediamine)cobalt(III) ions, giving a ratio of 1:2 for the heights of the first and second waves. In practice, however, presumably due to the rate of exchange and/or the formation constants involved, only one tris(ethylenediamine)cobalt(II) ion is formed from the reduction of two bis(ethylenediamine)-cobalt(III) ions. Thus at high pH (favoring free ethylenediamine and ligand exchange) the tris(ethylenediamine)cobalt(II) ion formed causes cancellation of one-half of the total wave height, which reappears at the more negative reduction potential of tris-(ethylenediamine)cobalt(III) ion.

A logical test of the mechanism proposed by MASON AND WHITE would be to add excess ethylenediamine to the solution of *trans*-dinitrobis(ethylenediamine)-cobalt(III) ion to see if the first wave is eliminated. A small amount of ethylenediamine should cause all the cobalt(II) ion formed at the electrode surface to undergo ligand exchange. The authors have found this to be the case.

It appears that any bis(ethylenediamine)cobalt(III) ion that is reduced more

easily (at a more positive potential) than the tris(ethylenediamine)cobalt(III) ion will undergo ligand exchange in basic solution. The aquothiocyanato- and dithiocyanatobis(ethylenediamine)cobalt(III) ions, for example, exhibit behavior similar to that of the dinitrobis(ethylenediamine)cobalt(III) ion. In basic solution, two waves are present, and the more negative one becomes approximately equal in height to the more positive one as the pH is increased (see Tables 1 and 3). Added ethylenediamine causes the complete disappearance of the first wave, as anticipated, and leaves only the single reversible wave at the half-wave potential of tris(ethylenediamine)cobalt(III) ion. From Table 5 the amount of free, unprotonated ethylenediamine necessary to eliminate the first wave is *ca.* 1 m*M*, which corresponds to the stoichiometric amount necessary to form tris(ethylenediamine)cobalt(II) from bis(ethylenediamine)-cobalt(II). Presumably, it requires slightly more than the stoichiometric amount of free ethylenediamine to render the wave reversible as demonstrated by the irreversibility of the reduction of tris(ethylenediamine)cobalt(III) ion without added ethylenediamine.

Ethylenediamine ligand exchange cannot, of course, account for the two waves observed in the reduction of the aquopentaamminecobalt(III) ion, since no ethylenediamine is present, nor can it account for the entire height of the single wave obtained in basic solutions of aquoammine- and aquohydroxobis(ethylenediamine)cobalt(III) ions. The acid–base behavior of the ions as a cause of the multiplicity of waves must also be considered. The water ligands of aquated cobalt(III) ions are known to ionize to form the corresponding hydroxo compounds, the first ionization constant being usually *ca.* 10^{-6} [11]. Normally the polarographic reduction of weak acids yields single waves, unless the interconversion of the conjugate acid–base pair is hindered by slow kinetics or the lack of available protons[12,13]. The double wave of the aquopentaamminecobalt(III) ion in unbuffered solution is attributed to the release of ammine ligands from the labile cobalt(II) reduction product at the electrode surface. The ammine groups deprotonate the aquopentamminecobalt(III) ions at the electrode surface, thus terminating the first wave. The conjugate base produced is reduced at a more negative potential. At high pH, the hydroxopentamminecobalt(III) ion is the electroactive species in solution and is reduced directly. In buffered solution, the pH is constant at the electrode surface and a single reduction wave that shifts to more negative half-wave potentials with increasing pH is observed.

The various aquated bis(ethylenediamine)cobalt(III) ions also exhibit separate reduction waves for the acid and base forms in unbuffered solution. Thus the middle wave at -0.25 V *vs.* SCE at pH 3.0–3.3 for the aquoamminebis(ethylenediamine)-cobalt(III) ion is due to the hydroxoamminebis(ethylenediamine)cobalt(III) species formed at the electrode surface through deprotonation by ethylenediamine from the labile cobalt(II) reduction product. As the pH is raised, the wave shifts negatively to merge with the wave for ligand exchange giving a composite wave of excessive slope at pH 3.4. The total wave appears to change slope with increasing pH as the hydroxoamminebis(ethylenediamine)cobalt(III) wave shifts to more negative potentials. In phosphate buffer solution, the two waves are not completely merged and both may be distinguished up to pH *ca.* 9.

The reduction of the aquohydroxobis(ethylenediamine)cobalt(III) ion apparently involves ligand exchange, which may account for no more than half the total wave height, merged with the wave for the reduction of the base-stable species such

that only one wave is observed in solution of pH 10 or more. As the pH is increased above 10, the slope becomes excessive and the apparent half-wave potential becomes more negative than that of the tris(ethylenediamine)cobalt(III) ion because the dihydroxo species is being reduced at a more negative potential. At pH 11, it is found that a solution containing both tris(ethylenediamine)cobalt(III) ion and aquohydroxobis(ethylenediamine)cobalt(III) ion gives two separate waves, one for each species. The most negative wave (that of the aquohydroxobis(ethylenediamine)cobalt(III) ion) is somewhat distorted due to the formation of cobalt oxides[14] at the electrode surface. If ethylenediamine is added to the solution, well-defined separate waves can be obtained up to pH 12, since the ethylenediamine co-ordinates with the cobalt(II) ion and prevents it from depositing on the electrode surface. Apparently, the dihydroxobis(ethylenediamine)cobalt(III) ion is of the same order of stability in slightly basic solution as the tris(ethylenediamine)cobalt(III) ion, and surpasses the stability of that ion as the pH is raised further. Comparable results were noted by BJERRUM AND RASMUSSEN[15] from spectrophotometric equilibrium studies. Thus, the polarographic wave observed in an unbuffered solution of the aquohydroxobis(ethylenediamine)cobalt(III) ion at a pH above *ca.* 10 is no longer composed partly of the ligand exchange wave but is due instead to the direct reduction of the dihydroxobis-(ethylenediamine)cobalt(III) ion.

An examination of Table 4 yields more information on the conditions under which the ligand exchange mechanism is operating. Comparison of samples 2 and 4 indicates that approximately 1 m*M* of free ethylenediamine (stoichiometric amount) is necessary to yield the reversible wave of tris(ethylenediamine)cobalt(III) ion. Similar results were noted for the dithiocyanatobis(ethylenediamine)cobalt(III) ion (see Table 5). The reversibility of sample 5 indicates that the mechanism operates efficiently down at pH 8.32 if sufficient ethylenediamine is present. The increase in slope for samples 11, 12 and 14 (pH values 9.21, 9.39 and 9.68, respectively), even with a large excess of ethylenediamine, probably indicates that the half-wave potential of the dihydroxobis(ethylenediamine)cobalt(III) ion has become slightly more negative than that of the tris(ethylenediamine)cobalt(III) ion; the waves are becoming separated in this pH range. The decrease at pH 10.70–10.71 (samples 6 and 9) is probably caused by the more complete buffering of the added ethylenediamine. As still more ethylenediamine is added at the same pH (sample 17) the slope increases again; the reasons for this are not known, although an activity effect is suggested.

The reduction characteristics of the aquothiocyanatobis(ethylenediamine)-cobalt(III) ion in unbuffered solution (Table 1) appear to be unique in that the first wave is highly responsive to pH, in contrast to the first wave of the other ions, and also no evidence of an intermediate wave representing the reduction of the hydroxothiocyanatobis(ethylenediamine)cobalt(III) ion is observed. It is believed that both anomalies are due to the proximity of the half-wave potentials of the aquo- and the hydroxothiocyanatobis(ethylenediamine)cobalt(III) ions. Because of this proximity one observes an extended composite wave for the acid and base species (note the excessive slope). As the solution is made basic, the acid form ceases to exist and the slope then declines to 0.10, a value comparable to that of the other ions studied.

The possibility of polymerization as a cause of the multiple waves associated with the aquated bis(ethylenediamine)cobalt(III) ions has been suggested[2]. WERNER[16]

has prepared dimers of the several aquated ions studied and it can be seen that the process of dimerization could be realized in basic solution, *e.g.*:

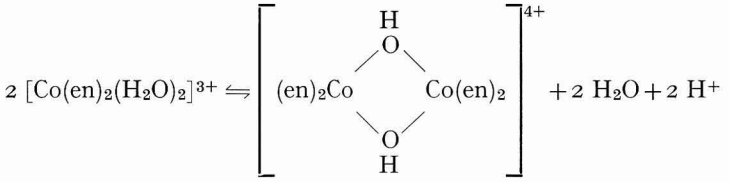

If a dimer or other polymer were indeed formed in basic solution, the increase in volume of the diffusing species would result in a decrease in the diffusion coefficient (from the Stokes–Einstein relationship, $D = kT/6\pi r\eta$). The diffusion current would then decrease in basic solution, a behavior opposite to that actually observed. RASMUSSEN AND BJERRUM[17] have shown, furthermore, that the hydrolysis of the dimer of the aquohydroxobis(ethylenediamine)cobalt(III) ion takes place far too slowly to explain the immediate changes in the polarogram caused by a pH change.

SUMMARY

The polarographic behavior of a series of aquated bis(ethylenediamine)cobalt-(III) ions has been studied in buffered and unbuffered aqueous solution. In unbuffered solution, multiple waves, the relative heights of which are dependent upon pH, were obtained for the one-electron reduction to the cobalt(II) state. The first (most positive) wave is due to the direct reduction of the aquobis(ethylenediamine)cobalt(III) ion in solution, while later (more negative) waves are due to ligand exchange and the corresponding hydroxo compound formed by deprotonation of the parent aquo species. In basic solution, the dihydroxobis(ethylenediamine)cobalt(III) ion gives a single wave at the more negative potential because this ion is more stable than tris(ethylene-diamine)cobalt(III) ion. In buffered solution, the multiplicity due to the acid and base forms of the aquated bis(ethylenediamine)cobalt(III) ions is eliminated.

REFERENCES

1 H. F. HOLTZCLAW AND D. P. SHEETZ, *J. Am. Chem. Soc.*, 75 (1953) 3053.
2 N. MAKI, Y. SHIMURA AND R. TSUCHIDA, *Bull. Chem. Soc. Japan*, 32 (1959) 150.
3 J. G. MASON AND R. L. WHITE, *J. Electroanal. Chem.*, 8 (1964) 454.
4 A. WERNER, *Ann.*, 386 (1912) 160, 161, 187.
5 F. EPHRAIM, *Ber.*, 56 (1923) 1536.
6 A. WERNER, *Ber.*, 40 (1907) 281.
7 J. B. WORK, *Inorganic Syntheses*, II (1946) 221.
8 C. J. NYMAN, E. W. MUHRBACH AND G. B. MILLARD, *J. Am. Chem. Soc.*, 77 (1955) 4194.
9 D. KONRAD AND A. A. VLČEK, *Collection Czech. Chem. Commun.*, 28 (1963) 595.
10 H. A. LAITINEN AND P. KIVALO, *J. Am. Chem. Soc.*, 75 (1953) 2198.
11 M. L. TOBE, *Sci. Progr. (London)*, 48 (1960) 483.
12 I. M. KOLTHOFF AND J. J. LINGANE, *Polarography*, Vol. 1, Interscience Publishers, New York, 1952, p. 269.
13 R. BRDICKA, *Collection Czech. Chem. Commun.*, 12 (1947) 122.
14 P. KIVALO, *J. Am. Chem. Soc.*, 77 (1955) 2678.
15 J. BJERRUM AND S. RASMUSSEN, *Acta Chem. Scand.*, 6 (1952) 1265.
16 A. WERNER, *Ann.*, 375 (1910) 1.
17 S. RASMUSSEN AND J. BJERRUM, *Acta Chem. Scand.*, 9 (1955) 735.

ELECTROANALYTICAL CHEMISTRY AND INTERFACIAL ELECTROCHEMISTRY
Elsevier Publishing Company, Amsterdam – Printed in The Netherlands

REVIEW

CHRONOPOTENTIOMETRY

MILAN PAUNOVIC
*Reduction Research Division, Reynolds Metals Company, Sheffield, Alabama, 35661 (U.S.A.)**
(Received September 2nd, 1966)

I. INTRODUCTION

The electrode reactions discussed in this review proceed by at least two consecutive steps:

1. Transport of the electrochemically-reacting species to and from the interface electrode–solution.

2. Transfer of electrons to or from electrochemically-reacting species (reactants).

The overall rate of the electrode reaction depends on the rate of the first step only or on the rate of both 1 and 2.

It will be assumed that mass transport occurs only by linear diffusion under the influence of a gradient of chemical potential (the concentration gradient). The concentration gradient is established by the consumption of reactant in the electrode reaction. It is assumed that the initial concentration of the reactant is homogeneous up to the electrode. The assumption that the concentration of electrochemically-reacting species before electrolysis is independent of the distance from the electrode implies that the double-layer structure is not considered in the following analysis.

Semi-infinite linear diffusion to a plane electrode in an unstirred solution will be considered.

Mass transport under the influence of a gradient of electrical potential is neglected because a large excess of supporting electrolyte is used.

The system for potential–time studies is composed of the test-, counter and reference electrodes as shown schematically in Fig. 1.

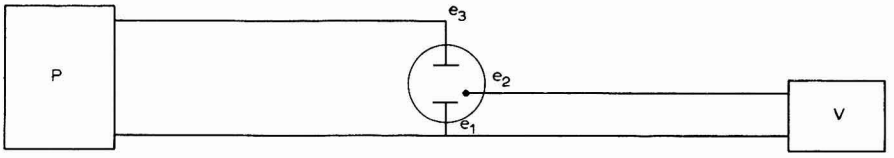

Fig. 1. Schematic diagram of apparatus for galvanostatic non-steady state electrolysis. (P), Constant-current power supply; (e_1), test electrode; (e_2), reference electrode; (e_3), counter electrode; (V), Potential–time recording instrument.

Constant current from the constant-current power supply, P, is applied between electrodes e_1 (test electrode) and e_3 (counter electrode). The potential of the test electrode, e_1, against the reference electrode, e_2, is recorded by the instrument V as a function of time.

* Present address: Photocircuits Corp., Glen Cove, N.Y. 11542 (U.S.A.)

Before electrolysis, the equilibrium,

$$O + ne \rightleftarrows R \tag{1}$$

is set up and determines the potential of the test electrode. O represents the oxidized species or reactant and R the reduced form or product.

When a pulse of a constant current is applied to the test and counter electrodes such that the reaction,

$$O + ne \rightarrow R \tag{2}$$

occurs at the test electrode the reactant O is consumed at the electrode and its concentration at the interface decreases. As the electrolysis proceeds there is a progressive depletion of the electrolyzed species at the interface of the working electrode. The depletion extends farther away in solution as the electrolysis proceeds. Thus, the concentration, C_O, is a function of the distance, x, from the electrode and the time, $C_O = C_O(x, t)$. Product R diffuses from the electrode and is also a function of x and t, $C_R = C_R(x, t)$.

At the transition time, τ, the concentration of reactant O at the electrode surface equals zero

$$C_O(0, \tau) = 0 \tag{3}$$

As a result of variation of the concentration of O at the electrode with time, the potential of the test electrode will also vary with time. The variation of potential with time during non-stready state galvanostatic electrolysis is shown schematically in Fig. 2.

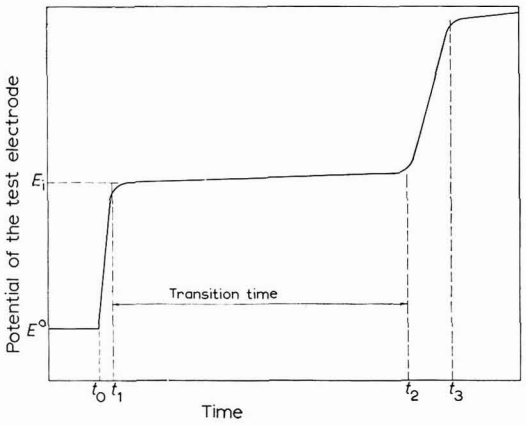

Fig. 2. Variation of potential of test electrode with time during galvanostatic non-steady state electrolysis. (E°), Equilibrium potential; (E_i), potential of test electrode at beginning of electrolysis at current density i.

Galvanostatic non-steady state electrolysis occurs during change in the concentration of the reactant at the electrode from its initial value C_O° to zero value. The duration of this non-steady state electrolysis is designated τ. Once functions $C_O = C_O(x, t)$ and $C_R = C_R(x, t)$ are known, a potential–time function in terms of transition time can be obtained.

Therefore, the first problem in the theory of potential–time curves in galvanostatic non-steady state electrolysis with total or partial control by diffusion, is to investigate the variation of concentration with time at the electrode.

This review is not intended to be a complete coverage of all the pertinent literature but rather a survey of basic ideas, principles and potentialities of the chronopotentiometric method. The mechanism of electrode processes is of particular interest to most electrochemists and is, therefore, given more thorough treatment.

II. FUNDAMENTALS OF THE THEORY

1. Variation of concentration, $C_O(x, t)$, $C_R(x, t)$, and transition time

A. Single reversible and irreversible electrochemical reaction. Kinetic scheme:

$$O + ne \rightarrow R \tag{4}$$

(i) Reactant O and product R are soluble species. This part of the theory is the same for reversible and irreversible electrochemical reactions. Change in concentration of the reactant, C_O, at the electrode, on switching on a constant current, was calculated by WEBER[1] and SAND[2,3] by solving the differential equation expressing Fick's law,

$$\frac{\partial C_O(x, t)}{\partial t} = D_O \frac{\partial^2 C_O(x, t)}{\partial x^2} \tag{5}$$

where D_O is the diffusion coefficient of reactant O. The differential equation was solved with the following initial and boundary conditions;

$$C_O(x, 0) = C^\circ, \tag{6.1}$$

$$C_O(x, t) \rightarrow C^\circ, \quad \text{for } x \rightarrow \infty \tag{6.2}$$

$$i/nF = D_O \left(\frac{\partial C_O(x, t)}{\partial x}\right)_{x=0} \tag{6.3}$$

where C° is the bulk concentration of O, i the current density and F the faraday. Condition (6.1) expresses that, initially, before electrolysis, the concentration of the solution is homogeneous at all distances, x, from the electrode, equal to the bulk concentration of reactant O.

The boundary condition (6.3) follows from the fact that, according to Faraday's law, regardless of the current-controlling factor, the current density at any time is given by

$$i_t = nF \frac{dN}{dt}, \tag{7}$$

where dN/dt is the number of moles that react at the electrode in unit time and nF is the charge involved in the reduction of one mole of substance O.

When the current-controlling factor is the rate of diffusion of reactant to the electrode and when the concentration gradient at the electrode is developed as a result of electrolysis, dN/dt is equal to the flux of the reactant at the electrode and is given by Fick's law,

$$\frac{dN}{dt} = D_O \left(\frac{\partial C_O(0, t)}{\partial x}\right)_{x=0} \tag{8}$$

The boundary condition (6.3) results from (7) and (8). The result of integration is[3]

$$C_O(x, t) = C^\circ - (2\lambda D_O^{\frac{1}{2}} t^{\frac{1}{2}}/\pi^{\frac{1}{2}}) \exp(-x^2/4D_O t) + \lambda x \operatorname{erfc}(x/2D_O^{\frac{1}{2}} t^{\frac{1}{2}}) \quad (9)$$

with

$$\lambda = \frac{i}{nFD_O} \quad (10)$$

$$\operatorname{erf}(\lambda) = \frac{2}{\pi^{\frac{1}{2}}} \int_0^{\lambda} \exp(-z^2)\, dz \quad (11)$$

and

$$\operatorname{erfc}(\lambda) = 1 - \operatorname{erf}(\lambda) \quad (12)$$

where z is an auxiliary variable. Similarly, for $C_R(x, t)$

$$C_R(x, t) = (2\lambda D_O t^{\frac{1}{2}}/D_R^{\frac{1}{2}}\pi^{\frac{1}{2}}) \exp(-x^2/4D_R t) - (\lambda x D_O/D_R) \operatorname{erfc}(x/2D_R^{\frac{1}{2}} t^{\frac{1}{2}}) \quad (13)$$

As an example, function $C_O(x, t)$ is plotted against x in Fig. 3 for various times of electrolysis.

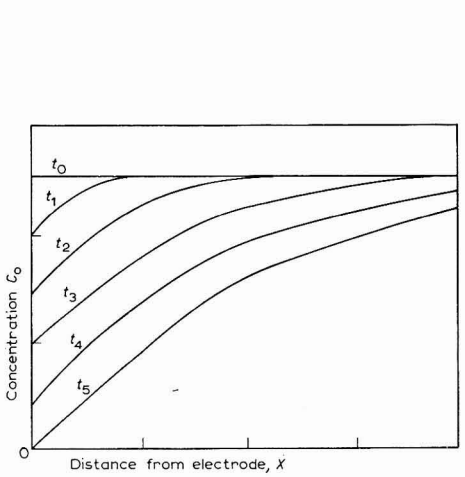

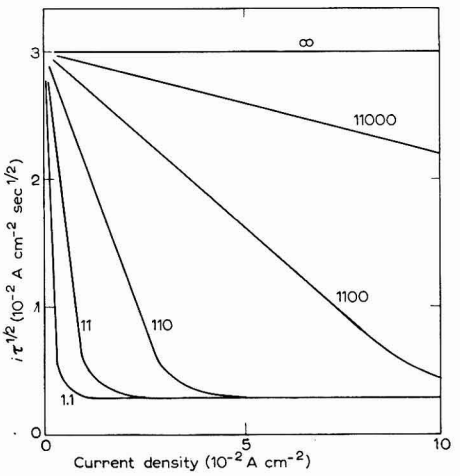

Fig. 3. Variation of concn. of reactant during non-steady state electrolysis. The number t_n on each curve is the time elapsed since the beginning of electrolysis $t_5 > t_4 \ldots > t_1$.

Fig. 4. Theoretical curves for variation of $i\tau^{\frac{1}{2}}$ with current density for the electrochemical reaction preceded by a chemical reaction. The number on each curve indicates the value of $(k_f + k_b)$ (DELAHAY AND BERZINS[6]).

Variation of concentration of reactant O at the electrode, $C_O(0, t)$, is obtained from eqn. (9) by introducing $x = 0$.

$$C_O(0, t) = C^\circ - 2it^{\frac{1}{2}}/nF\pi^{\frac{1}{2}}D_O^{\frac{1}{2}} \quad (14)$$

By introducing $x = 0$ into eqn. (13) one obtains

$$C_R(0, t) = 2it^{\frac{1}{2}}/nFD_R^{\frac{1}{2}}\pi^{\frac{1}{2}} \quad (15)$$

According to eqn. (14) the concentration C_O at the electrode changes with the square root of t.

For $t=\tau$, since $C_O(o, \tau)=o$ (eqn. (3)) it follows from eqn. (14) that,

$$\tau^{\frac{1}{2}}=\pi^{\frac{1}{2}} nFC_O^{\circ}D_O^{\frac{1}{2}}/2i \tag{16}$$

According to eqn. (16), $\tau^{\frac{1}{2}}$ is proportional to the bulk concentration of the substance reacting at the electrode and inversely proportional to the current density.

For a given system, assuming D_O independent of concentration, and for constant current density, eqn. (16) reduces to

$$\tau^{\frac{1}{2}}=\text{const.} \times C^{\circ} \tag{17}$$

Thus, $\tau^{\frac{1}{2}}$ is a linear function of C° and can be used for quantitative determinations of C°. Equation (16), and in the simplest form (17), are the fundamental equations of chronopotentiometric analysis.

(ii) Product R is insoluble. Kinetic scheme:

$$O + ne \rightarrow R \text{ (insoluble)} \tag{4a}$$

Concentration change, $C_O(x, t)$, and τ are the same as in Case A(i).

B. Complex mechanisms

(i) Two consecutive electrochemical reactions involving different substances. Kinetic scheme:

$$O_1 + n_1e \rightarrow R_1 \tag{18}$$

$$O_2 + n_2e \rightarrow R_2 \tag{19}$$

Reactant O_1 is reduced at less cathodic potentials. The theory of this type of electrolysis was developed by BERZINS AND DELAHAY[4].

If ionic species O_1 and O_2 are reduced at sufficiently different potentials, a potential–time curve exhibits two steps.

For the first reduction, at potential E_1, the theory of a single electrochemical reaction applies. The transition time, τ_1, for this first step is given by the eqn. (16).

After the elapse of a time τ_1, the situation at the test electrode can be described as follows: (a) at the transition time τ_1, the concentration of O_1 at the electrode is equal to zero and remains equal to zero as the electrolysis proceeds after time τ_1; (b) reactant O_1 continues to diffuse towards the electrode where it is immediately reduced.

Since this supply by diffusion of reactant O_1 is insufficient to maintain the impressed constant current, a part of the current at the test electrode is used for charging of the double layer until the potential reaches the value E_2 when reactant O_2 is reduced. Then the current at the working electrode is the sum of two components corresponding to the simultaneous reduction of substances O_1 and O_2.

After the transition time τ_1, the current density through the cell is given by the equation (analogous to the formula (6.3)),

$$i=nFD_{O_1}\left(\frac{\partial C_{O_1}(x, t')}{\partial x}\right)_{x=0}+n_2FD_{O_2}\left(\frac{\partial C_{O_2}(x, t')}{\partial x}\right)_{x=0} \tag{20}$$

where the time t' is defined by the equation

$$t'=t-\tau_1 \tag{21}$$

t being the time elapsed since the beginning of the electrolysis.

Transition time for the second step, τ_2, is reached when the concentration of the reactant O_2 at the electrode surface becomes equal to zero. The equation for τ_2 is

$$(\tau_1+\tau_2)^{\frac{1}{2}}-\tau_1^{\frac{1}{2}} = \pi^{\frac{1}{2}}n_2FD_{O_2}C_{O_2}^{\circ}/2i \tag{22}$$

where τ_2 is measured from the first transition time, τ_1. If eqn. (16) is used for τ_1, the second transition time is given by

$$\tau_2=(\pi F^2/4i^2)\ (2n_1n_2D_{O_1}^{\frac{1}{2}}D_{O_2}^{\frac{1}{2}}C_{O_1}^{\circ}C_{O_2}^{\circ}+n_2^2D_{O_2}C_{O_2}^{\circ}) \tag{23}$$

According to eqns. (22) and (23), transition time τ_2 depends on the concentration of reactants O_1 and O_2.

From eqn. (22) it follows that the plot of $[(\tau_1+\tau_2)^{\frac{1}{2}}-\tau_1^{\frac{1}{2}}]$ *vs.* $C_{O_2}^{\circ}$ is a straight line. This can be used for the quantitative determination of $C_{O_2}^{\circ}$.

Since, after transition time τ_1, reduction of O_1 and O_2 is simultaneous, the current efficiency for the reduction of O_2 is less than 100%. Thus, the transition time for the reduction of O_2 is greater than would be the case were the substance O_2 alone.

(*ii*) *Two-step electrochemical reaction of a single substance.* Kinetic scheme:

$$O_1+n_1e \rightarrow R_1 \tag{24}$$

$$R_1+n_2e \rightarrow R_2 \tag{25}$$

If reactants O_1 and R_1 are reduced at sufficiently separated potentials then the potential–time curve exhibits two steps; the treatment of this is similar to the treatment of the kinetic scheme with reactions (18) and (19).

For reaction (24) the theory of a single electrochemical reaction applies.

After time τ_1, and since the test electrode reaches potential E_2 corresponding to reduction of the intermediate R_1, the situation at the electrode is:

With respect to the reactant O_1,

(a) concentration of O_1 at the electrode at τ_1 and after τ_1 is equal to zero;

(b) reactant O_1 continues to diffuse toward the electrode and at the electrode is reduced directly to R_2 in a process involving (n_1+n_2) electrons.

With respect to the reactant R_1 (intermediate in reduction of O_1 to R_2),

(a) concentration of R_1 at the electrode at time τ_1, *i.e.*, initial concentration of the reactant for step (25), is a function of distance x from the electrode as a result of diffusion from the electrode during the first step (it is noteworthy that it was assumed that the initial concentration of reactant in the first step is homogeneous and independent of x);

(b) intermediate R_1 diffuses back towards the electrode; at the electrode, R_1 is reduced to R_2, as in eqn. (25).

Fact (a) considerably complicates the mathematical treatment of the present problem.

As a result of the simultaneous reduction of O_1 to R_2 and R_1 to R_2, the current through the cell after time τ_1 is made up of two components according to the equation[3]

$$i=(n_1+n_2)FD_O\left(\frac{\partial C_O(x,t')}{\partial x}\right)_{x=0}+n_2FD_{R_1}\left(\frac{\partial C_{R_1}(x,t')}{\partial x}\right)_{x=0} \tag{26}$$

with t' defined by eqn. (21).

The transition time τ_2 is given by the equation

$$\tau_2 = (\pi F^2 D\ (C^\circ)^2/4i^2)\ (2n_1n_2 + n_2^2), \tag{27}$$

or equation,

$$\tau_2 = \tau_1[2(n_2/n_1) + (n_2/n_1)^2] \tag{28}$$

obtained from eqns. (16) and (27).

(*iii*) *Electrochemical reaction preceded by a chemical reaction.* Kinetic scheme:

$$Y \underset{k_b}{\overset{k_f}{\rightleftarrows}} O \tag{29}$$

$$O + ne \rightarrow R \tag{30}$$

Substance Y is not directly reduced at the applied potential but is transformed to an electroactive form, O, by a prior chemical reaction (29).

From a quantitative treatment of kinetic scheme (29) and (30), one deduces that the presence of a prior chemical reaction can be detected in potential–time studies by using intermediate current densities, *i.e.*, using proper current densities for given values of k_f and k_b[5].

At very high current densities there is not enough time for chemical transformation (29) to occur. The amount of Y converted to O during time τ is negligible and the system behaves as if there were no preceding chemical reaction. The initial equilibrium value of reactant O controls the potential of the test electrode and the transition time.

At low current densities, the system also behaves as if there were no preceding chemical reaction because under these conditions slow consumption of reactant O at the electrode allows production of O and the system behaves as if all the reactant were in the O-form. Therefore, in the study of kinetic scheme (29–30) proper choice of current density is very important.

In kinetic scheme (29–30) the electrode reaction proceeds by three consecutive steps.

1. Transfer of Y and O to and from the interface.
2. Chemical transformation $Y \rightleftarrows O$.
3. Transfer of electrons to the electrochemically-reacting species O.

Assuming that step 3 is a reversible process, the rate of electrode reaction is determined by the rate of diffusion and the chemical transformation.

Since the concentration of reactant O, at point x and time t, is controlled by diffusion and chemical reaction (29), eqn. (5) has to be modified to take into account the change in concentration due to reaction (29). By adding the kinetic term to the right-hand side of eqn. (5) one obtains[6]

$$\frac{\partial C_O(x, t)}{\partial t} = D_O \frac{\partial^2 C_O(x, t)}{\partial x^2} + k_f C_Y(x, t) - k_b C_O(x, t) \tag{31}$$

where k_f and k_b are formal rate constants for the forward and backward processes in (29).

Assuming that the diffusion coefficient of substances O and Y are equal,

$D_O = D_Y = D$; then for $[(k_f + k_b)^{\frac{1}{2}} \tau^{\frac{1}{2}}] > 2$, the transition time is given by the equation

$$i\tau^{\frac{1}{2}} = \tfrac{1}{2}\pi^{\frac{1}{2}} nFC^\circ D^{\frac{1}{2}} - \{\pi^{\frac{1}{2}}/2K(k_f + k_b)^{\frac{1}{2}}\} i \tag{32}$$

where K is the equilibrium constant for reaction (29),

$$K = C_O/C_Y = k_f/k_b \tag{33}$$

In this case, the product $i\tau^{\frac{1}{2}}$ is a linear function of the current density. Figure 4 shows typical relationships between $i\tau^{\frac{1}{2}}$ and i for reactions with larger values of $(k_f + k_b)$.

A decrease in the product $i\tau^{\frac{1}{2}}$ with current density is a diagnostic criterion for the occurrence of a prior chemical reaction, *e.g.*, dissociation of a complex.

According to eqn. (32) the function $i\tau^{\frac{1}{2}}$ is not directly proportional to concentration C°. In order to get a linear dependence for $i\tau^{\frac{1}{2}}$ *vs.* C for an analytical application, the following method can be used[5]. For each sample, *i.e.*, each concentration, product $i\tau^{\frac{1}{2}}$ is determined at several current densities. A plot of $i\tau^{\frac{1}{2}}$ *vs.* i is extrapolated to zero current density. Accordingly, the effect of prior chemical reaction is eliminated and $i\tau^{\frac{1}{2}}$-values obtained by extrapolation can be plotted *vs.* concentration C° for analytical application.

The slope of the straight line $i\tau^{\frac{1}{2}} = f(i)$, from eqn. (32) is[6]

$$\frac{\partial (i\tau^{\frac{1}{2}})}{\partial i} = -\frac{\pi^{\frac{1}{2}}}{2} \frac{1}{K(k_f + k_b)^{\frac{1}{2}}} \tag{34}$$

If the equilibrium constant is known, one can calculate the rate constants, k_f and k_b, from (33) and (34).

If the value of $(k_f + k_b)^{\frac{1}{2}} \tau^{\frac{1}{2}}$ is smaller than 0.1, $i\tau^{\frac{1}{2}}$ is given by equation

$$(i\tau^{\frac{1}{2}})_{i \to \infty} = \tfrac{1}{2}\pi^{\frac{1}{2}} nFC^\circ D^{\frac{1}{2}}/\{1 + (1/K)\} \tag{35}$$

The limit of the product $i\tau^{\frac{1}{2}}$ is independent of the current density. Equation (35) can be used to calculate K.

(*iv*) *Electrochemical reaction followed by a chemical reaction.* Kinetic scheme:

$$O + ne \rightarrow R \tag{36}$$

$$R \underset{k_b}{\overset{k_f}{\rightleftarrows}} Z \tag{37}$$

Substance Z is not reduced or oxidized at the electrode at the potentials applied.

Since chemical reaction (37) does not effect variations of the concentration of reactant O, the transition time is given by eqn. (16).

The concentration, $C_R(0, t)$, is affected by transformation (37) and Fick's differential equation must be modified to account for this effect[7].

(*v*) *Electrochemical reaction is preceded by adsorption of electroactive species; slow establishment of adsorption equilibrium.* Kinetic scheme:

$$O(\text{adsorbed}) \overset{\text{slow}}{\rightleftarrows} O(\text{solution}) \tag{38}$$

$$O(\text{adsorbed}) + ne \rightarrow R \tag{39}$$

$$O(\text{solution}) + ne \rightarrow R \tag{40}$$

In the presence of adsorption of an electroactive species at the electrode, the current at the electrode is composed of two components according to the origin of ions: $i = i_{ads.} + i_{diff.}$. Current $i_{ads.}$ originates from the discharge of the ions coming from the adsorption layer at the electrode[8]. The diffusion current, $i_{diff.}$, is determined by the concentration gradient according to eqn. (6.3). The surface concentration, Γ, of adsorbable ionic species is a function of time, and $i_{ads.}$ is given by the equation,

$$i_{ads.} = -nF\frac{d\Gamma}{dt} \tag{41}$$

where $d\Gamma/dt$ is the decrease of concentration in the adsorption layer.

In this section it will be assumed that adsorption equilibrium is established before the electrolysis and that the rate of adsorption (and desorption) is a slow process. The time necessary for establishment of the equilibrium is supposed to be considerably longer than the transition time, τ.

It is assumed that a complete monolayer of reactant O is established prior to electrolysis and that this monolayer is reduced to a monolayer of the reduced species, R.

(*a*) *Electrode reactions (39) and (40) are consecutive.* In this mechanism two cases can be distinguished.

In *the first case*[5,8], ions discharged at the electrode initially are supplied exclusively from the adsorption layer. When the adsorption layer is exhausted, ions diffuse to the electrode.

The adsorbed species, O, are more easily reduced (*i.e.*, reduce at less cathodic potentials) than the solution species. A potential–time curve exhibits two steps, the first of which corresponds to the reduction of the adsorbed species (39), and the second to the solution species (40).

Transition time ($\tau_{ads.}$) can be calculated from Faraday's law[8] because the amount of adsorbed species is a constant value determined by the surface area of the electrode (in the adsorption of a complete monolayer). Since the reduction of $O_{ads.}$ is completed at time, $\tau_{ads.}$, the number of coulombs necessary for the reduction is $i\tau_{ads.}$, thus

$$\tau_{ads.} = nF\Gamma/i \tag{42}$$

where Γ is initial equilibrium amount of adsorbed O species in moles/unit area.

Equation (16) applies to the second step.

Thus,[8]

$$\tau = \tau_{ads.} + \tau_{diff.} \tag{43}$$

and

$$i\tau = nF\Gamma + (nFC)^2\pi D/4i \tag{44}$$

A plot of $i\tau$ *vs.* $1/i$ yields a straight line with an intercept $nF\Gamma$ and a slope proportional to C^2D.

In *the second case*[5,8], it is assumed that in the first step, the supply of ions is exclusively due to the concentration gradient at the electrode according to Fick's law, until $C_{x=0} = 0$. When the adsorbed species of O is less easily reduced (*i.e.*, reduces at more cathodic potential) than the solution species, eqn. (16) applies to the first step. After $\tau_{diff.}$, the situation at the electrode is qualitatively similar to that of

kinetic schemes (18–19), species $O_{ads.}$ and $O_{sol.}$ are reduced at the electrode simultaneously.

The transition time, τ_2 ($\tau_2 = \tau_{ads.}\tau_1 = \tau_{diff.}$), is given by the equation[5]

$$\tau_2 = (i/nF)\,(\tau_1+\tau_2)\,\arccos\{(\tau_1-\tau_2)/(\tau_1+\tau_2)\} + (2i/nF)\sqrt{\tau_1\tau_2} \tag{45}$$

According to Lorentz's approximate treatment, $(i\tau)^{\frac{1}{2}}$ is given by the equation[5,8]

$$(i\tau)^{\frac{1}{2}} = (nF\Gamma)^{\frac{1}{2}} + nFC(\pi D)^{\frac{1}{2}}/2i^{\frac{1}{2}} \tag{46}$$

A plot of $(i\tau)^{\frac{1}{2}}$ *vs.* $1/i^{\frac{1}{2}}$ yields a straight line with an intercept $(nF\Gamma)^{\frac{1}{2}}$ and a slope proportional to $CD^{\frac{1}{2}}$.

The more rigorous treatment is given by REINMUTH[5] and ANSON[9].

(*b*) *Electrode reactions (39) and (40) are parallel (simultaneous).* When reactions (39) and (40) are simultaneous during the entire electrolysis time, τ, the current i, assuming constant distribution of i into $i_{ads.}$ and $i_{diff.}$, is given by[8,10]

$$i = i_{ads.} + i_{diff.} \tag{47}$$

and

$$i\tau = nF\Gamma + \tfrac{1}{2}nFC(\pi D\tau)^{\frac{1}{2}} \tag{48}$$

A plot of $i\tau$ *vs.* $\tau^{\frac{1}{2}}$ yields a straight line with an intercept $nF\Gamma$ and a slope proportional to $CD^{\frac{1}{2}}$.

Equations (44), (46) and (48) with corresponding plots can be used as diagnostic criteria for distinguishing between the different mechanisms of electrode reactions.

(*vi*) *Electrochemical reaction is preceded by adsorption of the electroactive species; rapid establishment of adsorption equilibrium.* Kinetic scheme:

$$\text{O(adsorbed)} \overset{\text{rapid}}{\rightleftharpoons} \text{O(solution)} \tag{49}$$

$$\text{O(adsorbed)} + ne \rightarrow \text{R} \tag{50}$$

$$\text{O(solution)} + ne \rightarrow \text{R} \tag{51}$$

In this section it will be assumed: (a) that electrode reactions (50) and (51) are simultaneous and (b) that adsorption equilibrium is maintained during the entire non-steady state electrolysis due to the rapid rate of adsorption and desorption.

The current–transition time characteristics for this mechanism depend upon the adsorption isotherm that relates Γ to $(C_O)_{x=0}$.

For the linear isotherm and when $C(D\tau)^{\frac{1}{2}} \gg \Gamma$, the current–transition time equation is given by[8,10]

$$C\tau^{\frac{1}{2}} = \tfrac{1}{2}(\pi/D)^{\frac{1}{2}}\Gamma + nF(\pi/D)^{\frac{1}{2}}C^2/2i \tag{52}$$

A plot of $C/\tau^{\frac{1}{2}}$ *vs.* C^2/i yields a straight line with an intercept $(\pi/D)^{\frac{1}{2}}\Gamma/2$ and a slope proportional to $D^{\frac{1}{2}}$.

(*vii*) *Electrochemical reduction followed by oxidation and vice versa.* Kinetic scheme:

$$\text{O} + ne \rightarrow \text{R} \tag{53}$$

$$\text{R} - ne \rightarrow \text{O} \tag{54}$$

The electrochemical reduction of reactant O to R proceeds up to transition time τ. At time τ, the direction of current through the cell is reversed. After time τ, species R which had been produced during the first step is reoxidized to O.

The theory of a single electrochemical reaction (section 1A) applies to the first step.

Treatment of the second step is more complex because of variation of the initial concentration of reactant with distance from the electrode[4].

Variation of the concentration of reactant R before (at τ) and during reoxidation to O is shown in Fig. 5.

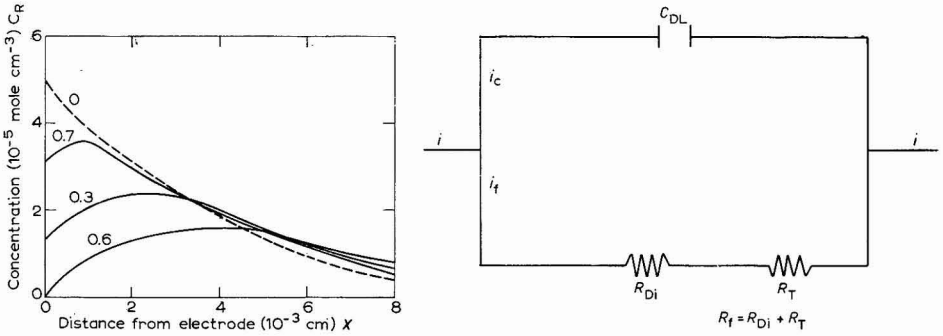

Fig. 5. Theoretical curves for variation of the concn., $C_R(x, t)$, before (at τ, *i.e.*, $t'=0$) and during re-oxidation. The number on each curve is the time in seconds elapsed after reversal of current at τ. (BERZINS AND DELAHAY[4]).

Fig. 6. Simplified equivalent circuit for single electrode reaction involving two consecutive steps, mass transport by diffusion and a charge transfer. (C_{DL}), Double-layer capacity of test electrode; (R_{Di}), diffusion resistance; (R_T), transfer resistance of electrode reaction; (R_f), resistance of electrode reaction.

Transition time for reoxidation step (54) is[4]

$$\tau' = \{\theta^2/(\theta+\lambda')^2 - \theta^2\}\tau \tag{55}$$

The functions θ and λ' are defined by equations,

$$\theta = i/nFD_R \tag{56}$$

$$\lambda' = i'/nFD_R \tag{57}$$

Where i and i' are the current densities in the first and second electro-chemical step, respectively, and D_R is the diffusion coefficient of substance R.

When $i=i'$, then $\theta=\lambda'$ and i' is given by

$$\tau' = \tfrac{1}{3}\tau \tag{58}$$

Relationship (58) holds when the reduced species, R, is soluble. In the case when R is insoluble and remains on the electrode[11]

$$\tau' = \tau \tag{59}$$

Relationship τ' to τ provides a very useful diagnostic criterion in electrode kinetics. This criterion is necessary in the study of the irreversible electrochemical reactions[11] where the potential–time function does not provide criteria for distinguishing between the cases with soluble and insoluble reduced forms, R.

C. Galvanostatic non-steady state electrolysis with a superimposed alternating current of constant amplitude. Kinetic scheme:

$$O + ne \rightarrow R \tag{60}$$

When alternating current with constant amplitude is superimposed on a galvanostatic pulse, the flux of the reactant O at the electrode is determined (according to eqn. (6.3)) by the sum of the direct current component ($i_{d.c.}$) and alternating component ($i_{a.c.}$)[3,12]

$$D_O \left(\frac{\partial C_O(x, t)}{\partial x}\right)_{x=0} = \frac{i_{d.c.} + i_{a.c.}}{nF} = \frac{i_{d.c.} + I \sin \omega t}{nF}, \tag{61}$$

where I is the amplitude and ω the angular velocity of the alternating current.

By solving Fick's equation for linear diffusion for the characteristic initial and boundary conditions, one obtains $C_O(0, t)$ as a function of C_O°, D_O, $i_{a.c.}$, ω and t.

2. Potential–time curves

A. Basic treatment

A simplified equivalent circuit for the single electrode reaction discussed in this review is shown in Fig. 6. The diffusion capacity, $C_{diff.}$, is neglected.

When a constant current is applied to the system shown in Fig. 6, current (electron flow) is used for[13,16].

(*a*) *Charging the double-layer capacity up to the potential at which electrode reaction can proceed with measurable velocity.*

(*b*) *Electrode reaction (charge transfer).*

Thus, the total current density, i, is given by

$$i = i_c + i_f \tag{62}$$

where i_c is capacitive, and i_f, faradaic current.

The potential of the test electrode at which a process is occurring, represented by the equivalent circuit in Fig. 6 during non-steady state galvanostatic electrolysis, varies with time according to the curve given in Fig. 2.

Three time intervals can be identified in the curve in Fig. 2.

(1) Time interval ($t = 0$–t_1). In this treatment the rise time across the circuit composed of the resistance and capacitance of the solution between the test electrode and the tip of the Luggin capillary (R_s, C_s) is neglected since it is 10^{-9} sec or less[17].

The first process after applying a current to the system is charging the double-layer capacity, C_{DL} in Fig. 6, from the reversible potential, E°, up to potential E_i when the electrode reaction begins at the measurable rate.

The time necessary to charge the capacity C in an RC circuit to 99.0% of the imposed voltage is

$$t_{v=0.99v_c} = 4.6\ RC \tag{63}$$

For example (in order to show the order of the magnitude) taking $C_{DL} = 50\ \mu F\ cm^{-2}$ and $R = 2\ \Omega$, $t_1 = 4.6 \times 10^{-4}$ sec.

(2) Time interval (t_2–t_1). When the potential E_i is reached the rate of change of

potential of the test electrode with time slows down since the potential is controlled by the electrochemical reaction.

The duration of this time interval is determined by the concentration of the reactant which is reduced or oxidized at the electrode and by the kinetics of the electrode reaction.

(3) Time interval (t_3–t_2). At time t_2, the concentration of the reactant at the electrode is equal to zero and the electron-transfer reaction cannot maintain the current constant because the supply of reactant to the electrode surface is insufficient. Starting from this point, a good portion of the impressed current will be used for charging the double-layer capacity up to the potential when the next electrode reaction commences. Simultaneously, the first electrode reaction continues to consume electrons from the electrode. Because only a part of the current is used for charging C_{DL}, the process is slower and takes a longer time than that in the time interval t_0–t_1, where at the beginning of the charging process almost all the current is used for the charging of C_{DL}. The distribution of the current (i) between components i_f and i_c (eqn. (62), Fig. 6) along the $E=f(t)$ curve during the three time intervals discussed is given in Fig. 7.

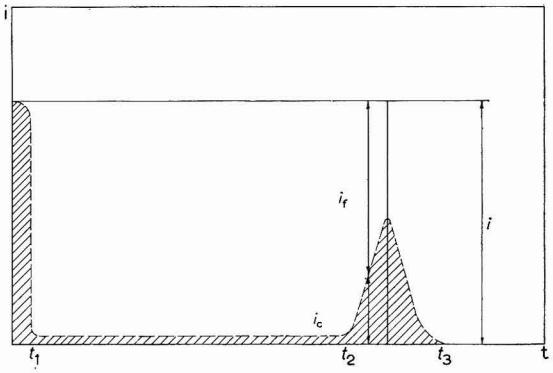

Fig. 7. Distribution of total current density, i, between components i_f and i_c along $E=f(t)$ curve shown in Fig. 2 (GIERST AND MECHELYNCK[15]).

The influence of the double-layer capacity on the shape of the potential–time curve is given qualitatively in the above discussion of E–t time intervals. It is obtained quantitatively from the equation for charging of the capacitor in the RC circuit (a series circuit)[16]

$$V_t = V_c(1 - e^{-t/RC}) \tag{64}$$

where

$V_t \rightarrow V_c$ when $t \rightarrow \infty$

The slope of curve (64) at $t=0$ is

$$\left(\frac{dV_t}{dt}\right)_{t=0} = \frac{V_c}{RC}. \tag{65}$$

Thus, for given values of R and V_c (in these discussions R and E_i) the rate of growth of

the function $E=f(t)$ up to potential V_c, *i.e.*, E_i, is controlled by the capacity which in our electrode system is the double-layer capacity.

If function (64) is approximated by a straight line, the tangent to the function at $t=0$, from the equation of the tangent (at x_0, $y=f'(x_0)x$) follows

$$V_t=(V_c/RC)t \tag{66}$$

Setting $V=V_c$, one gets

$$t=RC \tag{67}$$

If the approximation (66) is used to calculate the voltage after time $t=RC$, the capacitor C is charged to 100% V whereas this would be almost 63% using eqn. (64).

Therefore, in the first approximation, the slope of the $E=f(t)$ curve for the time interval (t_0-t_1) is given by eqn. (65) and the length of the time interval, *i.e.*, the approximate time necessary to reach the potential E_i (Fig. 2), by eqns. (63) and (67).

In the further theory of potential–time curves it will be assumed that experiments are conducted in such a way that t_1, the time necessary to charge the double layer, can be neglected in comparison with t_2 (*i.e.*, with the transition time τ) and the system will be treated as $i=i_F$ neglecting i_c (see eqn. (62), Fig. 6).

B. Single reversible electrochemical reaction. Kinetic scheme: (4)

The rate of reaction is controlled by diffusion only.

(*i*) *Reactant O and product R are soluble species.* The potential can be calculated as a function of time from the Nernst equation by using the time function, $C_O(0, t)$ and $C_R(0, t)$, as given by eqns. (14) and (15) in the logarithmic term.

Taking into account eqn. (16) for τ, in order to eliminate C°, $E=f(t)$ is given by[6]

$$E=E_{\tau/4}+(RT/nF)\ \ln\{\tau^{\frac{1}{2}}-t^{\frac{1}{2}})/t^{\frac{1}{2}}\} \tag{68}$$

with

$$E_{\tau/4}=E^\circ+(RT/nF)\ \ln\ (f_O D_R^{\frac{1}{2}}/f_R D_O^{\frac{1}{2}}) \tag{69}$$

where E° is the standard potential for the couple O–R and the f's are activity coefficients. For $t=\frac{1}{4}\tau$, $E=E_{\tau/4}$.

Equation (68) shows that a plot of the quantity $\ln\{(\tau^{\frac{1}{2}}-t^{\frac{1}{2}})/t^{\frac{1}{2}}\}$ *vs.* potential yields a straight line with slope RT/nF.

According to eqn. (69), $E_{\tau/4}$ is independent of C_O° and i, *i.e.*,

$$\frac{\partial E_{\tau/4}}{\partial \ln C^\circ}=0 \tag{70}$$

$$\frac{\partial E_{\tau/4}}{\partial \ln i}=0 \tag{71}$$

(*ii*) *Product of electrolysis, R, is insoluble.* Kinetic scheme: (4a)

With the assumption that the activity of the deposit (insoluble product) is equal to unity, $E=f(t)$ can be calculated using the Nernst equation with $C_O(0, t)$, from eqn. (14).

The result is[11]

$$E=E^{\circ\prime}+(RT/nF)\ \ln\ \{2i/nF(\pi D_O)^{\frac{1}{2}}\}+(RT/nF)\ \ln\ (\tau^{\frac{1}{2}}-t^{\frac{1}{2}}) \tag{72}$$

where $E^{\circ\prime}$ is the formal standard potential of the couple O–R.

The plot of $\ln(\tau^{\frac{1}{2}}-t^{\frac{1}{2}})$ *vs.* E yields a straight line with slope RT/nF. E-values for various values of t for the construction of this plot are taken from the experimental $E=f(t)$ curve.

By putting $t=\tau/4$ in eqn. (72) and by subsequent elimination of τ with (16), the potential at time $t=\tau/4$ is

$$E_{\tau/4}=E^{\circ\prime}+(RT/nF)\ln\tfrac{1}{2}C^{\circ} \tag{73}$$

From (73)

$$\frac{\partial E_{\tau/4}}{\partial \ln C^{\circ}}=\frac{RT}{nF} \tag{74}$$

$$\frac{\partial E_{\tau/4}}{\partial \ln i}=0 \tag{75}$$

C. Single irreversible electrochemical reaction. Kinetic scheme: (4)

The reaction is controlled by diffusion and charge transfer.

(*i*) *Reactant O and product R are soluble species.* The potential of the test electrode for an irreversible electrochemical reaction, neglecting backward reaction ($k_{f,h}\gg k_{b,h}$) is given by,

$$E=(RT/\alpha n_a F)\ln nFk_{f,h}^{\circ}\,C_O(0,t)-(RT/\alpha n_a F)\ln i \tag{76}$$

where n_a is the number of electrons involved in the rate-determining charge-transfer step, n the number of electrons involved in the overall reaction, α the transfer coefficient and $k_{f,h}^{\circ}$ the value of the formal rate constant for the forward electrochemical process when $E=0$.

Substituting $C_O(0,t)$ in eqn. (76) by the time function $C_O(0,t)$ given by eqn. (14), and introducing the transition time τ according to eqn. (16) one gets[6]

$$E=(RT/\alpha n_a F)\ln(\tau^{\frac{1}{2}}-t^{\frac{1}{2}})-(RT/\alpha n_a F)\ln(\pi^{\frac{1}{2}}D_O^{\frac{1}{2}}/2k_{f,h}^{\circ}) \tag{77}$$

or

$$E=(RT/\alpha n_a F)\ln(nFC^{\circ}k_{f,h}^{\circ}/i)+(RT/\alpha n_a F)\ln[1-(t/\tau)^{\frac{1}{2}}] \tag{78}$$

The plot of $\ln(\tau^{\frac{1}{2}}-t^{\frac{1}{2}})$ or $\ln[1-(t/\tau)^{\frac{1}{2}}]$ *vs.* E is a straight line the slope of which is $RT/\alpha n_a F$. Thus, αn_a can be calculated from the slope.

For $t=0$, eqn. (78) reduces to

$$E_{t=0}=(RT/\alpha n_a F)\ln(nFC^{\circ}k_{f,h}^{\circ}/i) \tag{79}$$

Therefore, potential at zero time depends on $k_{f,h}^{\circ}$, C° and i. The rate constant, $k_{f,h}^{\circ}$, can be calculated from eqn. (79).

The potential at time $t=\tau/4$ is

$$E_{\tau/4}=\varepsilon+(RT/\alpha n_a F)\ln(\pi^{\frac{1}{2}}nFC^{\circ}D_O^{\frac{1}{2}}/4i) \tag{80}$$

where ε is the second term in eqn. (77).

From (80) it follows[11], for constant current i,

$$\frac{\partial E_{\tau/4}}{\partial \ln C^{\circ}}=\frac{RT}{\alpha n_a F} \tag{81}$$

and for constant concentration C°

$$\frac{\partial E_{\tau/4}}{\partial \ln i} = \frac{RT}{\alpha n_a F} . \tag{82}$$

The rate constant, $k_{f,h}$, can be defined as a function of potential by two parametric equations with the parameter t representing the time[6];

(a) The first parametric equation is a function, $k_{f,h}=f(t)$, which can be derived from the equation

$$i/nF = k_{f,h} C_O(0, t) \tag{83}$$

which defines the rate of forward electrochemical reaction (backward reaction is neglected, $k_{f,h} \gg k_{b,h}$). Substituting $C_O(0, t)$ in eqn. (76) by (14) and eliminating C° by (16)

$$k_{f,h} = \pi^{\frac{1}{2}} D^{\frac{1}{2}}/2(\tau^{\frac{1}{2}} - t^{\frac{1}{2}}) \tag{84}$$

(b) The second parametric function is the experimental curve $E=f(t)$.

For assigned values of t, the corresponding values of $k_{f,h}$ can be computed from eqn. (84), the corresponding value of E can be read from the experimental curve $E=f(t)$ and the graph of the function $K_{f,h}=F(E)$ can be plotted.

The intercept of the function $k_{f,h}=F(t)$ at $E=0$ yields $k_{f,h}^\circ$.

(*ii*) *Product R is insoluble.* Since the potential of the test electrode does not depend on $C_R(0, t)$, eqn. (77) is valid here with all consequences.

D. Complex mechanisms

(*i*) *Electrochemical reduction followed by oxidation and vice versa.* Kinetic scheme (53–54)

(a) *Reversible electrochemical reaction.* The potential of the test electrode as a function of time after reversal of the current through the cell at the time τ is given by the equation[4]

$$E = E_{1/4} + \frac{RT}{nF} \ln \frac{\tau^{\frac{1}{2}} - \{(\tau+t')^{\frac{1}{2}} - 2t'^{\frac{1}{2}}\}}{(\tau+t')^{\frac{1}{2}} - 2t'^{\frac{1}{2}}} \tag{85}$$

where $t'=t-\tau$ and $E_{1/4}$ is defined by eqn. (69).

For the reoxidation process according to eqn. (85), the function $E=f(t)$ has the value $E_{1/4}$ when $t'=0.222\ \tau'$. For the first step (reduction), $E=f(t)$ has the value $E_{1/4}$ when $t=\tau/4=0.250\ \tau$. This can be used as a diagnostic criterion of reversibility of the process.

(*b*) *Irreversible electrochemical reactions.* Potential–time function for the reoxidation process in this case is

$$E = \frac{RT}{(1-\alpha')n_a' F} \ln \frac{\pi^{\frac{1}{2}} D_R^{\frac{1}{2}}}{2k_{b,h}^\circ} - \frac{RT}{(1-\alpha')n_a' F} \ln \left\{(\tau+t')^{\frac{1}{2}} - 2t'^{\frac{1}{2}}\right\} \tag{86}$$

A plot of $\ln\{(\tau+t')^{\frac{1}{2}} - 2t'^{\frac{1}{2}}\}$ *vs.* E yields a straight line with slope $RT/(1-\alpha')n_a' F$.

The rate constant $k_{b,h}$ can be calculated from $E_{t'=0}$ in an analogous way to the calculation of $k_{f,h}$ from eqn. (78) *i.e.*, (79).

Therefore, the current-reversal method can be used for the study of the kinetics of electrochemical reactions in both directions.

E. Galvanostatic non-steady state electrolysis with a superimposed alternating current of constant amplitude

This case has been studied so far only for reversible electrode processes[12].

The potential of the test electrode is the sum of a d.c. and an a.c. component. The alternating component of potential tends to infinity for $t=0$ and $t=\tau$. Theoretically calculated potential–time curves, $E_{d.c.}=f_1(t)$ and $E_{a.c.}=f_2(t)$, are shown in Fig. 8.

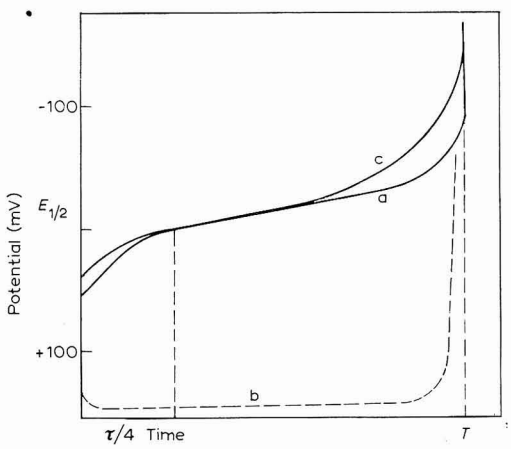

Fig. 8. Theoretical potential–time curves. (a), For conventional chronopotentiometry; (b), alternating component; (c), Fournier d.c. component (TAKEMORI *et al.*[12]).

Large variations of the alternating component of the potential should allow more precise determinations of the transition time than conventional chronopotentiometry.

III. VERIFICATION OF THE THEORY

Only verification of fundamental equations will be discussed. The discussion will include the transition-time equation (eqn. (16)) and the potential–time equations for single electrochemical reactions (eqns. (68), (72), (77) and (78)).

1. Transition-time equation

A. Historical

Equation (16) was derived by SAND[2] in 1901. This equation was verified by Sand (and other investigators up to 1950) by checking the independence of the product $i\tau^{\frac{1}{2}}$ of the current density for transition times of the order of several hours. In these experiments, owing to the length of electrolysis, mass transport was by convection as well as by diffusion. Reliable results were obtained in 1950 by GIERST AND JULIARD[13,14]. Potential–time curves were recorded by a cathode ray oscilloscope. Transition times ranged from a few minutes to fractions of a second. They found that the product $i\tau^{\frac{1}{2}}$ remains constant to within 0.6% for a ten-fold change of the current density (from 0.18 to 1.18 mA cm^{-2}).

LAITINEN AND FERGUSON[18] in 1957 investigated the validity of the transition-time equation for molten salt systems. They found that the plot of the product, $i\tau^{\frac{1}{2}}$, *vs.* C° gives a straight line which is in accordance with eqn. (16).

VOORHIES AND FURMAN[19] in 1959 showed the applicability of the equation to non-aqueous solutions by examining the constancy of the transition-time constant ($K = i\tau^{\frac{1}{2}}/C^{\circ}$) with variations in the transition time.

B. Factors that can cause deviations from the transition-time equation

The main factors that can cause deviation from the transition-time equation are: (i) coverage of the electrode by the adsorbed substances, (ii) surface roughness of solid electrodes, (iii) non-linearity of the diffusion field, (iv) convection and (v) double-layer effects. Each of these factors will be discussed briefly.

(*i*) *Coverage of the electrode by adsorbed substances that are neither reduced nor oxidized at the electrode.* The partial coverage of the electrode by the adsorbed substances that are neither reduced nor oxidized at the electrode can cause three classes of changes[20-22].

First, consider a decrease in available surface area for the electrode reaction as a result of a blocking of part of the electrode surface. This causes an increase in actual current density and decrease in τ.

Coverage of the electrode at a certain potential is a function of time, and kinetics of adsorption may require a considerable time (of the order of minutes) to reach the equilibrium surface concentration of the adsorbed substance[23,24]. The kinetic characteristics of adsorption can be additional parameters in E–t relationships.

Secondly, change in the kinetic parameters of the electrode reaction: the rate constant and the transfer coefficient, α[25]. In general, the rate constant and α decrease as a result of adsorption. The rate of the electrode reaction can be reduced to the extent that (k_f) corresponds to the irreversible behavior and the process can become activation-controlled if it was previously diffusion-controlled. The effect is change in the rate-determining step.

Thirdly, introduction of a new slow step into the reaction sequence: transfer of reactants across the thin adsorbed layer.

GIERST AND JULIARD[14] have registered linear decrease of $i\tau^{\frac{1}{2}}$ with current density in the electrolysis of a $3 \cdot 10^{-3}$ M cadmium solution with the addition of gelatin.

(*ii*) *Surface roughness of solid electrodes.* Variation of concentration, $C_O(x, t)$, $C_R(x, t)$, and transition time was calculated for semi-infinite linear diffusion to a plane electrode. Equation (16) is therefore valid for a planar flat electrode. For the rough electrode the diffusion is not strictly linear. The nature of diffusion depends on the nature of the geometry of the roughness. For the first approximation model, the uneven surface of the electrode can be represented as a sinusoidal type of imperfection. For a sinusoidal uneveness there is a spherical contribution to diffusion.

There is no exact theory for non-steady state diffusion to a rough electrode.

For the steady-state conditions at the electrode it was shown[16,26] that at distances large compared with the amplitude of the sinusoidal type of imperfection (uneveness), the concentration profile is unaffected by the uneveness of the electrode. In terms of thickness of diffusion layer, this extreme condition can be stated in this way: for thickness of the diffusion layer large in comparison with the amplitude of

the imperfections of the electrode, eqn. (14) is valid[5]. For these conditions the diffusional area is the same as the projected area of the electrode and the roughness factor is equal to 1 (f=real/geometric (apparent) surface area).

With decreasing distance from the electrode, which is tantamount to decreasing thickness of the diffusion layer, uneveness of the surface becomes more important and the real diffusional area increases; hence, the roughness factor, f, also increases. This can be seen in Fig. 9.

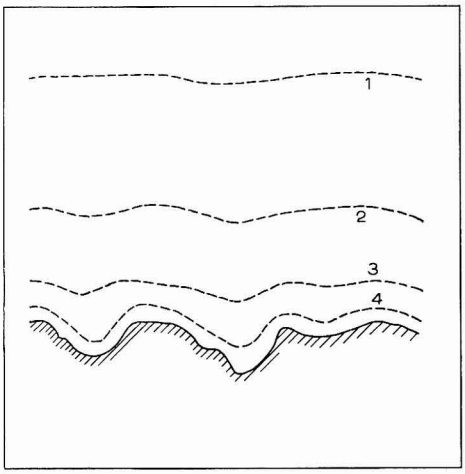

Fig. 9. Schematic representation of diffusion layer on a rough electrode. Increase in roughness factor with decrease in thickness of diffusion layer in the order of 1–4 (LORENZ[8]).

When one encounters larger real diffusional areas and larger f's for the same imposed current, there is a correspondingly lower real current density ($i_{real}=I/P_{real}=I/f\times P_{apparent}$) and therefore a longer time of electrolysis.

One can thus expect positive deviations from constancy of the product $i\tau^{\frac{1}{2}}$ with increasing current density resulting from roughness of the electrode.

(*iii*) *Non-linearity of the diffusion field.* The plane indicator electrode should be designed in such a way that it provides conditions for uni-directional diffusion only along lines that are normal to the surface. For precise measurements and precise checking of the validity of eqn. (16), a planar electrode should be shielded[27,28]. These conditions can be approximated satisfactorily for analytical applications by the use of a platinum foil electrode positioned in such a way that the current lines are normal to the plane surface. An unshielded planar disc electrode can be used as a micro-electrode.

Under certain conditions eqn. (16) may be valid for spherical electrodes and cylindrical wire electrodes[29,30]. When the dimensions of an electrode are large compared with the diffusion-layer thickness, then the electrode surface referred to the diffusion layer approximates an infinite plane.

Deviations from the transition-time equation are very often noticed in the use of all types of electrodes mentioned including the shielded planar electrode.

Diffusion to the unshielded planar electrode occurs not only in directions

normal to the surface, but also in arbitrary directions. There are spherical contributions to the diffusion to a planar circular electrode. Non-linearity of the diffusion field around the electrode can be a cause of deviations from theoretical equations. When the thickness of the diffusion layer is large by comparison with the dimensions of the electrode, the diffusional field is to the first approximation, linear. As the thickness of the diffusion layer decreases, the departure from linearity increases.

Therefore, since the thickness of diffusion layer is given by $\sqrt{D\tau}$, one would expect deviation due to non-linearity of diffusion for longer transition times, *i.e.*, lower current densities.

Positive and negative deviations from the constancy in $i\tau^{\frac{1}{2}}$–τ plots were observed by many investigators[29,31]. One example is shown in Fig. 10.

Increase at long transition time was explained by spherical contributions to the diffusion.

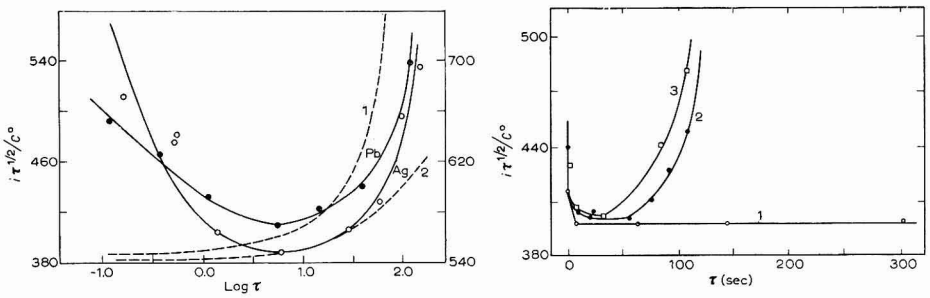

Fig. 10. Variation of $i\tau^{\frac{1}{2}}/C^\circ$ with log τ for reduction of Ag(I) and Pb(II) at unshielded disc electrode. Left axis, Ag(I), 5.00 mM in 0.2 M $NaNO_3$ soln.; τ measured at *ca.* −0.24 V *vs.* satd. mercurous sulfate electrode. Right axis, Pb(II), 5.00 mM in 0.2 M $NaNO_3$ soln.; τ measured at *ca.* −0.72 V *vs.* S.C.E. (---), Calcd. for spherical diffusion for $n=1$, $D=1.95\times10^{-5}$ cm^2 sec^{-1}, $C^\circ=5.00$ mM, for an *effective radius* of (1), 0.13 and (2), 0.26 cm (BARD[29]).

Fig. 11. Variation of $i\tau^{\frac{1}{2}}/C^\circ$ with τ for reduction of Ag(I) at shielded electrode. Ag(I), 5.00 mM in 0.20 M KNO_3 and 0.01 M HNO_3. Electrode 1.00 cm^2. Orientation of electrode: (1) horizontal, diffusion upward; (2), horizontal, diffusion downward; (3), vertical (BARD[29]).

(*iv*) *Convection.* Measurements with a shielded planar electrode can also show deviations. Deviations can be caused by natural convection if the indicator electrode is not properly oriented. The electrode should be oriented in such a way that the density gradient produced as a result of electrode reaction does not cause natural convection (less dense solution should be above the denser solution)[27]. The influence of orientation of the electrode can be seen from Fig. 11.

It is seen from Fig. 11 that the transition-time constant is independent of τ for large values of transition time in the absence of natural convection.

(*v*) *Double-layer effect.* The effect of charging of the double layer on the transition-time constant can be qualitatively estimated[14,29] by assuming that the charging of the double layer occurs constantly during time τ with the constant capacitive current, $i_c=C_{DL}\Delta E/\tau$.

With this assumption from eqns. (62) and (16), the total current density is

$$i=nF\pi^{\frac{1}{2}}D^{\frac{1}{2}}C^\circ/2\tau^{\frac{1}{2}}+C_{DL}\Delta E/\tau \qquad (87)$$

and the transition time constant

$$i\tau^{\frac{1}{2}}/C^{\circ} = nF\pi^{\frac{1}{2}}D^{\frac{1}{2}}/2 + (C_{DL}/C^{\circ})\ (\Delta E/\tau^{\frac{1}{2}}) \tag{88}$$

For constant concentration C°,

$$i\tau^{\frac{1}{2}}/C^{\circ} = K + K'/\tau^{\frac{1}{2}} \tag{89}$$

Equations (88) and (89) give the transition-time constant as a function of τ. It follows from these equations that with decreasing τ, the second term in eqn. (88) *i.e.*, (89), increases. Therefore, positive deviations are expected for small values of τ. For large values of τ, the second term can be neglected and the charging of the double layer does not contribute to the deviations.

The upper limit for the current density can be calculated[3] from the relationship Q_c/Q_e where Q_c is the quantity of electricity used for charging of the C_{DL} and Q_e the quantity of electricity used for the electrode reaction.

$$Q_c/Q_e = C_{DL}\Delta E/i\tau = 4iC_{DL}\Delta E/\pi n^2F^2(C^{\circ})^2D_O \tag{90}$$

The relationship between the critical (minimum) applied current density, i_K, and the limiting current density, i_L, has been derived by RYABUKHIN[32].

(*vi*) *Adsorption of electroactive species and products of reaction.* The concomitant electrolysis of electroactive species diffusing to and adsorbed on the electrode yields larger values of the transition time and consequently produces deviations from the transition-time equation. Transition time–current relationships for these cases are discussed in the sections II-B and IV-4.

(*vii*) *Oxide formation.* The formation or reduction of an oxide film may precede, follow or occur simultaneously with the electrode reaction studied. The effect of this complicated process is the same as in the case of adsorption of an electroactive species: increase in the chronopotentiometric constant with increasing current density.

ANSON AND LINGANE[33] and BARD[34] derived equations for the correction of experimental data to yield the transition time for the electrode reaction of interest.

2. Potential–time equations for single electrochemical reactions

Equation (68) was derived and verified for the first time by KARAOGLANOFF[35] in 1906. The results were unsatisfactory since the transition times measured were of the order of several hours. In 1954, DELAHAY AND MATTAX[36] obtained results that were in agreement with the theory for electrolysis in aqueous solutions. Plots of the logarithmic term in eqns. (68) and (77) *vs.* time were linear for transition times of the order of one minute.

INMAN AND BOCKRIS[37] in 1962 showed the validity of eqns. (68) and (72) for electrolysis in molten salts. LAITINEN AND RHODES[38] in 1962 measured variations of $E_{\tau/4}$ with concentration in accordance with eqn. (74).

IV. APPLICATIONS TO SELECTED PROBLEMS

1. Applications in electroanalytical chemistry

The analytical application is based on eqn. (16) according to which $i\tau^{\frac{1}{2}}$ *vs.* concentration gives a straight line. This can be used as a calibration curve[39,40]. The plot of $\tau^{\frac{1}{2}}$ *vs.* concentration should extrapolate to $\tau^{\frac{1}{2}} = 0$ sec for $C^{\circ} = 0$. Transition time $\tau^{\frac{1}{2}} > 0$ sec for $C^{\circ} = 0$ observed by LAITINEN AND GAUR[39] was attributed to impurities in the supporting electrolyte. Residual transition times can be expected more often in molten-salt systems than in aqueous systems because of higher ionic concentrations[39].

The precision of the concentration determination depends upon the constancy of temperature of the solution being analyzed, stability of the current, and precision of transition-time measurements. The fluctuations in the temperature that can be tolerated are determined by the temperature coefficient of the diffusion coefficient. Linearity of the $i\tau^{\frac{1}{2}}$–C plot requires constant D.

Reproducibility of the transition-time measurements was studied[3] for the reduction of 0.001–0.01 M solutions of iodate ion in 1 N NaOH at the current densities from about 1–10 mA cm^{-2} and transition times from about 58–54 sec. The average deviation from the mean value of τ was $\pm 0.4\%$. The maximum deviation was 1.27%. Since C° is proportional to $\tau^{\frac{1}{2}}$, the average deviation for concentration is $\pm 0.2\%$ and the maximum, $\pm 0.65\%$.

For molten salt systems in the millimolar concentration range, the accuracy is between 2 and 4%[41]. LAITINEN AND FERGUSON[18] studied the precision of transition-time measurements for the reduction of a 2.08 mM solution of cadmium chloride at 15.8 μA cm^{-2}. The standard deviation was $\pm 4.0\%$ for an average transition time of 2.077 sec.

The microelectrode in this study was not shielded. Linearity of the $\tau^{\frac{1}{2}}$–C° plot in the concentration range about 2–80 mM is within $\pm 2.6\%$.

It is clear that there is insufficient data for conclusive judgement on the precision of the chronopotentiometric method having in mind the principal factors that can cause deviations from transition-time eqn. (16) and the results so far available.

2. Applications to the determinations of diffusion coefficients

The diffusion coefficient of the reacting species can be obtained from two types of plots that give straight lines on the basis of eqn. (16).

First, when $i\tau^{\frac{1}{2}}$ is plotted *vs.* i for constant concentration of the reactant, the intercept with the $i\tau^{\frac{1}{2}}$-axis is $(\pi^{\frac{1}{2}}nFC^\circ D_O^{\frac{1}{2}})/2$. Since the product $i\tau^{\frac{1}{2}}$ is independent of i, the plot should be a straight line parallel to the i-axis[14].

Secondly, the slope of the $i\tau^{\frac{1}{2}}$ *vs.* C plot is[18] $nF\pi^{\frac{1}{2}}D^{\frac{1}{2}}$.

In the first case from the intercept, and in second from the slope, one can calculate the diffusion coefficient, D.

When D is plotted *vs.* i/T, on the basis of determinations of the diffusion coefficient D at different temperatures, one can calculate the activation energy for the diffusion of reacting species[42,43].

3. Applications in electrode kinetics and elucidation of mechanisms of electrochemical reaction

The kinetics of electrochemical and chemical reactions can be studied by the galvanostatic non-steady state electrolysis as shown above.

A knowledge of the kinetics enables the mechanism of electrochemical reactions to be elucidated. Four diagnostic criteria were proposed[11]:

(a) A linear plot of some logarithmic function of time and τ *vs.* potential, and the slope of that plot.

$$E = \varphi\{\ln F(t, \tau)\}; \quad \frac{\partial\varphi\{\ln F(t, \tau)\}}{\partial E}$$

(b) Variation of the quarter-time potential with the logarithm of the imposed current density.

$$\frac{\partial E_{\tau/4}}{\partial \ln i}$$

(c) Variation of the quarter-time potential with the logarithm of the bulk concentration of the species that reacts at the electrode

$$\frac{\partial E_{\tau/4}}{\partial \ln C^{\circ}}$$

(d) The ratio of the transition times in the current-reversal method

$$\tau/\tau'$$

These four diagnostic criteria for the Kinetic Scheme discussed are summarized in Table 1.

TABLE 1

DIAGNOSTIC CRITERIA FOR THE KINETIC SCHEMES DISCUSSED

Kinetic scheme	$F(t, \tau)$	$\frac{\partial \varphi\{lnF(t,\tau)\}}{\partial E}$	$\frac{\partial E_{\tau/4}}{\partial \ln C^{\circ}}$	$\frac{\partial E_{\tau/4}}{\partial \ln i}$	τ/τ'
$O+ne \rightleftarrows R$	$\tau^{\frac{1}{2}}-t^{\frac{1}{2}}/\tau^{\frac{1}{2}}$	RT/nF	0	0	$\frac{1}{3}$
$O+ne \rightleftarrows R_{(insol.)}$	$\tau^{\frac{1}{2}}-t^{\frac{1}{2}}$	RT/nF	RT/nF	0	1
$O+ne \rightarrow R$	$\tau^{\frac{1}{2}}-t^{\frac{1}{2}}$ or $\{1-(t/\tau)^{\frac{1}{2}}\}$	$RT/\alpha n_a F$	$RT/\alpha n_a F$	$-RT/\alpha n_a F$	$\frac{1}{3}$ or 0
$O+ne \rightarrow R_{(insol.)}$	$\tau^{\frac{1}{2}}-t^{\frac{1}{2}}$ or $\{1-(t/\tau)^{\frac{1}{2}}\}$	$RT/\alpha n_a F$	$RT/\alpha n_a F$	$-RT/\alpha n_a F$	$\frac{1}{3}$ or 0

Diagnostic criteria for the occurrence of a prior chemical reaction is $i\tau^{\frac{1}{2}}=f(i)$, given by eqn. (32).

Diagnostic criteria for other kinetic schemes are given by REINMUTH[11].

Whether species A is an electroactive species or not can be determined by studying the dependence of $k_{b,h}^{\circ}$ on the concentration of A[44].

The product of the first step, *i.e.*, the intermediate species for stepwise electrode reactions, can be ascertained on the basis of the determinations of n for the first step, using eqns.[33,43] (28), (68), (72) and (77).

4. Study of the adsorption of electroactive species

Adsorption of an electroactive species on an electrode surface is detected qualitatively by increase in the value of the chronopotentiometric constant, $i\tau^{\frac{1}{2}}/C$ (or $i\tau^{\frac{1}{2}}$ product), above the theoretical value and the increase of this constant with increasing current density. The qualitative appearance of the chronopotentiogram is a function of the concentration of the electroactive species and the applied current[45,48].

The quantitative calculation of the amount of adsorbed electroactive species from transition-time measurements involves extrapolation of current–transition-time functions (eqns. (44), (46), (48) and (52)) to $\tau=0$. Γ calculated from these intercepts depends upon the equation chosen for extrapolation. Thus, an accurate calculation of Γ on this basis requires a knowledge of the mechanism of the electrode reactions, *i.e.*, the corresponding i–τ equation. The mechanism is usually ascertained by *the best fit*

criterion on comparison of the experimental i–τ relationship with the several theoretical equations. Constancy of the diffusion coefficient, D, over a range of solution concentrations is an auxiliary criterion[45].

MURRAY suggested the use of ramp current ($i=\beta t$) chronopotentiometry as a diagnostic test[49].

MURRAY AND GROSS[45] discussed the experimental conditions that are of importance in carrying out measurements for distinguishing between different electrode mechanisms. They were able to come to definite conclusions on the mechanism of electrode reactions in the case of adsorption of lead and mercury(II) on a mercury electrode.

Because the current–transition-time characteristics of different mechanisms are not widely different, it is not always possible to reach clear conclusions in distinguishing between different theoretical mechanisms.

The feasibility of distinguishing between different cases, and the limitations of the chronopotentiometric method in the quantitative study of adsorption was discussed by LAITINEN AND CHAMBERS[50]. They found that desorption in the region of potentials involved in transition-time measurements, gives high transition times, and a high, and concentration-dependent diffusion coefficient.

TATWAWADI AND BARD[10] calculated Γ for riboflavin on a mercury electrode using different theoretical equations and, in general, obtained good agreement between the values of Γ obtained by chronopotentiometric and electrocapillarity measurements. In the same study, it was found that a system with simultaneous adsorption of reactants and products can be interpreted by intermediate mechanisms.

HERMAN, TATWAWADI AND BARD[46] used the current-reversal method to study adsorption.

5. Study of complex ions

The theory of kinetic scheme (29–30) can be applied to the study of the mechanism of reduction of complex ions[6] and the kinetics of formation and dissociation of complex ions[51].

INMAN AND BOCKRIS[52] calculated the formation constants of a series of complex ions formed in the molten-salt solution $Cd(NO_3)_2+NaNO_3+KNO_3$, by determining the quarter-time potentials. On the basis of knowledge of the successive formation constants and the rate constants for formation and dissociation of the slowest dissociating complex, BOCKRIS *et al.*[53,54] calculated the lifetime of the slowest dissociating complex ion in the series.

V. INSTRUMENTATION AND EXPERIMENTAL TECHNIQUE

1. Cells

Basically, three types of cells can be used—with one, two or three separate compartments. The system can contain two or three electrodes. In two-electrode systems, the reference electrode is also the auxiliary electrode and in this case should be of large area in order to avoid polarization.

GIERST AND JULIARD[14] in 1953 used a two-electrode system, with a slow-growing mercury drop ($P\simeq$ 1 mm^2) as a test electrode and a large reversible counter electrode ($P\simeq$ 300 mm^2), in a single compartment.

A three-electrode system was used in 1953 by DELAHAY AND BERZINS[6]. In an H-shape cell, a mercury pool of constant area was used as a test electrode, platinum as an auxiliary, and saturated calomel as a reference electrode. In a three-electrode system it is possible to minimize the ohmic drop.

A liquid bismuth electrode was used by VAN NORMAN[55].

LINGANE[56] used a system with a solid indicator electrode. An all-glass, single-compartment cell with three electrodes has been designed for studies in molten salts[37].

The cell used for studies of molten fluorides was designed by SENDEROFF, MELLORS AND REINHART[43].

2. Solution preparation

Special care for the purity of solvent and solute must be taken for the study of molten-salt systems. LAITINEN, FERGUSON AND OSTERYOUNG[57] have described the technique of melt preparation; they used a residual-current criterion to follow the degree of purification of the molten-salt solvent.

Purification of molten fluorides is described by SENDEROFF, MELLORS AND REINHART[43].

3. Electrode pre-treatment

The importance of pre-treatment of the surface of the solid electrode has been discussed by ANSON AND LINGANE[33] and VOORHIES AND FURMAN[58].

There are two main types of pre-treatment; (i) pre-treatment to prepare a chemically-pure metal surface free from oxides, or with well-defined and reproducible oxide layers; (ii) surface polishing of the solid electrodes to avoid any roughness effect[39].

In the study of deposition of metals, the solid electrode can be cleaned of deposited metal by anodic polarization between experiments[18]. The electrode can become rougher with deposition of high-melting metals.

4. The electrolysis circuit

Constant-voltage power supply and constant-current power supply can be used as current sources. Current should be maintained constant to within $\pm 0.1\%$. A series of high-voltage batteries can be used as a current supply.

A constant-voltage power supply (PS) usually with output voltage of 200–300 V is connected to the electrolytic cell in series with variable resistances, R_1 and R_2 (Fig. 12a). The current is adjusted by resistance R_1 and the exact value determined by measuring the ohmic drop across the calibrated resistance, R_2, with a potentiometer, P. The electrolytic cell is by-passed during current measurements (R_3).

A relay is used for switch SC. A switch with a rise or decay time less than 1 μsec is described by MATTSON AND BOCKRIS[59].

When a constant-current supply is used, the resistance R_1 is omitted.

A switching circuit[60] with a rise time of 10^{-7} sec is shown in Fig. 12b.

A switching circuit with an initially biased electrode is described by OSTERYOUNG[61].

5. Recording of the potential–time curves

The voltage between the test electrode, e_1, (Fig. 12a) and the reference

electrode, e_2, *vs.* time can be recorded by means of a recording potentiometer or a cathode-ray oscilloscope.

A recorder with a fast response (0.5 sec for full span) is usually used for recording potential–time curves with transition times longer than 2 sec[18]. The time-base of the recorder can be calibrated by simultaneous timing with the electric timer[29].

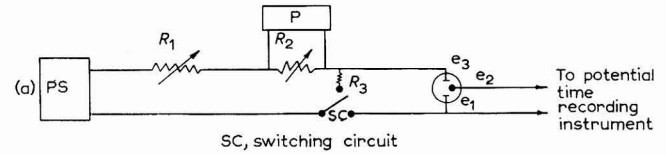

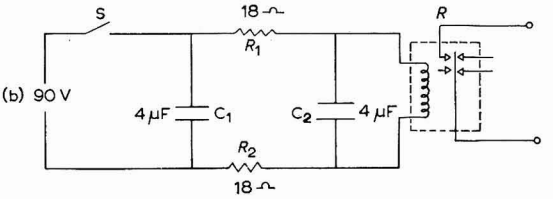

Fig. 12. (a), Elementary electrolysis circuit; (b), switching circuit (SC) with a rise time of 10^{-7} sec; (R), 275B western electric relay; (S), microswitch (DEVANATHAN AND SELVARATNAM[60]).

A cathode-ray oscilloscope is usually used for recording the potential–time relationship for an electrolysis of shorter duration[6]. The time-base of the oscilloscope is calibrated by an oscillator that has been calibrated against a time mark generator[29].

6. Automatic determination of transition time

In electroanalytical applications, once the electrode processes are known and potential–time curves interpreted, it is necessary to record the transition time only, in order to determine the concentration of the reacting species. This can be done automatically using the instrument described by SARTIAUX[62].

The electrolysis circuit is the same as in Fig. 1 or Fig. 12a. The test electrode, e_1, and reference electrode, e_2, are connected to the potentiometer, P_2. A relay connects the potentiometer and timer circuit. The potentiometer P_2 is set at a value corresponding to the potential of the test electrode at which the transition time is measured. The relay is set to switch off the timer circuit at the transition-time potential.

The electrolysis and the timer are started simultaneously by means of the fast switch. When the transition time is reached, the relay opens the timer circuit. The reading at the timer gives directly the transition time. The scale of the timer can be calibrated to give directly the concentration of the species being determined.

For measurement of transition times longer than one second, closing as well as opening of the fast switch can be done manually[56].

An electronic instrument for automatic measurement of the transition time has been designed by GIERST AND MECHELYNCK[15].

7. The recording of the first derivative of potential–time curves

The circuit used for the recording of the first derivative of a potential–time

curve is described by IWAMOTO[40]. Automatic determination of transition time is possible with the differential technique under certain conditions.

8. Electrolysis with superimposed alternating current

The alternating current through the cell can be measured directly, or the characteristics of the cell can be measured by means of an a.c. bridge. Both methods are described in DELAHAY's monograph[3].

ACKNOWLEDGEMENTS

It is a pleasure to thank Dr. N. E. RICHARDS and Mr. E. R. RUSSELL for valuable comments during the preparation of the manuscript.

SUMMARY

Basic ideas, principles, potentialities and recent developments of chronopotentiometry, as a method of electrochemical studies, are reviewed.

Single and complex mechanisms of electrode reactions are discussed and the sequence of occurrences on the electrode during galvanostatic non-steady state electrolysis analyzed. Derivations of fundamental relationships, $\tau = f(i)$ and $E = F(t)$, (transition time–current and potential–time) are discussed on the same basis.

Applications of the chronopotentiometric method of study in the following fields are reviewed: electroanalytical chemistry, diffusion, electrode kinetics, mechanism of electrochemical reactions, adsorption of electroactive species and the study of complex ions.

Instrumentation and experimental technique are briefly reviewed.

REFERENCES

1 H. F. WEBER, *Wied. Ann.* 7 (1879) 536.
2 H. J. S. SAND, *Phil. Mag.*, 1 (1901) 45.
3 P. DELAHAY, *New Instrumental Methods in Electrochemistry*, Interscience Publishers, Inc., New York, 1954, chap. 3 and 8.
4 T. BERZINS AND P. DELAHAY, *J. Am. Chem. Soc.*, 75 (1953) 4205.
5 W. H. REINMUTH, *Anal. Chem.*, 33 (1961) 322.
6 P. DELAHAY AND T. BERZINS, *J. Am. Chem. Soc.*, 75 (1953) 2486.
7 P. DELAHAY, C. C. MATTAX AND T. BERZINS, *J. Am. Chem. Soc.*, 76 (1954) 5319.
8 W. LORENZ, *Z. Elektrochem.*, 59 (1955) 730.
9 F. C. ANSON, *Anal. Chem.*, 33 (1961) 1123.
10 S. V. TATWAWADI AND A. J. BARD, *Anal. Chem.*, 36 (1964) 2.
11 W. H. REINMUTH, *Anal. Chem.*, 32 (1960) 1514.
12 Y. TAKEMORI, T. KAMBARA, M. SENDA AND I. TACHI, *J. Phys. Chem.*, 61 (1957) 968.
13 L. GIERST AND A. JULIARD, *Proc. Intern. Comm. Electrochem. Thermodyn. Kinet., 2nd Meeting, Tamburini, Milan, 1950.*
14 L. GIERST AND A. L. JULIARD, *J. Phys. Chem.*, 57 (1953) 701.
15 L. GIERST AND P. MECHELYNCK, *Anal. Chim. Acta*, 12 (1955) 79.
16 W. H. REINMUTH, *Anal. Chem.*, 33 (1961) 485; J. J. MCMULLEN AND N. HACKERMAN, *J. Electrochem. Soc.*, 106 (1959) 341.
17 M. ENYO, Thesis, University of Pennsylvania, Pa., 1960.
18 H. A. LAITINEN AND W. S. FERGUSON, *Anal. Chem.*, 29 (1957) 4.
19 J. D. VOORHIES AND N. H. FURMAN, *Anal. Chem.*, 31 (1959) 381.
20 R. PARSONS, *Advan. Electrochem. Electrochem. Eng*, (1961) 1.

21 P. DELAHAY, *Anal. Review of Physical Chemistry*, Anal. Review Inc., Palo Alto, California, 1957, p. 228.
22 P. DELAHAY, *Record Chem. Progr. Kresge-Hooker Sci. Lib.*, 19 (1958) 83.
23 P. DELAHAY AND I. TRACHTENBERG, *J. Am. Chem. Soc.*, 79 (1957) 2355.
24 P. DELAHAY AND C. T. FIKE, *J. Am. Chem. Soc.*, 80 (1958) 2628.
25 H. A. LAITINEN AND W. J. SUBCASKY, *J. Am. Chem. Soc.*, 80 (1958) 2623.
26 C. WAGNER, *J. Electrochem. Soc.*, 101 (1954) 225.
27 I. M. KOLTHOFF AND J. J. LINGANE, *Polarography*, Vol. 1, Interscience Publishers, Inc., New York, 1952, chap. 2.
28 J. J. LINGANE, *Electroanalytical Chemistry*, Interscience Publishers, Inc., New York, 1958, chap. XXII.
29 A. J. BARD, *Anal. Chem.*, 33 (1961) 11.
30 G. MAMANTOV AND P. DELAHAY, *J. Am. Chem. Soc.*, 76 (1954) 5323.
31 P. J. LINGANE, *Anal. Chem.*, 36 (1964) 1723.
32 YU. M. RYABUKHIN, *Zh. Fiz. Khim.*, 37 (1963) 694.
33 F. C. ANSON AND J. J. LINGANE, *J. Am. Chem. Soc.*, 79 (1957) 1015.
34 A. J. BARD, *Anal. Chem.*, 35 (1963) 340.
35 Z. KARAOGLANOFF, *Z. Elektrochem.*, 12 (1906) 5.
36 P. DELAHAY AND C. C. MATTAX, *J. Am. Chem. Soc.*, 76 (1954) 874.
37 D. INMAN AND J. O'M. BOCKRIS, *J. Electroanal. Chem.*, 3 (1962) 126.
38 H. A. LAITINEN AND D. R. RHODES, *J. Electrochem. Soc.*, 109 (1962) 413.
39 H. A. LAITINEN AND H. C. GAUR, *Anal. Chim. Acta*, 18 (1958) 1.
40 R. T. IWAMOTO, *Anal. Chem.*, 31 (1959) 1062.
41 C. H. LIU, K. E. JOHNSON AND H. A. LAITINEN, *Electroanalytical Chemistry of Molten Salts in Molten Salt Chemistry*, edited by M. BLANDER, Interscience Publishers, Inc., New York, 1964.
42 S. SENDEROFF AND G. W. MELLORS, *J. Electrochem. Soc.*, 113 (1966) 66.
43 S. SENDEROFF, G. W. MELLORS AND W. J. REINHART, *J. Electrochem. Soc.*, 112 (1965) 840.
44 J. H. ROBERTS, JR. AND D. T. SAWYER, *Electrochim. Acta*, 10 (1965) 989.
45 R. W. MURRAY AND D. J. GROSS, *Anal. Chem.*, 38 (1966) 392.
46 H. B. HERMAN, S. V. TATWAWADI AND A. J. BARD, *Anal. Chem.*, 35 (1963) 2210.
47 W. LORENZ AND H. MUHLBERG, *Z. Elektrochem.*, 59 (1955) 736.
48 W. LORENZ AND E. O. SCHMALZ, *Z. Elektrochem.*, 62 (1958) 301.
49 R. W. MURRAY, *J. Electroanal. Chem.*, 7 (1964) 242.
50 H. A. LAITINEN AND L. M. CHAMBERS, *Anal. Chem.*, 36 (1964) 5.
51 H. GERISCHER, *Z. Physik. Chem.*, 2 (1954) 79.
52 D. INMAN AND J. O'M. BOCKRIS, *Trans. Faraday Soc.*, 57 (1961) 2308.
53 J. O'M. BOCKRIS, D. INMAN, A. K. N. REDDY AND S. SRINIVASAN, *J. Electroanal. Chem.*, 5 (1963) 476.
54 H. BLOOM AND J. O'M. BOCKRIS, *Fused Salts*, edited by B. R. SUNDHEIM, McGraw-Hill Book Co., New York, 1964, chap. 1.
55 J. D. VAN NORMAN, *Anal. Chem.*, 33 (1961) 946.
56 J. J. LINGANE, *J. Electroanal. Chem.*, 1 (1959/60) 379.
57 H. A. LAITINEN, W. S. FERGUSON AND R. A. OSTERYOUNG, *J. Electrochem. Soc.*, 8 (1957) 516.
58 J. D. VOORHIES AND N. H. FURMAN, *Anal. Chem.*, 30 (1958) 1656.
59 E. MATTSON AND J. O'M. BOCKRIS, *Trans. Faraday Soc.*, 55 (1959) 1586.
60 M. A. V. DEVANATHAN AND M. SELVARATNAM, *Trans. Faraday Soc.*, 56 (1960) 1820.
61 R. A. OSTERYOUNG, *Anal. Chem.*, 37 (1965) 429.
62 J. SARTIAUX, Thesis, University of Brussels, 1952. (P. DELAHAY, Ref. 3, chapter 16).

Elsevier Publishing Company, Amsterdam – Printed in The Netherlands

BOOK REVIEWS

Theory and Principles of Electrode Processes, by B. E. CONWAY, The Ronald Press Company, New York, 1965, vii+303 pages, $7

The production of a book on electrode processes by as well-known an electrochemist as Professor CONWAY is naturally a matter of considerable interest. The volume under review, which is a useful addition to the literature of the subject, follows the intention of the series in that the interests of the author form the outstanding feature of the book.

Chapters 1 and 2, introductory, but with some original contribution by the author, treat potential differences at interphases and the ionic double layer; the material is presented in a clear manner well supported by references.

The particular interests of the author become more apparent in Chapters 3 and 4 dealing with the problem of adsorption of the ionic reactant, and in Chapter 5 on the behaviour of neutral molecules and ions; Chapters 6 and 7 are much preoccupied with the handling of the electron transfer step and the problem of adsorption. This is certainly the best part of the book and although the presentation is rather formal, indeed there is little experimental detail anywhere in the text, the treatment is authoritative and valuable. However, whilst it is axiomatic that an understanding of these very central problems are most necessary for an overall insight into electrode processes, the presentation is such as to imply, and certainly to a newcomer to the field, that a combination of essentially galvanostatic experiments together with the interpretation of Tafel slopes would take one far along the path of the elucidation of any electrode process. This approach is further developed in the very long section on application to selected problems often in an interesting and informative manner, but includes treatments by such methods of, for example, the difficult problems of the kinetics of formation of anodic films and of metal deposition where, in point of fact, there is considerable doubt as to the effectiveness of their application. This approach has therefore led, in the reviewer's opinion, through the nature of the selectiveness forced by the nature of the series, to an imbalance of treatment, and the very considerable modern developments in potentiostatic methods, a.c. methods, including Faradaic rectification and impedance, and relaxation methods in general, have been given almost negligible attention by comparison. As far as the reviewer can see, this deficiency has not been made good by reference to other authorities or even by stressing the need for an understanding much deeper than that displayed in the present volume.

In comparison with the breadth of electrochemical studies a text of the length of the present book is in any case necessarily selective. Hydrogen evolution (in detail), oxygen evolution, metal deposition, anodic film formation and corrosion and passivity are given some attention, as implied previously; organic electrochemistry, a rapidly growing area of interest, does receive some attention but predominantly one reaction, the Kolbe reaction, an interest of the author's, is the central point of the discussion; some basic mechanisms are given a brief outline in an Appendix. A brief account of semi-conductor electrodes is given and a final short chapter on the gas–metal interface makes a somewhat unexpected appearance.

This is not really an introductory book. It certainly will be read with interest, displaying, as it does, the author's important personal contribution to certain aspects of electrode processes, but there must be some disappointment in that matters of importance are not included. The experienced electrochemist will find the text valuable in that he will know how to relate the content of the book to the wider problems, and he will already have a general appreciation of additional necessary techniques. The rather formal treatment with absence of precise experimental information makes it essential for a graduate student using the text to have adequate advice through supervision in order to supplement the monograph from other sources.

The book has an attractive format and the price is very reasonable and it is certainly a text that the practising electrochemist can afford and would find useful to have on his shelves.

H. R. THIRSK, University of Newcastle upon Tyne

J. Electroanal. Chem., 14 (1967) 475–476

Electronic Structures of Molecules by RAYMOND DAUDEL, Pergamon Press, Oxford, 1966, 233 pages, 50s.

This book is a translation of *Structure Electronique des Molecules* (1962), and is an introduction to the quantum-mechanical theory of molecular structure based on Professor DAUDEL's third-year lecture course at the Sorbonne. The author's aim is to provide a general introductory outline of the main types of theoretical approaches that have proved useful in recent years; these are described in more detail in another book, *Les Fondemonts de la Chimie Théorique*. A translation of this larger work is also in progress.

The first two chapters deal with one- and two-electron systems and with diatomic molecules, and include useful brief summaries of the most recent work. The third chapter discusses diatomic molecules, including the s.c.f. approach; there is also a brief account of projection operator formalism. Chapter four is concerned with the interpretation of bond angles in terms of hybridisation ratios; Walsh's method is included here. The next six chapters deal with the electronic properties of organic molecules (mainly hydrocarbons), and compare different methods of calculating orbital and ionization energies. The last chapter (11) deals briefly with electronic properties of molecules of biological interest. This discusses very many topics in a short space, and in the reviewer's opinion a list of references to the original papers would have been preferable.

There are 435 references in the body of the book, to publications in the field of quantum chemistry, which will be of considerable help to new workers in the field. The translation (anonymous) appears on the whole to have been competently carried out. There are, however, some minor oddities—*e.g.*, "empiric" for "empirical" (p. 129) and the phrase "unmarried electrons" (p. 213) (perhaps "spinsters" would be more appropriate?).

Electronic Structure of Molecules is a most useful guide to a rapidly expanding field, and the exposition has the clarity that one has learned to expect from Professor DAUDEL.

N. S. HUSH, University of Bristol

J. Electroanal. Chem., 14 (1967) 476

Electrometallurgy of Chloride Solutions, edited by V. V. STENDER, Consultants Bureau, New York, 1965, pages viii and 138, $20.00.

This special research report consists of 20 short papers presented at Dnepropetrovsk on the occasion of the Fifth All-Union Seminar on Applied Electrochemistry in October, 1962. They are all concerned with aspects of electrolysis, of electrowinning and electro-refining from chloride-containing systems. Most of the work is concerned with aqueous solutions although molten salt systems are also considered.

Cathode performance is shown to be often improved by the addition of chloride, and in several systems it is shown to lead to lower ohmic losses and greater current efficiencies. Detailed discussions are given of the corresponding cathodic deposition of manganese, zinc, cadmium, chromium, nickel, lead and various alloys. The related anode processes give rise to chlorine, and a good deal of consideration is given to the economics of chlorine production and recovery by electrolytic means.

The papers are of variable quality, some being rather simple, inconclusive and supported entirely by Russian references. Others, however, are sophisticated and, in showing a proper awareness of interfacial phenomena, perhaps demonstrate the integrated nature of pure and applied electrochemistry in the USSR. Considerations of electrocapillarity, of outer-layer potentials etc. rub shoulders with qualitative descriptions of metal morphology.

This collection is therefore a useful one, for the interesting facts that are recorded, for the various descriptions of the electrolyses of chloride-containing systems, and, not least, for the review of the recent *state of the art* in the USSR.

G. J. HILLS, University of Southampton

Fundamental Principles of Chemical Analysis, by WILLIAM F. PICKERING, Elsevier Publishing Company, Amsterdam, London, New York, 270 pp., £3.3.-, 1966.

The author states in the preface, that the challenge in the growth of analytical chemistry could be met by the preparation of a small text devoted solely to the fundamental principles of chemical analysis. This book is his attempt to answer this challenge.

This book is a compact one; 260 pages, packed with fundamentals, twelve chapters, including chapters on (i) determinations based on phase separations, (ii) electrical transformations, (iii) ionic equilibria, (iv) energy transitions (including all spectroscopic techniques), (v) statistics and sampling and (vi) chromatographic separations. One of the best chapters is the one discussing the selection of an analytical method. Frankly, the book is very concentrated, but it is often too skimping in dealing with a topic, especially in fast growing areas, for example atomic absorption spectroscopy, or X-ray spectroscopy. No mention is made of nuclear magnetic resonance or electron spin resonance.

Thus, although this book is to be commended in some ways, possibly for up to second year undergraduates, it is felt that (without malice) this book does not meet the challenge.

G. NICKLESS, University of Bristol

Colloid Chemistry, by A. SHELUDKO, Elsevier Publishing Company, Amsterdam, 1966, 277 pages, £4.

This book is based largely on a course of lectures given by the author in the Chemistry Faculty of the University of Sofia, Bulgaria. The first edition was published in Bulgarian in 1957 and a second, and revised edition, was published in Russian in 1960. The present book is a translation into English of the Russian edition, with revisions.

Taken as a whole, the book has much to commend it but there appear to be some omissions in the early chapters of the book in the sections on investigation of macromolecules. For example, the ultracentrifuge described on page 61 is of a type seldom used now in the western world and although quite a lot of space is devoted to sedimentation, the excellent book by SCHACHMAN (published 1959) is not mentioned nor is the important Archibald method for obtaining molecular weights. In the discussion of light scattering, several pages are devoted to the effects of an electric field on the light scattered by particles in the Raleigh region, but the dissymmetry and Zimm methods for examining macromolecules are not mentioned.

However, such omissions are compensated for by the excellence of some of the later chapters which contain accounts of fields where Professor SHELUDKO himself has made contributions. These deal mainly with the thermodynamic approach to the subject. One must single out particularly chapter 6 which is devoted to the subject of thin films, a field where significant contributions have recently been made in understanding the forces acting in colloidal systems. This chapter gives an excellent elementary review of the fundamentals and also indicates where the work is relevant to such problems as flotation, foams, coalescence of emulsion droplets, etc.

An interesting and valuable feature of this book is that a serious attempt has been made to generalise and give some rational account of the subject of colloid chemistry at a level that many undergraduate and most post-graduate students should be able to understand. There is also a useful collection of references to Eastern European and Russian literature. The production is excellent and there are few misprints in the text.

R. H. OTTEWILL, University of Bristol

The Electron Microprobe, edited by T. D. McKINLEY, K. F. J. HEINRICH AND T. B. WITTRY, Wiley, London and New York, 1966, 1035 pages, 210 s; $27.50.

There must be many users of electron-probe microanalysers who could not be present at the Washington conference who will welcome this almost complete report of the proceedings, and not a few of those present who will wish to have a permanent record of the proceedings.

The papers are divided into four groups covering light element analysis, quantitative analysis, new techniques, and general applications, respectively.

The first part deals with progress in the analysis of elements below sodium in the periodic classification; work on both non-dispersive and dispersive methods of detection is described, the latter involving both diffraction gratings and multilayer stearate crystals. Practical problems in this field, such as the importance of specimen contamination are also covered.

The section on quantitative analysis will undoubtedly be well-thumbed as it contains an excellent selection of essentially practical papers. One of the best features of this section is the number of tabulated factors allowing fluorescence corrections (after Wittry) and Philibert's $f(\chi)$-values to be read off directly. Heinrich's tables of mass absorption coefficients are becoming widely accepted and are reproduced in full. The growing importance of the computer in this field is evident in the attention given to the use of computers for the calculation of multicomponent corrections; a particularly interesting feature is the space devoted to discussion of iterative procedures, a subject often ignored.

The papers on instrumentation are of general rather than immediate interest and it is to the section on applications that many people will turn and find a wealth of rewarding detail. Particularly interesting are the number of papers giving calculation examples, and evidence (such as the footnote on page 605) of careful editing in the interests of clarity.

The book is expensive and is not likely to find its way to many private libraries, but it is a must for every laboratory using the technique. The title of the book, however, may be misleading to the beginner for it is not a treatise on the subject but a collection of papers presenting many different and, to the beginner, confusing points of view on the use of the electron-probe microanalyser.

G. SHAW, Pilkington Bros. Ltd., Lancashire

Trace Analysis: Physical Methods, edited by G. H. MORRISON, Interscience Publishers, Inc., 1966, 120s, xx + 582 pp.

The intention of the book is to try to bring together those facets of science which, when combined together, make a contribution to the problem of trace-element analysis. Each chapter has been written by a person active in his respective field, since it was felt no one person would have sufficient expertise to write authoritatively on all topics.

May it be said straight away, that the book is arranged in a very logical manner, beginning with a discussion of the basic terminology of what a *trace* is, followed by discussion of how one tries to choose a suitable analytical method. Thus questions of sensitivity, accuracy and precision, and selectivity are answered. The next chapters attempt to focus attention on the importance of trace impurity in (i) physical, and (ii) biological sciences. If the reviewer is to be honest, he considers the role of the trace element over-emphasized (in a book which is based on analytical chemistry), that insufficient discussion is given to the analytical problems involved, and that only hints at the problems are given. Perhaps this was the intention. The final chapter of the introduction is a concise and detailed account of the separation and pre-concentration procedures necessary to achieve the isolation of the trace component in analysis.

The next seven chapters are descriptions of the various analytical techniques that are used in trace analysis, from spectrophotometry to mass spectrometry. They are all good chapters, clear and precise. It may be said by some that this or that has been forgotten or I would not have placed the accent on that topic. One further comment is called for. These chapters seem to concentrate on metallic elements, and *trace* is used in the sense of an element and not a compound *e.g.*, pesticides, etc.

Finally, the book is completed with a chapter on non-specific methods for the analysis of solids, a chapter which should stimulate the interest of all analysts in techniques which may take over where our cherished methods begin to fail.

The book is well produced, free from mistakes, and should be on the shelves of all laboratories concerned with trace analysis. The book is worth its somewhat high cost.

G. NICKLESS, University of Bristol

JOURNAL OF ELECTROANALYTICAL CHEMISTRY AND INTERFACIAL ELECTROCHEMISTRY, VOL. 14 (1967)

AUTHOR INDEX

JOURNAL OF ELECTROANALYTICAL CHEMISTRY AND INTERFACIAL ELECTROCHEMISTRY, VOL. 14 (1967)

SUBJECT INDEX

Vol. 14 No. 4 JOURNAL OF ELECTROANALYTICAL CHEMISTRY AUGUST 1967
AND INTERFACIAL ELECTROCHEMISTRY

CONTENTS

SPOT TESTS IN ORGANIC ANALYSIS

Seventh English Edition, completely revised and enlarged

by FRITZ FEIGL in collaboration with VINZENZ ANGER

6 x 9″, xxiii + 772 pages, 19 tables, over 2000 lit.refs., 1966, Dfl. 85.00, £8.10.0, $30.00

This 7th edition has involved complete revision and reorganisation of the subject in order to present a still clearer picture of the multitudinous applications open to organic spot test analysis. The amount of new work which is appearing has certainly necessitated expansion, but the author has kept this to a minimum by omitting the chapter on spot test techniques (which are covered in the companion volume *Spot Tests in Inorganic Analysis*) and by limiting the number of tables and structural formulae.
Comparison with the 6th edition reveals the following differences:

	Number in 6th Edn.	7th Edn.
Preliminary tests	32	45
Functional group tests	70	109
Individual compound tests	133	148
Detection of particular structures and types of compounds	0	74
Differentiation of isomers etc.	0	54
Applications in the testing of materials etc.	111	131

In total the book now gives in 561 sections information on more than 900 tests compared with 600 tests in 346 sections in the preceding edition.

An important feature is the inclusion of a large number of recently developed tests and comments which have not hitherto been published in any form.

It is the author's hope that this work will help to correct the widespread impression that physical instrumentation is always superior to chemical methods for solving analytical problems. Each of the chapters presents instances of problems for which no solutions by physical means have yet been developed, or for which the rapid spot tests are equal or superior to the expensive instrumental procedure.

CONTENTS: 1. Development, present state and prospects of organic spot test analysis. 2. Preliminary (exploratory) tests. 3. Detection of characteristic functional groups in organic compounds. 4. Detection of structures and certain types of organic compounds. 5. Identification of individual organic compounds. 6. Application of spot tests in the differentiation of isomers and homologous compounds. Determination of constitutions. 7. Application of spot reactions in the testing of materials, examinations of purity, characterization of pharmaceutical products, etc... Appendix: Individual compounds and products examined. Author index. Subject index.

FROM REVIEWS OF THE SIXTH EDITION

... This new book, like its author, is unquestionably a giant on the analytical scene...
Journal of the Royal Institute of Chemistry

... Die Tatsache, dass Feigls klassisch gewordenes Werk, welches überall mit Begeisterung aufgenommen wurde, bereits in 6. Auflage erscheint, ist an sich Empfehlung genug... Es ist also eine wahre Fundgrube für neue Experimentaluntersuchungen...
Chimia

... Even in these days of physical instrumentation there is ample room for the techniques described in this book which were originated and largely developed by Prof. Feigl. They are mostly very quick and very economical on materials. They sometimes present solutions to problems so far insoluble by expensive physical methods...
Laboratory Practice

ELSEVIER PUBLISHING COMPANY
AMSTERDAM LONDON NEW YORK

147E